8-5-2020 4:30 PM

A Biomechanical Investigation into the Effect of Experimental Design on Wrist Biomechanics and Contact Mechanics

Clare E. Padmore, *The University of Western Ontario*

Supervisor: James A. Johnson, *The University of Western Ontario*
Co-Supervisor: Graham JW King, *Roth | McFarlane Hand and Upper Limb Centre*
A thesis submitted in partial fulfillment of the requirements for the Doctor of Philosophy degree in Biomedical Engineering

Abstract

The wrist is one of the most commonly injured joints, and injury can have serious sequelae if pathological healing ensues. Strides have been made to understand normal and pathological wrist biomechanics using experimental approaches, which has contributed to improved patient care. The present work advances our understanding of the influence of experimental techniques and joint motion measurement techniques on *in-vitro* wrist biomechanical cadaveric studies, and applies the knowledge learned to a common clinical entity of scapholunate insufficiency.

First, the relative contributions of the carpal rows to wrist motion were assessed, in addition to the identification of limitations of current biomechanical testing techniques. The radiocarpal joint contributed more motion to wrist flexion, the midcarpal joint contributed more to wrist extension, while near neutral wrist position there was a relatively equal contribution from both joints. Passive motion joint simulation, forearm position, and coordinate system selection and joint congruency were all identified as areas needing investigation.

In order to assess the effect of joint coordinate system (JCS) selection on resulting wrist angle, four JCS were compared to determine JCS selection on wrist angle characterization. Subtle differences were found between JCSs, and the findings support the use of any of the analyzed methods. Additionally, to quantify joint congruency at the wrist, validation and application of a previously described a non-invasive CT-based technique to measure joint congruency at the wrist is described.

The effect of forearm orientation on wrist joint biomechanics was then evaluated. Radioscaphoid joint contact was found to be sensitive to forearm orientation and wrist angle, while radiolunate joint was not sensitive to changes in forearm orientation. Scaphoid angular rotation was found to vary with forearm position, but only at the extremes of wrist flexion-extension.

The present work advances wrist biomechanics knowledge and will help to improve the clinical management of acute and chronic wrist injuries.

Keywords

Wrist, carpus; biomechanics, contact mechanics, orthopedics

Lay Summary

The wrist is a complex joint made up of eight carpal bones and an intricate network of soft tissue structures. It is one of the most commonly injured joints, and injury can have serious implications if abnormal healing occurs. Previous studies have sought to understand normal and injured wrist biomechanics using a variety of experimental methods, which has contributed to improved patient care. However, the influence of study design and experimental devices (*i.e.* joint motion simulators) on study results have yet to be examined. A rigorous experimental framework and an understanding of how each decision made during the development of a study is of utmost importance. The potential consequences of not understanding base assumptions when designing testing apparatus or studies may lead to biased data reporting and thus misguided data interpretation. Furthermore, highly standardized experimental designs will lead to more accurate and repeatable results. Reliable results are paramount in knowledge translation as they affect an investigator's or clinician's ability to trust outcomes and advance research and clinical management of wrist pathologies. The results from this body of work will help investigators gain a greater understanding of how assessment techniques and experimental design affect results and will help improve overall wrist biomechanics research.

Co-Authorship Statement

Chapter 1:

Sole Authorship: Clare Padmore
Manuscript Review: Nina Suh, James Johnson, Graham King

Chapter 2:

Study Design & Data Collection: Clare Padmore, Braden Gammon, Masao Nishiwaki
Analysis: Clare Padmore, Helen Stoesser
Manuscript Preparation: Clare Padmore
Manuscript Review: Nina Suh, James Johnson, Graham King, Dan Langohr

Chapter 3:

Study Design: Clare Padmore, Dan Langohr
Data Collection: Duncan Iglesias
Data & Statistical Analysis: Clare Padmore
Manuscript Preparation: Clare Padmore
Manuscript Review: Nina Suh, James Johnson, Graham King

Chapter 4:

Study Design: Clare Padmore, Dan Langohr
Data Collection: Clare Padmore
Data & Statistical Analysis: Clare Padmore
Manuscript Preparation: Clare Padmore
Manuscript Review: Nina Suh, James Johnson, Graham King

Chapter 5:

Study Design: Clare Padmore, Nina Suh, Graham King
Data Collection: Clare Padmore, Andrea Chan
Data & Statistical Analysis: Clare Padmore
Manuscript Preparation: Clare Padmore
Manuscript Review: Nina Suh, James Johnson, Graham King, Dan Langohr

Chapter 6:

Study Design: Clare Padmore, Nina Suh
Data Collection: Clare Padmore, Andrea Chan
Data & Statistical Analysis: Clare Padmore
Manuscript Preparation: Clare Padmore
Manuscript Review: Nina Suh, James Johnson, Graham King, Dan Langohr

Chapter 7:

Sole Authorship: Clare Padmore
Manuscript Review: Nina Suh, James Johnson, Graham King, Dan Langohr

Acknowledgments

The preparation and completion of this body of work could not have been possible without the guidance, support and leadership of many individuals. First and foremost, I would like to thank my supervisors: Dr. Jim Johnson, Dr. Nina Suh, and Dr. Graham King. They provided me with unparalleled support, guidance, mentorship, and leadership throughout my training at the Roth | McFarlane Hand and Upper Limb Centre. It was not only their knowledge and expertise, but their leadership to which I owe my success. I am humbled to have had the opportunity to learn from the best and am grateful for not only the opportunities they afforded me, but also the belief they had in me. I will forever carry with me the lessons they have taught me.

I also would also like to acknowledge all those who directly or indirectly impacted my time at the HULC lab. You were all instrumental in the completion of this work, and I feel grateful to have been a part of a great team. I would also like to give a special thank you to Team Wrist. We persevered through long testing days, and countless projects. I know the future of Team Wrist is bright, and you will continue to produce exceptional research.

Finally, I could not made it through this humbling process without the unwavering love and support of my family. To my sisters, Kathryn and Jenn, you have always been my biggest supporters; thank you for always being my rocks.

Table of Contents

List of Figures

Chapter 1

1 Introduction to Wrist Kinematics, Biomechanics and Contact Mechanics

OVERVIEW

The goal of this work is to assess and advance biomechanical assessments of the wrist joint. This chapter introduces the biomechanics of the wrist, with a particular focus on the carpus. The anatomy of the carpus, including the osseous anatomy and soft tissue structures are reviewed. The current state of literature regarding joint motion simulation and tracking strategies are also discussed. This is followed by current contact mechanics assessment approaches. Additionally, common clinical disorders of the carpus and their effect on wrist biomechanics will be reviewed. In summary, this introductory chapter outlines the motivation for the study, as well as the objectives and hypotheses regarding these investigations.

1.1 The Hand and Wrist

1.1.1 Osseous Anatomy

The wrist is a complex collection of bony and soft tissue structures that connect the hand to the long bones of the forearm (Figure 1-1).[1] The wrist is surrounded by an elaborate network of soft tissues including ligaments that connect the carpal bones to one another as well as to the long bones of the forearm and the metacarpal bones of the hand. Additionally, tendons from the muscles of the forearm attach to the carpus and metacarpals and are responsible for actuating wrist motion.

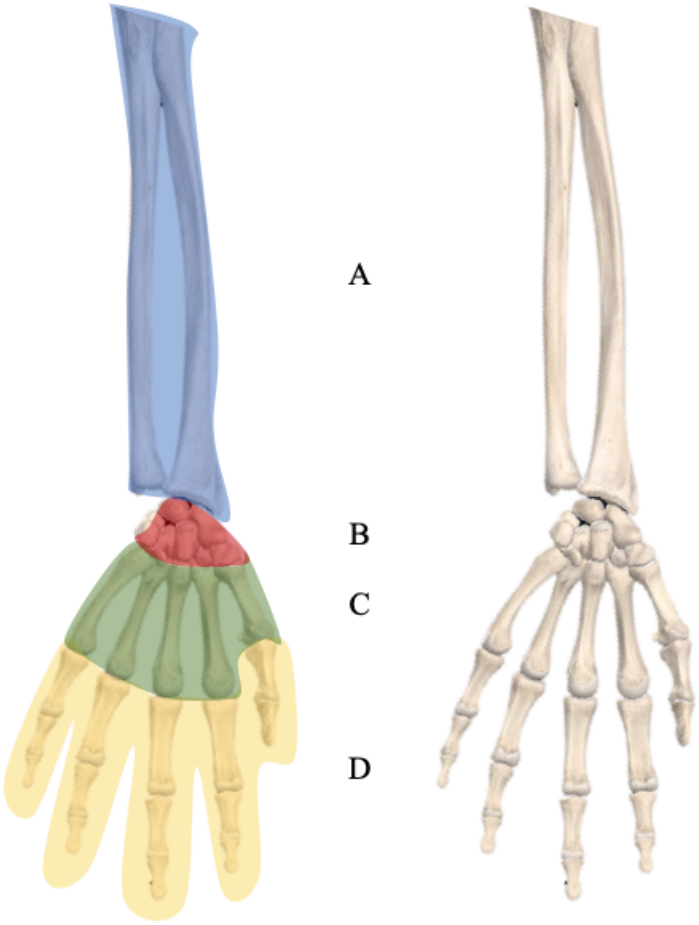

Figure 1-1: Osseous Anatomy of the Forearm, Hand and Wrist.

Bony anatomy of the right forearm, wrist, and hand demonstrating groupings of bones of interest. (A) Radius and Ulna, (B) Carpals, (C) Metacarpals, and (D) Phalanges.

1.1.1.1 Osteology of the Carpus and Wrist

The carpus is composed of eight bones: the scaphoid, lunate, triquetrum, pisiform, hamate, capitate, trapezoid, and trapezium (

Figure 1-2). The carpal bones are classified as short bones and provide stability through their numerous articulations with adjacent carpal bones as well as the distal radius, distal ulna, and the 1st through 5th metacarpals. The eight carpal bones can be divided into two horizontal rows.[2] The proximal row that contains the scaphoid, lunate, triquetrum and pisiform articulates with the distal radius as well as the ulnar triangular fibrocartilage complex,[3] forming the radiocarpal and ulnocarpal joints, respectively. Distally, the carpus contains the capitate, hamate, trapezoid, trapezium, articulate with the metacarpals.[4] The distal row of carpal bones also articulates with the proximal row of carpal bones; this articulation is called the midcarpal joints.

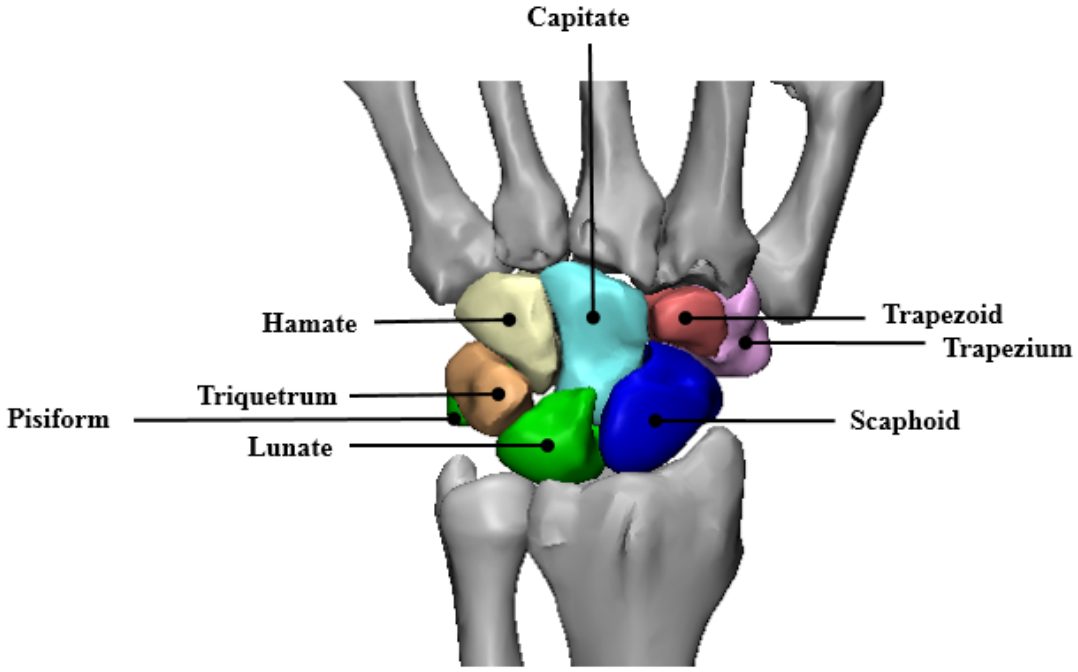

Figure 1-2: Bony Anatomy of the Carpus.

Dorsal view of the carpus, with all the carpal bones highlighted and labeled.

1.1.1.1.1 Radius

The radius is the shorter of the two parallel long bones that make up the forearm and located laterally to the ulnar when placed in a neutral anatomic position. At the distal end of the radius, the diaphysis diverges forming two articulating surfaces. The first articulating concave surface is the sigmoid notch, located on the medial side, which articulates with the distal ulnar forming the distal radioulnar joint. The second articulation formed by the distal articular surface of the radius is defined by a triangular fossa for the articulation with the scaphoid and a quadrangular fossa for the articulation with the lunate (

Figure 1-3).[5] The fossae are separated by the cartilaginous sagittal ridge known as the interfacet prominence, forming a congruent articulation between the proximal scaphoid and lunate. Furthermore, the lateral edge of the distal radius extends more distally, forming the radial styloid process. This conical shaped osseous projection constrains the proximal pole of the scaphoid and is the site of attachment for the radioscaphocapitate ligament.

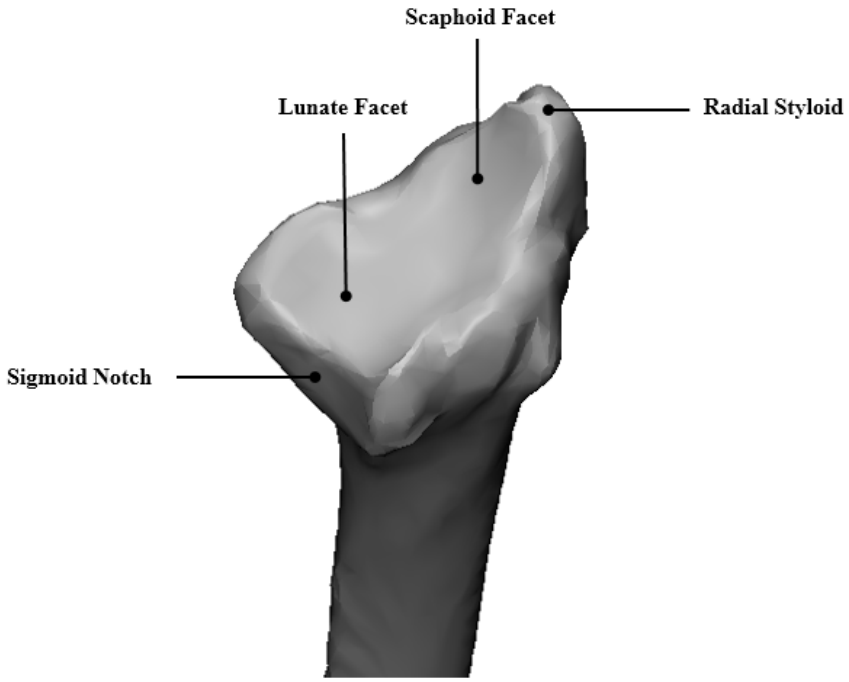

Figure 1-3: Anatomy of the Distal Radius.

An ulnar view of the distal radius. The concave triangular scaphoid fossa and the quadrangular lunate fossa, along with notable anatomical features are highlighted.

1.1.1.1.2 Scaphoid

The scaphoid is the largest of the carpal bones in the proximal row of carpus and is a stabilizing link between the proximal and distal rows (Figure 1-4).[6] The scaphoid has four articular facets covering approximately 42% of its entire surface and is boat or peanut shaped.[7] When the scaphoid is sitting in a neutral position, the long axis of the scaphoid is obliquely oriented in both the sagittal and coronal planes. Belsole et al. reported that the average three-dimensional angle between the long axis of the scaphoid and the long axis of the capitate was 73 degrees.[8]

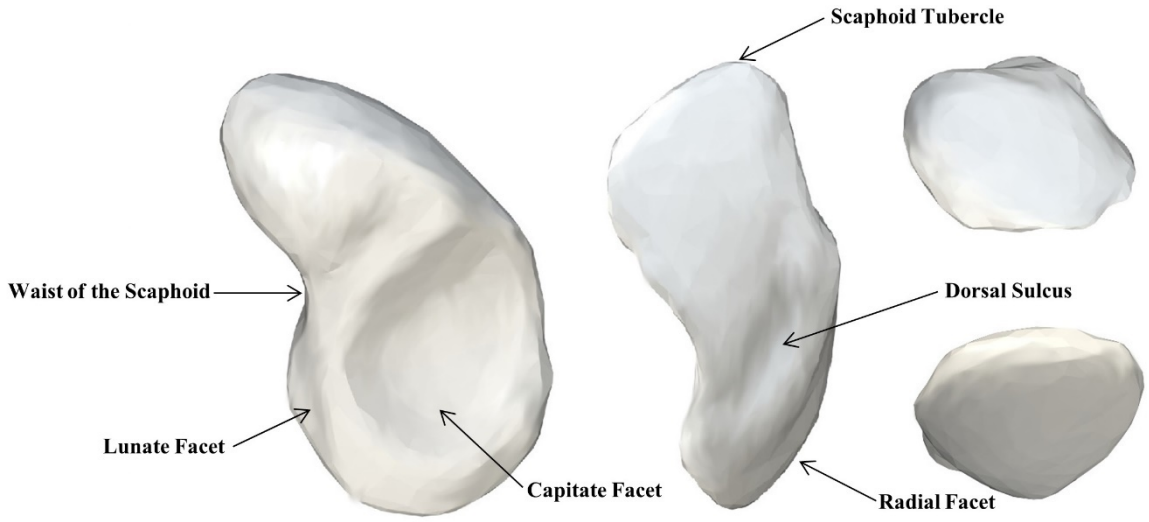

Figure 1-4: Osseous Anatomy of the Scaphoid.

Bony anatomy of the left scaphoid with associated landmarks. (A) Medial View, (B) Dorsal View, (C) Distal Articular Surface, (D) Proximal Articular Surface.

1.1.1.1.3 Lunate

The lunate is often considered the keystone bone of the carpus. It is approximately semilunar in shape and articulates between the scaphoid and triquetrum in the proximal carpal row (Figure 1-5). In roughly 65% of the population, the distal articular surface is divided into two facets: a radial facet for the capitate and ulnar facet for the hamate. This is referred to as a type II lunate. The remaining 35% of the population has a single facet for the capitate and this type of lunate is referred to as type I lunate.[9] The distal edge of the two non-articulating surfaces of the lunate are referred to as the dorsal and volar poles the lunate and are thought to have a stabilizing role with respect to the head of the capitate by preventing dorsal-volar subluxation during flexion-extension.

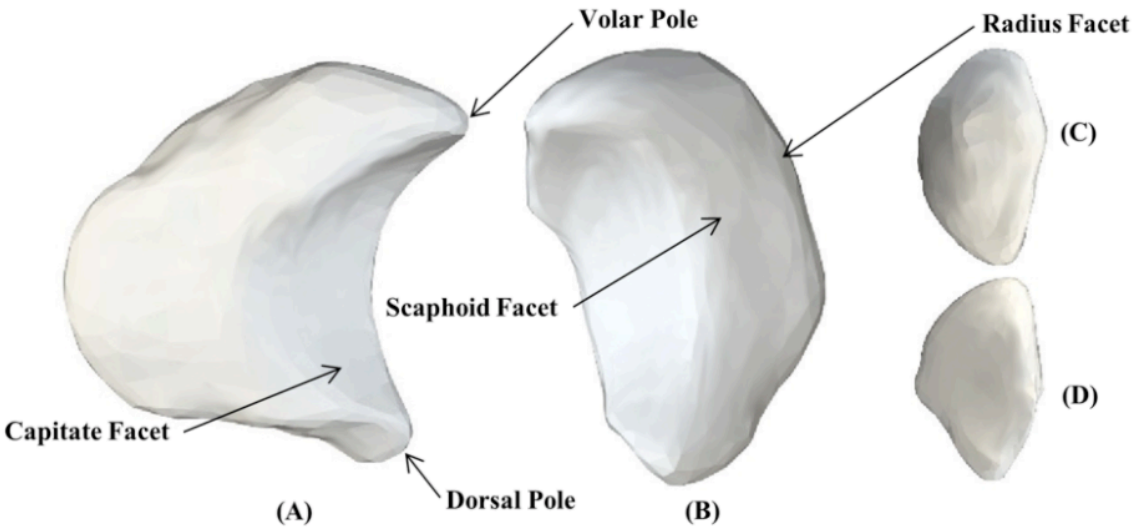

Figure 1-5: Osseous Anatomy of the Lunate.

Bony anatomy of a left lunate with landmarks highlighted. (A) Distal Articular Surface, (B) Proximal Articular Surface, (C) Medial View, (D) Lateral View.

1.1.1.1.4 Capitate

The capitate is the largest carpal bone and resides centrally in the distal carpal row. It comprises the basis of the transverse carpal arch forming a rigid central column of the hand and wrist. Distally it articulates with the third and fourth metacarpal. There is minimal motion at this joint and functionally the capitate acts as an extension of the base of the third metacarpal. On the radial aspect of the capitate lies the scaphocapitate joint. On the ulnar aspect, the capitate articulates with the hamate. Proximally, the capitate sits within the lesser convexity of the lunate, which allows for flexion and extension at the mid-carpal joint.

1.1.2 Wrist Joints

1.1.2.1 Radiocarpal Joints

The radiocarpal joint is critical to normal hand and wrist function. Formed by the multiple articulations of the scaphoid, the lunate and distal part of the radius, the radiocarpal joint is responsible for more than half of the range of motion of the wrist. The radiocarpal joint is an elliptical joint (a modified ball and socket)[5], with the biconvex proximal surfaces of the scaphoid and lunate articulating with the shallow lateral and medial biconcave facets on the articular surface of the distal radius, respectively, which are separated by a narrow anteroposterior crest. The importance of the radiocarpal joint to wrist motion is demonstrated by the fact that fusion significantly reduces flexion by approximately 76% (range, 73% to 80%), extension by approximately 64% (range, 60% to 68%), radial deviation by approximately 60%, and ulnar deviation by approximately 50%.[10–12]

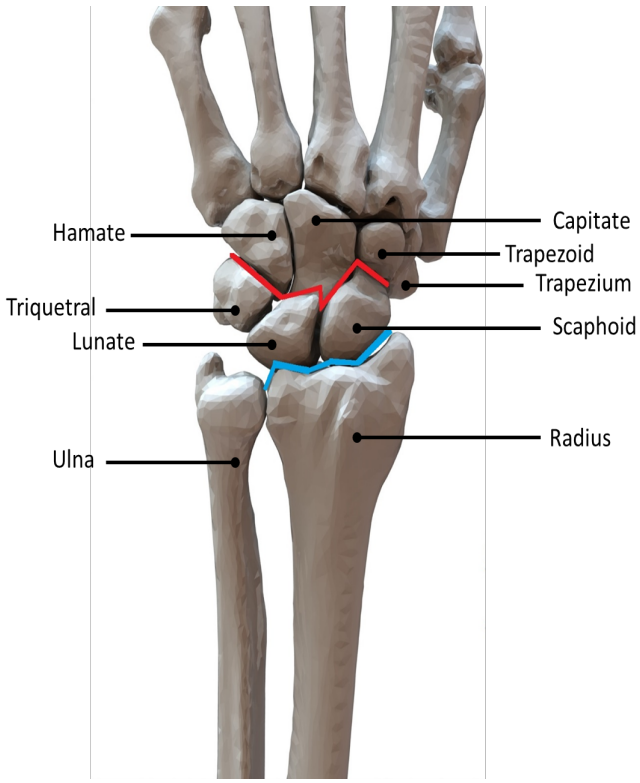

Figure 1-6: Midcarpal and Radiocarpal Wrist Joints.

*Dorsal view of the left wrist showing the radiocarpal **(blue line)** and midcarpal **(red line)** joints.*

1.1.2.2 Midcarpal Joints

The midcarpal joint is sigmoid in shape, with a concave-distal arc radially and a concave-proximal arc ulnarly. Overall, the amount of the proximal surfaces of the capitate and hamate covered by articular cartilage substantially exceeds the surface area of the actual contact with the distal surfaces of the scaphoid, lunate, and triquetrum for any given wrist position. Most of the stabilizing ligaments of the midcarpal joint are volar and lateral. The dorsal capsule is less robust and therefore vulnerable to trauma.[5]

The contribution of the midcarpal joint to normal wrist flexion-extension is complex. Patterson et al. showed that during global wrist motion, the radiolunate joint contributes more to the motion during flexion than that of the capitolunate joint, while the capitolunate joint contributes more during extension.[13] Suggesting that the midcarpal joint contributes most in maximum extension whereas the radiocarpal joint contributes most in maximum wrist flexion.

However, others studies have reported differing results. If only the central part of the carpus (the capitate-lunate-radius linkage) is considered, the radiocarpal and midcarpal motion is equally divided in only one-third of wrists.[10] In the remaining two-thirds, approximately 60% of the global flexion occurs at the lunocapitate interval, whereas 66% of extension is radiocarpal dependent. However, if motion is recorded at the radial aspect (the radius-scaphoid-trapezium linkage), more than two-thirds of the global arc of movement occurs at the radioscaphoid interval. Although radiocarpal and midcarpal contribution has been extensively studied, there remains uncertainty. The conflicting results may be due to different experimental protocols, data collection techniques or data processing methodologies.

1.1.3 Ligamentous Anatomy

Ligaments are bundles of fibrous connective tissue that act to bind bones together to provide stability across an articulation. The carpus contains an intricate network of ligaments that provide stability to the carpal bones during functional motion. Carpal ligaments can be divided into several groupings that are defined by their location within the carpus and the organization of the joint capsule. Capsular ligaments are defined as crossing the radiocarpal joint, the midcarpal joint, or crossing both.[14] Moreover, the ligaments are identified by location on the dorsal or volar aspect of the hand. The dorsal capsular wrist ligaments can be clearly seen after dissection of the extensor retinaculum, whereas the volar capsular ligaments are difficult to discern and appear to blend together. There are also two categories of wrist ligaments: intrinsic and extrinsic ligaments.[15] Intrinsic carpal ligaments originate and insert only onto carpal bones, providing a rigid framework for the wrist joint. Conversely, extrinsic ligaments bridge carpal bones to the metacarpals or the distal radius. The principle name of each ligament typically stems with the bone of origin as the prefix and the bone of insertion as the suffix.

The magnitude of motion allowed by each ligament, is a function of factors including orientation and laxity, and defines the degree of motion of the bones that are connected to the ligament. Multiples ligaments crossing a joint, implies multiple directions of constraint.

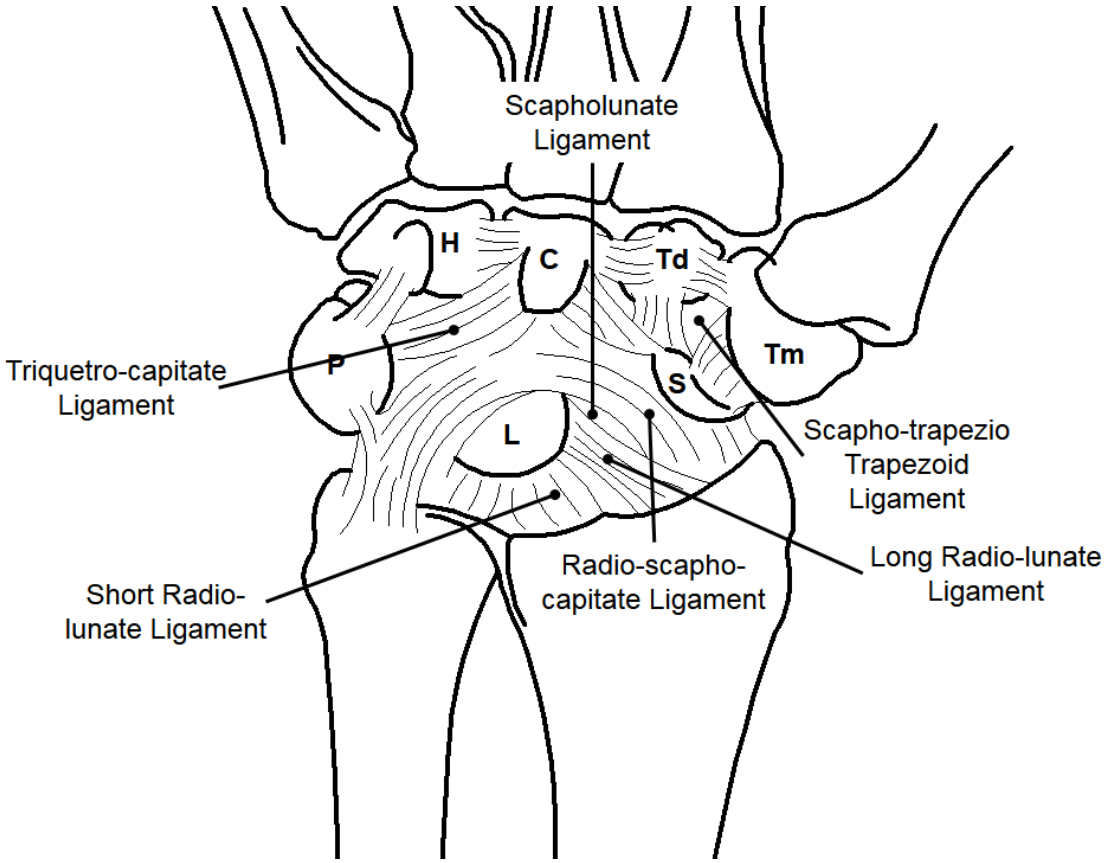

Figure 1-7: Volar Ligaments of the Wrist.

Schematic of the volar ligaments of the right hand.

1.1.3.1 Scapholunate Interosseous Ligament

The scapholunate (SL) interosseous ligament is uniquely "C" shaped and spans the interval between the dorsal, volar and proximal edges of the scapholunate (SL) joint surface.[16] This arrangement allows the distal portion of the SL joint surface to be directly exposed to the midcarpal joint space whereas the proximal interosseous component of the SL ligament isolates the surfaces from the radiocarpal joint. The three sub-regions of the SL ligament each have different material and anatomic properties. The dorsal component of the SL ligament is the most critical stabilizer of the SL joint acting as the primary restraint to distraction as well as torsional and translational moments.[17–19] It is a true ligament characterized by its thick transversely oriented collagen fibers. The volar component of the SL ligament, although considerably thinner than the dorsal component, plays a role in the rotational stability of the

SL joint. The proximal or membranous component of the SL ligament provides little restraint to abnormal carpal motion and it is histologically defined as a fibrocartilaginous structure.

1.1.3.2 Scaphotrapezium-Trapezoid Ligament

The origin of the scaphotrapezium-trapezoid (STT) ligament is distal to the attachment site of the RSC ligament on the lateral cortex of the distal pole of the scaphoid. Moving distally, the STT diverges to form two distinct bands, the scaphotrapezoid and the scaphotrapezium ligaments. Forming the dorsolateral STT joint capsule, both bands course distally attaching to the dorsal cortical surfaces of the trapezoid and trapezium. Before attaching to the respective bones, the fibers from each ligament interdigitate with surrounding ligaments attaching in the same region, with no clear divisions between them. Forming the volar STT joint capsule, the fibers of the STT ligament appear as a flat sheet of longitudinally oriented fibers.

1.1.3.3 Radioscaphocapitate Ligament

The radioscaphocapitate (RSC) ligament is the most radially positioned of the volar radiocarpal ligaments, attaching proximally to the radial styloid process as well as the radial region of the volar margin on the distal radius.[16] In part, the RSC ligament aids in the formation of both the volar floor and radial wall of the radiocarpal joint capsule. Moving distally from the radius, the RSC ligament courses ulnarly towards the scaphoid, first inserting onto the lateral aspect of the waist. The second insertion point of the RSC ligament on the scaphoid is from the radial aspect of the waist and volarly throughout the region of the margin of the proximal pole. The remaining portion of the ligament continues ulnarly and distally passing the volar and proximal aspects of the scaphocapitate (SC) joint space and attached on the volar aspect of the head of the capitate. The distalmost fibers of the RSC ligament integrate with the SC ligament to insert onto the volar surface of the waist of the capitate.

1.1.4 Musculature

The essential function of muscle is the ability to contract making it possible to produce joint motion. Muscles of the human body are classified as one of three types of tissue: smooth, cardiac, or skeletal. Skeletal muscle fibers are tubular, multinucleated, striated and unlike smooth and cardiac muscle contract voluntarily under nerve control. Skeletal muscles are

attached to the skeleton via fibrous connective tissues known as tendons. The fibers within the muscle generate tension across a joint by contracting, shortening in length, and producing a moment arm to manipulate the position of the joint. The magnitude of force is dependent on the size, type, and insertion point from the joint center of the muscle. As skeletal muscles contract, the bone of origin remains stationary while the bone of insertion is manipulated. Tendons do not actively change length as the muscle contracts, however, may undergo slight alterations due to their viscoelastic nature.

Most of the time a single muscle is not solely accountable for joint motion. Rather, a group of synergistic muscles aid in the motion with the muscle applying the greatest load being termed the primary mover. Additionally, as muscles contract, they typically have antagonist pairs which bring about joint motion in an opposite direction to provide stability to the motion.

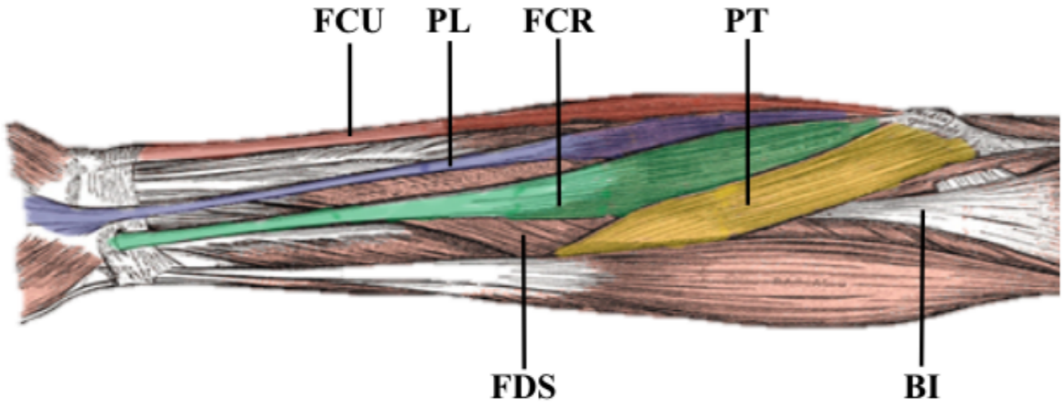

Figure 1-8: Volar Forearm Compartment Musculature.

This figure does not contain all muscles located on the volar aspect of the forearm, as many of these contribute to flexion and motion at the elbow and do not contribute significantly to stabilization of the carpus.

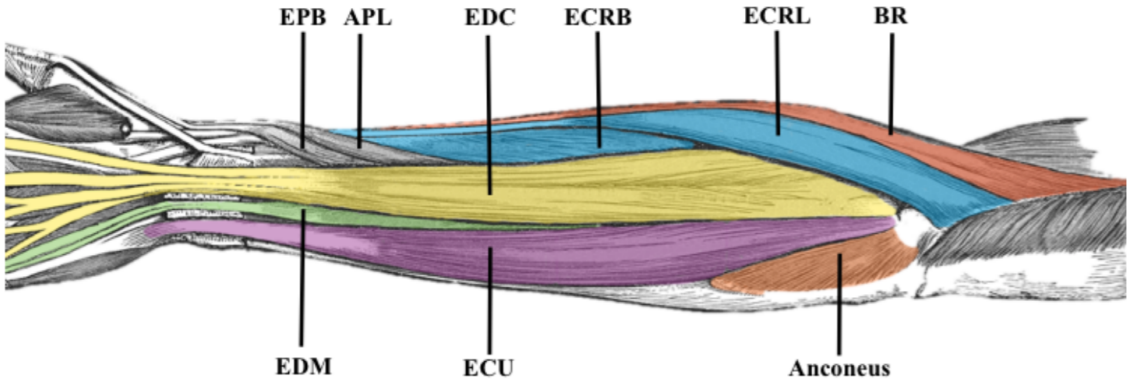

Figure 1-9: Dorsal Forearm Compartment Musculature.

This figure does not contain all muscles located on the dorsal aspect of the forearm, as many of these contribute to extension and motion at the elbow and do not contribute significantly to stabilization of the carpus.

Motion of the wrist is primarily achieved via six muscles: the flexor carpi radialis (FCR), flexor carpi ulnaris (FCU), extensor carpi radialis brevis (ECRB)(Figure 1-8), extensor carpi radialis longus (ECRL), and extensor carpi ulnaris (ECU) (Figure 1-9).[5,16] The wrist flexors are found in the volar compartment of the forearm and the extensors in the dorsal compartment. Wrist rotation is primarily controlled via four muscles, the biceps (both heads), supinator, pronator teres and the pronator quadratus (PQ). Gordon et al. reported loading ratios for both pronation and supination. Gordon et al. found that during pronation, the pronator teres contributed 56%, while the pronator quadratus contributed 44%. It was also found that during supination, the two heads of the biceps contributed 67%, while the supinator contirbuted 33%.[20]

1.2 Kinematics of the Carpus and Wrist

1.2.1 Range of Motion

The wrist is a hypermobile joint capable of multi-planar motions including but not limited to flexion-extension (FEM), radial-ulnar deviation (RUD), pronation-supination (PSM), and dart-thrower (DTM) motion. A well-balanced combination of joint architecture and tendon forces prevent ligaments and articular surfaces from carrying excessive load.

All wrist movements are accomplished through the complex motions of the eight carpal bones relative to the radius and ulna. As there are no tendinous attachments on the proximal carpus, the static and dynamic stability, particularly the proximal row, is dependent on the shape of the carpal articulations, the joint capsule, and the surrounding ligaments and other soft tissues.

Injury or deterioration of the ligaments due to age or disease may result in instability of the wrist and altered carpal biomechanics. Instability often progresses to osteoarthritis at the radiocarpal and midcarpal joints, leading to pain stiffness and weakness in patients. In recent years, research reporting on normal carpal biomechanics has been published and has furthered our knowledge; however, further studies would be beneficial to broaden our understanding of these complex articulations.

1.2.2 Carpal Kinematics

1.2.2.1 Row and Column Theory

Bryce and Destot were the first to describe kinematic function of the wrist in terms of two distinct rows arranged proximally and distally, known as row theory.[22] The lunate and triquetrum together comprise the proximal carpal row, which is referred to as the intercalated segment, because it lacks musculotendinous attachments, and is interposed between two other moving bones as part of an articulated link.[21] Consequently, proximal carpal row motion occurs indirectly from the motion of the distal row of carpal bones.[22–24] The distal row (trapezium, trapezoid, capitate, and hamate) is tightly bound to the metacarpals and essentially moves as a rigid unit. It has been observed that the scaphoid functions as the bridge, or connecting rod, between the rows because it coordinates the motion of the two rows.[25] Early studies of carpal function speculated that wrist flexion and extension occurred between the two rows at the midcarpal joint, while ulnar and radial deviation occurred through the articulation of the scaphoid with the radius at the radiocarpal joint.[26]

Alternative theories have been suggested, one of which conceptualizes the carpus into three columns: the radial, central, and ulnar columns. The radial column is thought to consist of the scaphoid, trapezium and trapezoid.[25] While the central column consists of the capitate, hamate and lunate, and the ulnar column consists of the triquetrum. The column theory suggests that flexion-extension occurs through the central column, and wrist radial-ulnar deviation occurs through rotation of the scaphoid and triquetrum about the central column.

Other theories, in addition to row and column theory, have been proposed to explain the mechanics of the wrist.[27,28] However, currently no theory exists that fully explains wrist mechanics. Several investigators have postulated that the shape of the carpal bones determines the type of wrist kinematic behavior[29]; however, conclusive evidence of this has yet to be found. For simplicity, the forthcoming chapters will discuss wrist biomechanics using the row theory description of the wrist.

1.2.2.2 Flexion-Extension

Planar wrist FEM motion occurs around the sagittal axis of the hand (Figure 1-10). The wrist joint can typically reach anywhere from 65 to 90 degrees of flexion and 55 to 75 degrees of

extension, demonstrating a 160-degree motion arc.[16] The total range of planar wrist FEM is a result of the combination of motion between the radiocarpal and midcarpal joints.[30] Wrist FEM is limited by the dorsal radiocarpal ligaments during wrist flexion and a combination of the volar ligaments and dorsal aspect of the radius during extension.

A variety of different methodologies have been employed to examine carpal kinematics during wrist flexion-extension. These kinematic studies have observed that the proximal row of carpal bones do not move as a single rigid body, even though they are rotating in the same plane. Using a passive motion wrist simulator with constant tendon loads across the wrist, Stoesser et al. examined carpal kinematics in the intact wrist during FEM.[31] They reported that the scaphoid rotates at a greater extent throughout flexion and extension compared to the lunate. In agreement with Stoesser et al.[31], Ruby et al.[23] reported that from full flexion to full extension of the wrist, the scaphoid rotates 80 degrees with respect to the radius, whereas the lunate rotates only 58 degrees.[23] Garcia-Elias et al. have also reported that not only does the scaphoid extend in wrist extension, but also supinates (6 degrees), and deviates in the radial direction (4 degrees), and by contrast the lunate pronates slightly (5 degrees) in addition to extending.[12] Garcia-Elias also found that the scaphoid and lunate flex and ulnarly deviate in the wrist flexion. The bony architecture of the scaphoid is thought to contribute to its significant mobility.

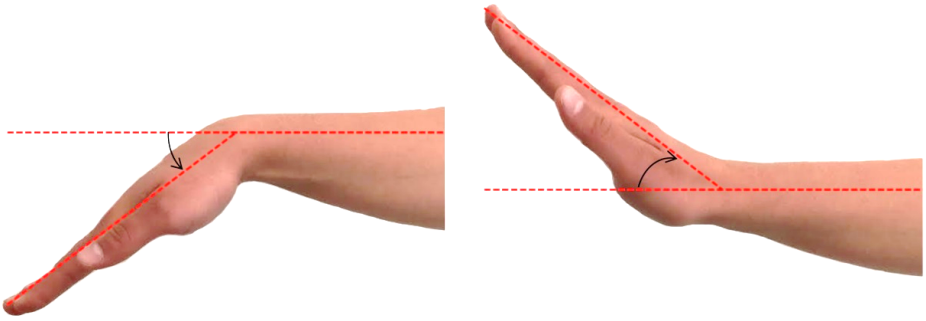

Figure 1-10: Range of Wrist Motion: Flexion – Extension.

Motion of the wrist joint in flexion (left) and extension (right).

1.2.2.3 Pronation-Supination

Pronation supination motion (PSM) largely occurs at the proximal and distal radioulnar joints of the forearm (Figure 1-11). The ulna is thought to stay almost stationary while the radius, through a combination of rolling and sliding, rotates around the ulna to achieve pronation and supination. Morrey et al. found that on average the wrist and forearm exhibits 68 degrees of pronation and 74 degrees of supination.[32] The pronation supination axis lies obliquely through the center of the radial head and the fovea of the ulnar head. The radioulnar ligaments at the DRUJ are the principal constraint to wrist supination while wrist pronation is limited by the crossing of the radial and ulnar shafts. PSM is also limited by the interosseous membrane that binds the radius to the ulna.

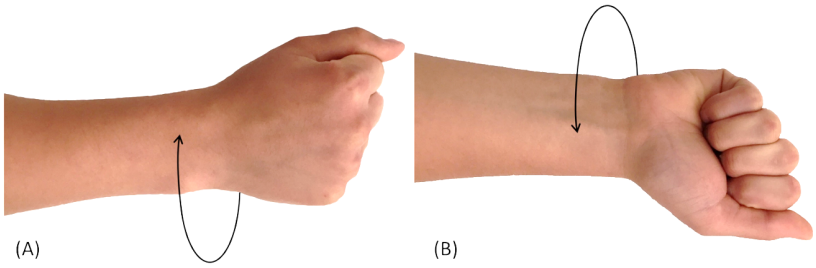

Figure 1-11: Range of Wrist Motion: Pronation-Supination.

Pronation-Supination. Motion of the wrist joint in pronation (A) and supination (B).

1.2.2.4 Radial Ulnar Deviation

Planar wrist radial-ulnar deviation (RUD) occurs around the medial-lateral axis of the wrist (Figure 1-12). On average the wrist has a 60-degree range of motion, deviating radially between 15 and 25 degrees and ulnarly, between 30 and 45 degrees.[33] RUD motion is limited through carpal interaction with the radial styloid and the tightening of the ulnar collateral ligaments in radial deviation and the tightening of the radial collateral ligaments in ulnar deviation. Radial deviation of the wrist results in scaphoid and lunate flexion.[34] In contact, ulnar deviation of the wrist results in extension of both the lunate and scaphoid.

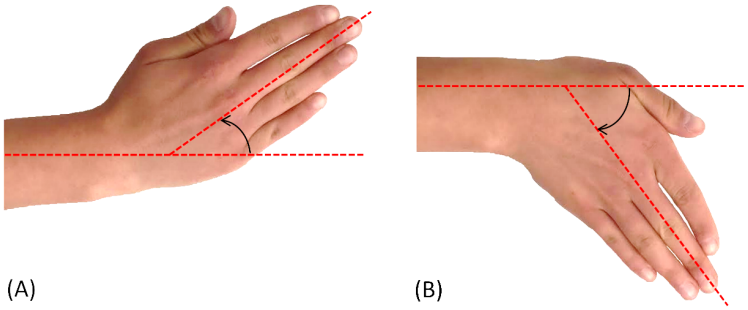

Figure 1-12: Range of Wrist Motion: Radial-Ulnar Deviation.

Radial-Ulnar Deviation. Motion of the wrist joint in radial (A) and ulnar (B) deviation.

1.2.2.5 Dart Throw Motion

Due to the complexity of the carpus, multidirectional movements can be achieved and has been considered to have given humans an evolutionary advantage by allowing enhancement of power swings (*i.e.* hammering), as well as improvements in hand precision for the use of weapons, tools and instruments.[35,36] The term dart-thrower motion (DTM), was first introduced by Palmer et al,[37] who described the functional movement. DTM describes an oblique plane that incorporates flexion-extension along with radial ulnar deviation (15° of radial deviation with 30°of wrist extension proceeding to 15° of ulnar deviation with 30°of wrist flexion) (Figure 1-13).

DTM has emerged as an important concept linking *in-vivo* and *in-vitro* kinematic analyses with clinical wrist function.[38] It has been deemed a suitable motion for rehabilitation protocols following reconstructions of the scapholunate interosseous ligament because the scaphoid and lunate are thought to be effectively protected. Crisco et al, reported that scaphoid and lunate motion approached zero at wrist positions along the dart thrower's path, which indicated that these bones are essentially fixed in their neutral position along this path of wrist motion.[39] In agreement with Crisco, Ishikawa et al.[40] and Dimitris et al.[41] performed cadaveric studies and found that during dart-thrower motion, scaphoid and lunate motion was minimized. Furthermore, the distal carpal row is thought to function as a 1-bone system pivoting around the scaphoid from radial extension to ulnar flexion. These investigators postulated that due to

the limited scaphoid and lunate motion, that the radiocarpal joint protected from wear during the dart-thrower motion.[25]

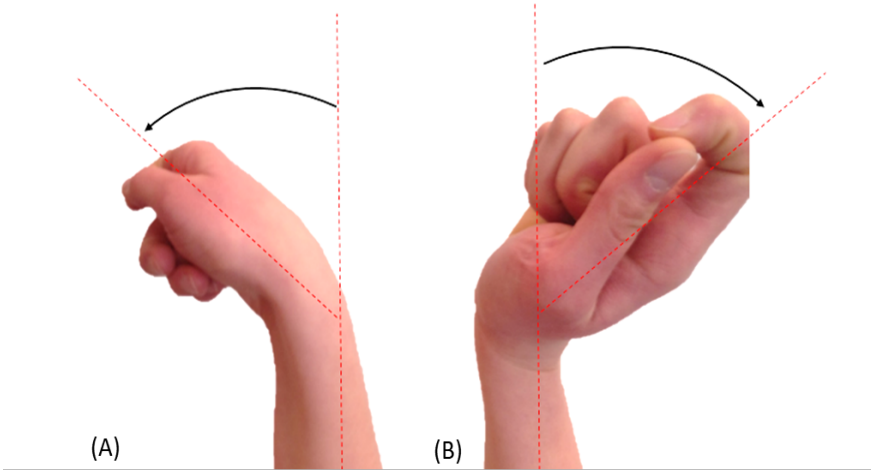

Figure 1-13: Range of Wrist Motion: Dart-Thrower Motion.
Motion of the wrist joint in forward dart-thrower (A) and reverse dart-thrower (A) motion.

1.3 Assessment of Wrist Kinematics & Biomechanics

To examine wrist joint mechanics, surgical repair techniques, and arthroplasty designs *in-vitro* cadaveric models are often used. A variety of different testing devices and simulators have been developed to investigate the kinematics of the wrist joint and can be classified as passive or active motion simulators. Both testing methods have associated strengths and limitations that affect the validity of the results.

1.3.1 *In-vitro* Joint Motion Simulators

Static and passive wrist motion simulators were the first devices used to examine carpal kinematics. The majority of these simulators used hanging weights to apply forces to the flexor and extensor tendons of the forearm *via* cables to produce compressive loading within the wrist.[26,42] Other simulators used pneumatic actuators to apply constant loads to the muscles of the forearm, while passively moving the wrist through a range of motion (Figure 1-14).[43,44] These passive simulators were able to facilitate a multitude of biomechanical and clinically

relevant studies; however, they were unable to mimic physiologic conditions observed *in-vivo,* calling the relevance of their results into question. Passive motion simulators often produce less repeatable motion pathways, and thus, there are higher rates of error in reported outcomes.[45]

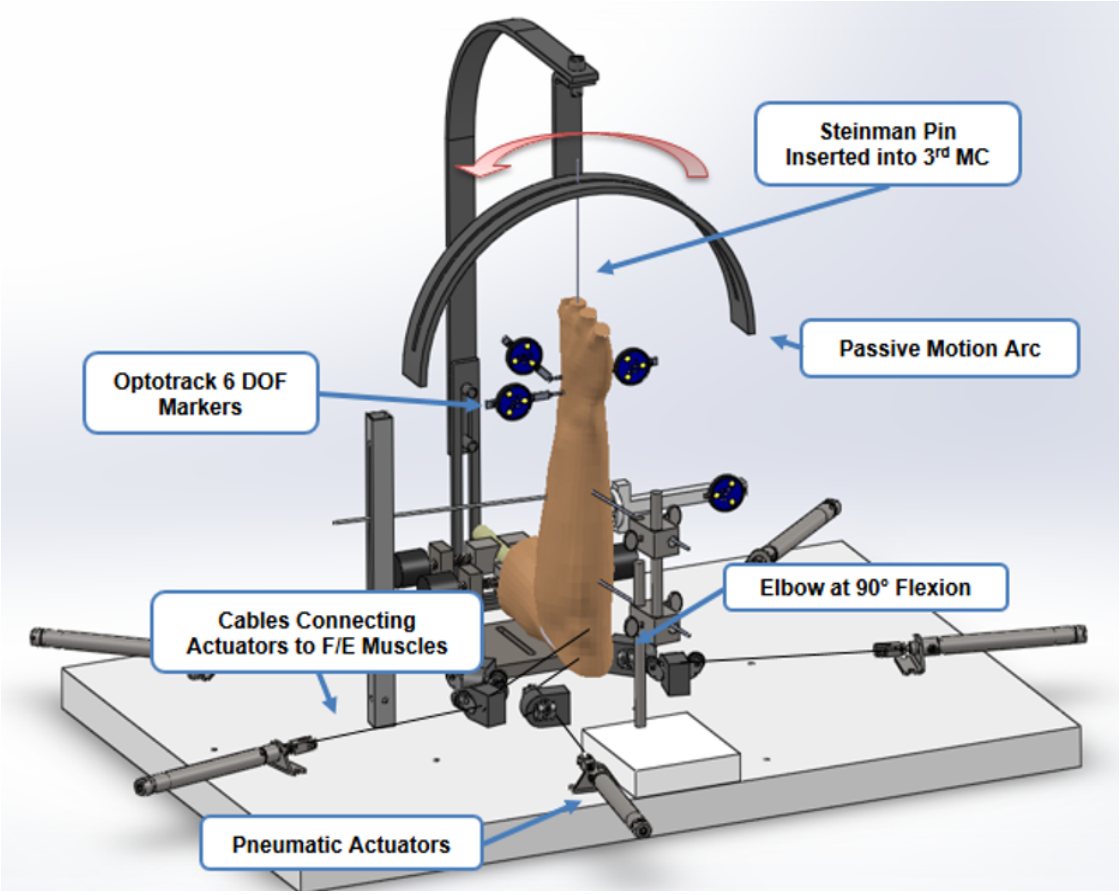

Figure 1-14: Nishiwaki's Motion Wrist Simulator.

Wrist motion simulator developed by Nishiwaki et al. to test the effect distal radius malunion deformities.

Active motion wrist simulators are thought to better simulate physiologic conditions, as they apply force directly to the muscle tendons of interest to manipulate joint position. Algorithms designed to exploit the antagonistic relationships of opposing forearm muscles groups (*i.e.* flexors and extensors muscles) allow for more accurate modelling of *in-vivo* scenarios. Motion of the wrist is generally controlled through force-position algorithms, such as a proportional-integral-derivative (PID) controller, that works to move the wrist in a controlled manner from one position to the next while balancing the antagonistic muscle pairs. The primary mover

muscle in the direction of the motion is position controlled to maintain a continuous angular velocity while the opposing muscles hold the constant muscle tone load set for the simulator. To reverse the direction of motion, the position-force algorithm switches so that the muscles previously under position control maintains a tone load while the antagonist acts to change position of the joint. Servomotors equipped with force transducers have generally been used to actuate the muscles of interest while providing force feedback. Due to incomplete understanding of native EMG and tendon force data, the inputs upon which the control systems operate are often based on estimates.

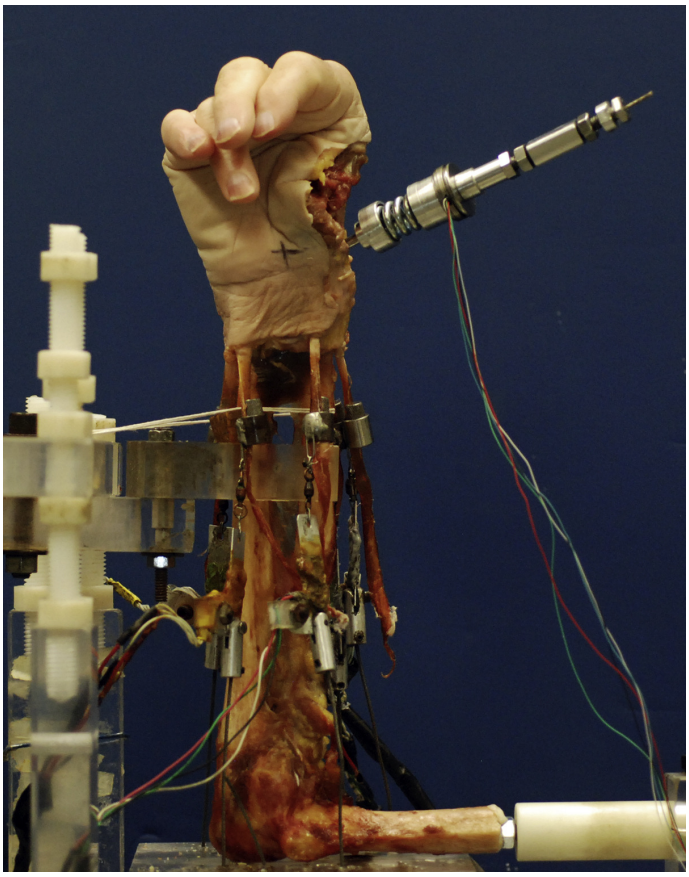

Figure 1-15: Active Motion Wrist Joint Simulator from Werner et al.[46]

Demonstrated is an active motion wrist simulator with electromagnetic feedback facilitating closed-loop control and reproducible motion of the wrist (Reprinted with permission from The Journal of Hand Surgery).

To our knowledge, Werner et al. was the first to a create a wrist motion simulator capable of active wrist motion (Figure 1-15).[45–48] Erhart et al. also described an active motion simulator which tracks wrist motions using active optical markers, and uses linear pneumatic actuators to induce motion following an antagonistic pair algorithm with the arm fixated vertically at 90 degrees flexion and a static forearm rotation.[48] For this simulator, the lines of action of the muscles are more accurately represented as they pass through their respective origins before diverting to the actuators.

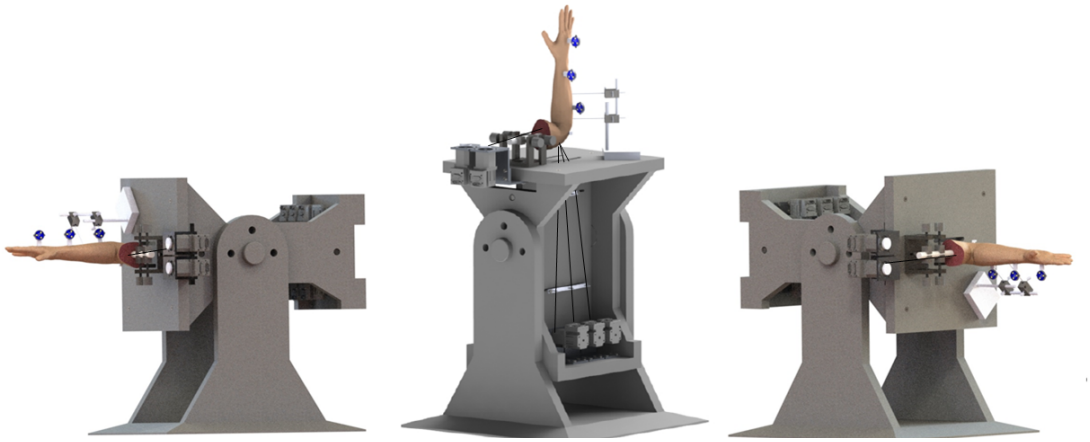

Figure 1-16: Iglesias et al Active Motion Wrist Simulator.

Active motion wrist simulator highlighting three different gravity loaded positions.

More recently, Iglesias et al.[45] developed an active motion joint simulator capable of replicating physiologic joint motion in three forearm orientations (Figure 1-16). The simulator achieves joint motion by using a motor manifold of seven servomotors which are controlled with a closed-loop feedback PID controller. These motors which are attached to the flexor and extensor tendons of the forearm (ECU, ECRL, ECRB, FCU, FCR, PT, and biceps brachii) facilitate the actuation of both the wrist and forearm. Each servomotor is instrumented with strain gauges to provide force feedback to the PID controller of the wrist simulator. Like Erhart et al., this joint motion simulator employs optical tracking to provide real-time information to its PID controller. The simulator has the capacity to replicate active flexion-extension, radial-ulnar deviation, dart-thrower motion as well as forearm rotation.

Shah et al. also recently developed an active motion wrist joint simulator. Similar to the wrist joint motion simulator developed by Iglesias et al., the simulator is capable of replicating physiologic wrist joint motion in several forearm orientations by using a combination of force and position feedback.[47] As the role of gravity in wrist biomechanics is poorly understood, the simulators developed by Iglesias et al and Shah at al are the first two wrist joint motion simulator that afford investigators' the opportunity to investigate the effect of forearm orientation on biomechanical outcome measure. Most prior biomechanical studies have been performed in a single gravity forearm position. In a study performed by Shah et al. where they examined three gravity positions, they reported higher tendon loads in the horizontal position, compared the other to two tested gravity positions (Figure 1-17).[49] The results of the study by Shah et al. and the forthcoming results from this body of work have clinical implications to the development of rehabilitation protocols for wrist pathologies and surgical interventions.

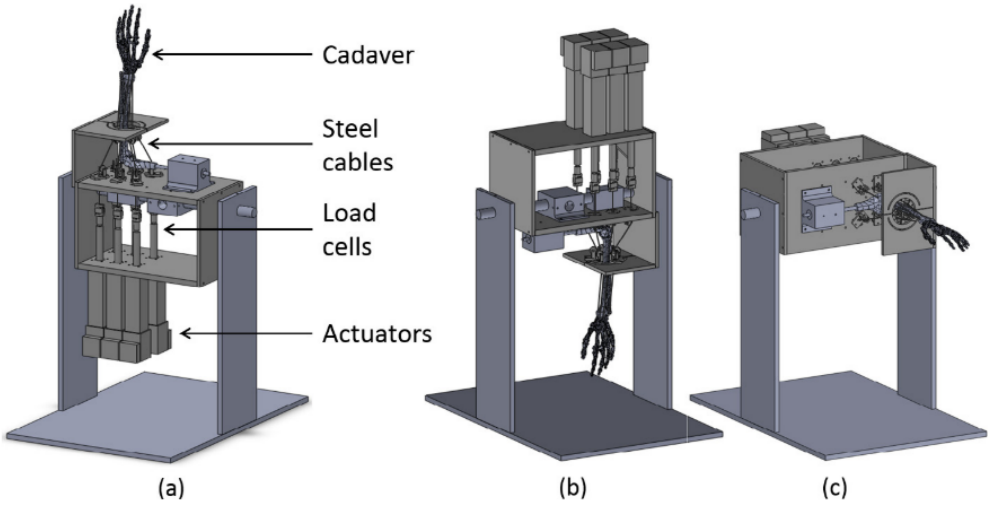

Figure 1-17: Shah et al. Active Motion Wrist Simulator.[47]

Active Motion wrist simulator highlighting three different gravity loaded positions. Detail (a) vertically upward (b) vertically downward and (c) horizontal (Reprinted with permission from The Journal of Biomechanics).

1.3.2 Motion Measurement

Traditionally, range of wrist motion has been measured with the help of tools such as goniometers. In general, goniometers are low-costs, lightweight and portable, and their measurements of clinical wrist angle are the gold standard.[50] Throughout the years, new 3-dimensional (3D) tracking methods have been developed to enable to dynamic analysis of kinematics.

1.3.2.1 Optical Tracking

Optical tracking is a motion capture technique that determines the real-time position and orientation of objects, using either passive or active markers attached to the objects of interest. Active optical tracking operates in the near-IR range (900 nm wavelength). LEDs are used as markers and are tracked by three collinear CCD units that form the camera module. The LEDs are fired sequentially and detected by each CCD unit. The central unit then uses the process of triangulation based on the known geometric configuration and firing sequence of each LED and the known fixed distance between the CCD elements. A minimum of three non-collinear LEDs are necessary for determining six degrees-of-freedom (DOF) pose information. Optical tracking units have high accuracy and reliability. One of the main limitations of optical tracking is line-of-sight.

1.3.2.2 Electromagnetic Tracking

Electromagnetic tracking uses small electromagnetic field sensors in an electromagnetic field of know geometry. In DC based tracking systems, static magnetic field measurements are used. The magnetic field is turned on and off at a certain frequency, allowing eddy currents to decay sufficiently to mitigate distortions caused by common conductive metals such as stainless steel, titanium and aluminum. A disadvantage of these systems is their lower accuracy relative to optical systems. However, the accuracy has been shown to improve with strict environmental control and line of site issues are not a problem.

1.3.3 Coordinate Systems

In biomechanical studies, anatomical joint coordinate systems (JCS) are used to describe the relative motion between two body segments, with each body segment having its own body coordinate system. To create anatomical coordinate systems on body segments, anatomical

landmarks are used to define the axes of the coordinate systems. Based on the points selected, the orientation of the coordinate system will vary. A clinically relevant coordinate system is imperative to create meaningful data and a standardized methodology for coordinate system creation is essential so that results from different biomechanical investigations can be compared without bias.

The International Society of Biomechanics (ISB) has previously published coordinate system recommendations for the hand and wrist in 2005.[51] However, most research groups have developed their own unique method of coordinate systems creation due to the short comings of the ISB recommendations. This has made it difficult to compare results between studies and build on past research. Several studies have recognized that there are inconsistencies in results in current literature and have attributed these to differences in the orientation of the radial coordinate system. A reliable and repeatable wrist coordinate system needs to be adopted by all investigators to promote objective comparisons between studies, which will consequently advance research.

1.4 Assessment of Contact Mechanics

Kinematics are useful in evaluating the motion pathway of bones, however, when events occurring at the articulation are of interest, such as changes in joint contact area or contact location, assessment methods which examine joint congruency are typically used. Historically, direct methods such as casting or pressure sensitive films have been used to quantify joint congruency; however, numerous indirect methods of quantifying joint congruency now exist as well. Both direct and indirect methods have their advantages as well as their drawbacks.

1.4.1 Direct Methods of Assessing Joint Contact

1.4.1.1 Pressure Sensitive Films

Viegas et al. studied the contact area and pressure at the radiocarpal joint using pressure-sensitive film (Fuji).[52] The results of this study found that the contact areas accounted for only 20.6% of the available joint surface and that there was a shift in contact area dorsally as the wrist extended.

Dynamic pressure sensitive films have also been employed, with the most common type being Tekscan® (Tekscan Inc, South Boston, MA). Tekscan® uses a piezoresistive material, and

records changes in the output voltage from the film. The voltage can then be converted into a contact pressure via calibration of the dynamic film; thus outputting not only contact area but contact pressure as well.[53] The advantages of this method include the need to only place it once within the joint to acquire recordings in numerous loaded positions. Drawbacks are similar to conventional film and are related to the inherent thickness of the film (0.1mm) altering the joint, as well as the semi-destructive nature of placing the film within the joint.

1.4.1.2 Casting

Casting is a technique where a polymer (Reprosil®) is inserted into the joint space and left to set following the reduction of the joint and application of physiologic joint force. The resulting cast often will have a section which is devoid of material; this section represents the articular joint contact at the joint of interest. This direct method of measuring joint contact area has some drawbacks. In order to inject the polymer into the joint space, the soft tissue surrounding the joint must be significantly disturbed. Additionally, casts can only capture a single static posture, and successive castings to capture an entire incremented range of motion is lengthy. Furthermore, due to the small size of the joints of the wrist, casting is very challenging.

1.4.2 Indirect Methods of Assessing Joint Contact

Due to the aforementioned limitations of direct methods of quantifying joint contact, indirect methods employing modern day imagining techniques have been developed in recent years. These approaches are often driven by computed tomography (CT) or magnetic resonance imaging (MRI) and can quantify the interaction that occurs in the joint without violating the joint itself.

1.4.2.1 Imaged Based Methods

Lalone et al. developed a CT based joint congruency technique to assess joint mechanics at the elbow. The technique was based on bone and cartilage registration from CT space to test day experimental space. Registration is defined as the determination of the relationship between a point in one space and the homologous point in another space. If the registration can be reduced to a single rotation and translation, then the registration is considered rigid. Registration methods are also categorized according to input source, *i.e*. three-dimensional (3D) images (e.g. CT), two-dimensional (2D) projection images (e.g., X-ray fluoroscopy), and 3D points

obtained via digitization. Due to landmarks within the body being difficult to identify, the use of fiducial markers was adopted by Lalone et al. and other researchers to enable easier registration between the two spaces of interest. The use of fiducial markers acting as identification of intrinsic points coupled with least square error transformation technique allows for rapid registration of spaces. Although Lalone et al. was able to refine this CT-based technique for assessing contact mechanics at the elbow, further refinement and further development of the technique is necessary to gain the accuracy required to apply this technique to smaller articulations, such as those in the carpus.[54]

Others have also exploited the 3D visualization abilities of computed tomography. However, more common than registration of CT images to kinematic data, is the successive acquisition of CT images across a motion arc. These investigations frequently examine kinematics in addition to arthrokinematics, which pertains to the movement of bone surfaces in a joint. Rainbow et al. has performed a variety of studies of the carpus, employing the successive CT images technique.[27,55,56] Crisco et al. performed their first CT based study in 1997.[57] Since that first CT based study, Crisco et al. has developed a database of wrist carpal bone anatomy and kinematics, from which predictive models are being constructed.[58]

Gated CT, also known as four-dimensional (4D) CT has gained traction in the musculoskeletal (MSK) research field in recent years with advances in imaging technology.[59,60] During a 4D-CT, multiple traditional CT scans are acquired over a period of time, thus permitting the review of dynamic physiology motion. In the MSK setting, 4D-CT is used to examine a range of joint motion, such as flexion-extension, in an effort to better understand the joint congruency across physiologic motion. 4D-CT, as all data acquisition methodologies, does have limitations. Often speed of patient motion is required to be slow as to not induce motion artifact into the captured images. Additionally, post imaging segmentation is often required to at least be in part manual, as many patients of interest are arthritic and have reduced joint space. Radiation dose is also of concern with imaging studies, and only allow for limited assessment.

Attempts have been made to assess carpal kinematics using 4D CT. Choi et al. assessed radial, ulnar, pronation, and supination motions in two healthy patients over a scan time of four or ten seconds.[61] Choi et al found sufficient image quality in all scans apart from the imaging of pronation supination for the four second scan time. These finding are consistent with the

findings of Dobbe at al., who found that imaging of objects rotating along the same axis as the CT scanner resulted in image artifact.[62]

1.5 Disorders of the Hand and Wrist

The wrist joint is often vulnerable to injury due to its numerous bones, and soft tissue structure. In the native state, the intricate balance of joint geometry and tendon forces across the wrist prevents the ligaments and capsular structures from carrying excessive loads.[5] Any disruption to this balance, because of an injury or disease, may result in abnormal force transmission and altered kinematics across the wrist joint. As a result, the joint often becomes unstable due to the progressive stretching of the surrounding capsule and stabilizing ligaments. Wrist pain is one of the most common complaints heard by clinicians. Often the principal cause of pain is obvious, but a complete examination is necessary in order to diagnose the critical underlying pathologies. Wrist pain may occur as a result of injury or trauma, either repetitive stress or sudden impact, or as a result of a degenerative disease. A comprehensive understanding of the intricate anatomy and kinematics of the hand is necessary to effectively diagnose and treat injuries of the wrist.

1.5.1 Carpal Instability

Carpal instability is another major cause of wrist pain. Carpal instability is defined as the wrist joint's inability to transfer loads without subsequent changes in stress on the surrounding ligaments and articular cartilage and the inability to maintain a functional range of motion without changes in intercarpal alignment. Instability generally occurs due to ligament disruption, articular cartilage damage, or as a sequela of a carpal fracture. The most common cause of carpal instability is injury to the scapholunate ligament within the proximal row (Figure 1-18).

Figure 1-18: Carpal Instability, in the form of scapholunate interval widening.

Radiographic evidence of scapholunate instability. Ulnar deviation of the wrist showing characteristic diastasis of the scapholunate interval.

The proximal carpal row is considered an intercalated segment with no direct control mechanisms attached to it, causing its motion to be entirely dependent on the mechanical signals of the surrounding articulations. Isolated injury to the SL ligament, although insufficient to cause abnormal carpal alignment, is often a precursor to abnormal joint kinematics, cartilage wear, and further degenerative changes.[10] SL instabilities are typically initiated through a fall on an outstretched hand, resulting in attenuation, a partial tear or a complete tear of the SL ligament. A partial SL tear may progress to a complete tear eventually causing SL dissociation, a dorsal intercalated segmental instability (DISI), or a pattern of wrist arthritis termed scapholunate advanced collapse (SLAC).[63–66] Currently there is no gold

standard in the management of carpal instabilities but rather the treatment strategy is tailored to the stage and degree of injury present. Some typical treatment options include: splinting, casting, arthroscopic debridement, reduction, pinning, direct repair with or without dorsal capsulodesis, and arthrodesis.[16]

Figure 1-19: Dorsal Intercalated Segmental Instability (DISI) deformity of the wrist illustrated on clinical x-ray.

(A) Scapholunate injury of the wrist without DISI deformity. (B) Scapholunate injury of the wrist with DISI deformity, showing the characteristic extension of the lunate relative to the scaphoid.

1.5.2 Arthritis

Arthritis may occur with age or secondary to a previous injury and can cause the healthy articular cartilage to erode triggering painful bone on bone contact. The most common types of arthritis to affect the hand and wrist are osteoarthritis, rheumatoid arthritis, and post-traumatic arthritis. Osteoarthritis is a degenerative disease, most commonly affecting older people, which causes cartilage deterioration, pain, and joint stiffness. Rheumatoid arthritis is an autoimmune disease-causing chronic inflammation, pain, stiffness, and swelling of multiple joints. This disease commonly affects the wrist causing damage to the articular cartilage, bone, and surrounding tendons and ligaments. Post-traumatic arthritis occurs following injury to the wrist, such as a fracture or torn ligament. It can either affect the articular cartilage directly or cause a delayed onset of cartilage loss. There is currently no cure for arthritis, but depending on the severity of the disease, there are numerous non-surgical and surgical treatment strategies including: steroid injections, anti-inflammatory medications, proximal row carpectomy, partial or total carpal fusion, and total wrist arthroplasty.

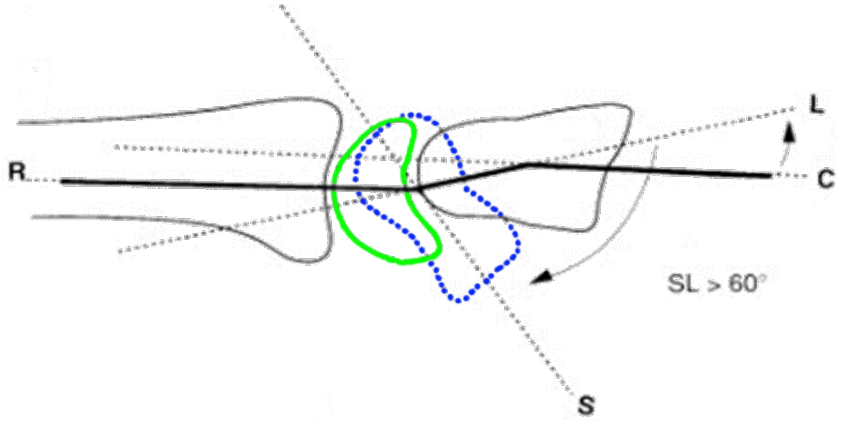

Figure 1-20: Rotation of the scaphoid and lunate in Dorsal intercalated segment instability (DISI).

A DISI deformity is a common carpal instability, where the scaphoid (blue) falls into a flexed position while the lunate(green) extends. DISI deformity is often observed in scapholunate ligament insufficiency or other ligamentous injuries.

Figure 1-21: Scapholunate advanced collapsed (SLAC).

SLAC wrist is a progressive pattern of wrist arthritis resulting from dissociation of the scaphoid and lunate. SLAC wrist can be described by the Watson classification which identifies three stages of SLAC progression. Stage I – arthritis between scaphoid and radial styloid. Stage II – arthritis between scaphoid and entire scaphoid facet of the radius. Stage III – Arthritis between capitate and lunate.

The most common pattern of wrist arthritis is the SLAC wrist.[64,65] This progressive sequence of degenerative change is caused by articular alignment problems between the scaphoid and the radius.[64,67] Beginning at the radioscaphoid joint, the arthritis progresses between the capitate and the lunate, where the capitate begins to migrate proximally and there is dissociation between the scaphoid and lunate; these changes are secondary to carpal collapse. Approximately 55% of all naturally occurring degenerative arthritis is found to occur in the SLAC wrist pattern.[64]

1.6 Thesis Rationale

When compared to other orthopedic fields, the current state of wrist biomechanical research is in its infancy. Past work has begun to quantify the intricacies of the native wrist as well as injury states; however, due to the complexity of the wrist, there remains to be a unified understanding of the basic biomechanics of the carpus. The unification of research begins with the assessment of current research strategies to investigate carpal biomechanics and contact mechanics. A comprehensive review of current methodologies to generate wrist coordinate systems would be beneficial to standardize wrist biomechanics literature so comparisons among studies can be made.

Joint congruency and contact area are both difficult parametric values to obtain in a non-invasive manner. The carpus provides significant challenges in both its motion pathways (kinematics), its osseous and articular morphology, as well its small scale. Clinical entities of the wrist often become chronic and progress to degenerative disease, such as arthritis. As such, the implementation of an accurate non-invasive joint congruency methodology would greatly improve the understanding of wrist congruency and contact mechanics.

The goal of this work is to advance current wrist biomechanics and contact mechanics research strategies. These findings will help unite investigators in their experimental methodologies and will provide valuable knowledge of the intact and pathological wrist.

1.7 Objectives

1. To determine the radiocarpal and midcarpal contributions to global wrist motion:
2. To assess current methodologies for generating wrist coordinate systems and compare how coordinate system selection effects the calculation of global wrist joint angle;
3. To develop and validate a CT-based joint congruency method to determine a reliable threshold value which accurately represents articular contact;
4. To assess the effect of forearm orientation on carpal kinematics and radiocarpal contact mechanics during physiologic active wrist motion;
5. To apply the biomechanical approaches established herein, the effect of forearm orientation was evaluated on an injury model- particularly scapholunate insufficiency and

determine which forearm orientation provides the greatest stability to the scapholunate joint.

1.8 Hypotheses

The following hypotheses were formulated:

1. *The radiocarpal and midcarpal will contribute equally to global wrist motion;*
2. *A single coordinate system generation method will emerge as most consistent in describing wrist angle and will provide the smallest deviation from clinically measured wrist angle;*
3. *A CT-based joint congruency technique will assess wrist joint congruency with the same or less degree of error as the gold standard, Tekscan®;*
4. *The gravity flexion and gravity extension forearm orientations will emerge as vulnerable wrist positions, causing increased joint contact in the native wrist;*
5. *The gravity flexion position will cause greater alterations in scapholunate kinematics and contact after scapholunate ligament injury as compared to the neutral and gravity extension positions.*

1.9 Thesis Overview

Chapter 2 describes the investigation of the relative contributions of the radiocarpal and midcarpal joints to flexion-extension wrist motion and describes the limitations of current biomechanical testing design.

Chapter 3 compares four previous described wrist joint coordinate systems and examines the effect of wrist coordinate system selection on resulting wrist angle by describing the accuracy and repeatability of each selected joint coordinate system.

Chapter 4 describes the application and validation of CT-based joint congruency method for assessing joint congruency at the wrist. Tekscan® will be used to validate the CT-based joint congruency technique and an appropriate threshold level to accurately and reliably predict joint contact area will be determined.

Chapter 5 examines the sensitivity of radiocarpal contact mechanics and carpal kinematics to forearm orientation during wrist flexion-extension and dart-thrower motion.

Chapter 6 will apply the previous kinematic and biomechanical knowledge gained from previous chapters to a common clinical entity of scapholunate insufficiency. The effect of forearm orientation on scapholunate injuries will be discussed and with specific interest in the development of rehabilitation protocols.

Chapter 7 provides a general cumulative discussion of this dissertation's work and furnishes interplay and association of the conclusions in the different chapters included in this work, in addition to describing future directions.

1.10 References

1. Lewis OJ, Hamshere RJ, Bucknill TM. The anatomy of the wrist joint. *J Anat*. 1970;106(Pt 3):539-552. http://www.ncbi.nlm.nih.gov/pubmed/4987391%0Ahttp://www.pubmedcentral.nih.gov/articlerender.fcgi?artid=PMC1233428.

2. Bryce TH. Certain Points in the Anatomy and Mechanism of the Wrist-Joint Reviewed in the Light of a Series of Röntgen Ray Photographs of the Living Hand. *J Anat Physiol*. 1896;31(Pt 1):59-79.

3. Frank HN. Netter Atlas of Human Anatomy 7th Ed 2018. 2018.

4. Linscheid RL, Dobyns JH. Dynamic carpal stability. *Keio J Med*. 2002. doi:10.2302/kjm.51.140

5. Sabbag K, Meals R, Cooney WP. *The Wrist: Diagnosis and Operative Treatment*. Vol 26. 2nd ed. (Kluwer W, ed.). Philadelphia, Balitmore, New York, Lodon, Buenos Aires, Hong Kong, Sydney, Tokyo; 2001. doi:10.1053/s0363-5023(00)90002-9

6. Patterson RM, Elder KW, Viegas SF, Buford WL. Carpal bone anatomy measured by computer analysis of three-dimensional reconstructions of computed tomography images. *J Hand Surg Am*. 1995;20(6):923-929. doi:10.1016/S0363-5023(05)80138-8

7. Standring S. Gray's Anatomy E-Book: The Anatomical Basis of Clinical Practice. *Elsevier Heal Sci*. 2010:1562. doi:10.1088/1751-8113/44/8/085201

8. Belsole RJ, Hilbelink DR, Llewellyn JA, Stenzler S, Greene TL, Dale M. Mathematical analysis of computed carpal models. *J Orthop Res*. 1988;6(1):116-122. doi:10.1002/jor.1100060115

9. Nakamura K, Beppu M, Patterson RM, Hanson C a, Hume PJ, Viegas SF. Motion analysis in two dimensions of radial-ulnar deviation of type I versus type II lunates. *J Hand Surg Am*. 2000;25(5):877-888. doi:10.1053/jhsu.2000.9411

10. Kaufmann RA, Pfaeffle HJ, Blankenhorn BD, Stabile K, Robertson D, Goitz R.

Kinematics of the Midcarpal and Radiocarpal Joint in Flexion and Extension: An In Vitro Study. *J Hand Surg Am*. 2006;31(7):1142-1148. doi:10.1016/j.jhsa.2006.05.002

11. Got C, Vopat BG, Mansuripur PK, Kane PM, Weiss APC, Crisco JJ. The effects of partial carpal fusions on wrist range of motion. *J Hand Surg Eur Vol*. 2014;41(5):479-483. doi:10.1177/1753193415607827

12. Garcia-Elias M, Cooney WP, An KN, Linscheid RL, Chao EYS. Wrist kinematics after limited intercarpal arthrodesis. *J Hand Surg Am*. 1989. doi:10.1016/S0363-5023(89)80077-2

13. Patterson RM, Nicodemus CL, Viegas SF, Elder KW, Rosenblatt J. High-speed, three-dimensional kinematic analysis of the normal wrist. *J Hand Surg Am*. 1998;23(3):446-453. doi:10.1016/S0363-5023(05)80462-9

14. Berger R a. The Anatomy of the Ligaments of the Wrist and Distal Radioulnar Joints. *Clin Orthop Relat Res*. 2001;383(383):32-40. doi:10.1097/00003086-200102000-00006

15. Berger RA. The ligaments of the wrist: A current overview of anatomy with considerations of their potential functions. *Hand Clin*. 1997;13(1):63-82.

16. Goldner RD, Urbaniak JR. *Green's Operative Hand Surgery*.; 2011. doi:10.1016/B978-1-4160-5279-1.00048-4

17. Short WH, Werner FW, Green JK, Masaoka S, Walter H. Short, MD, Frederick W. Werner, MME, Jason K. Green, BS, and Shunji Masaoka, MD P. Biomechanical Evaluation of Ligamentous Stabilizers of the Scaphoid and Lunate. *J hand surg am*. 2002;27(6):991-1002. doi:10.1053/jhsu.2002.35878.Biomechanical

18. Berger RA. The Gross and Histologic Anatomy of the Scapholunate Interosseous Ligament. *J Hand Surg Am*. 1996;21(2):170-178. doi:10.1016/S0363-5023(96)80096-7

19. Werner FW, Dimitris C, Joyce DA, Harley BJ. Force in the Scapholunate Interosseous Ligament during Physiological Wrist Loading. *J Hand Surg Am*. 2015;40(8):1-9. doi:10.1016/j.jhsa.2015.04.007

20. Gordon KD, Pardo RD, Johnson JA, King GJW, Miller TA. Electromyographic activity and strength during maximum isometric pronation and supination efforts in healthy adults. *J Orthop Res*. 2004;22(1):208-213. doi:10.1016/S0736-0266(03)00115-3

21. Gould HP, Berger RA, Wolfe SW. The origin and meaning of intercalated segment. *J Hand Surg Am*. 2015;40(12):2471-2472. doi:10.1016/j.jhsa.2015.09.013

22. Savelberg HHCM, Otten JDM, Kooloos JGM, Huiskes R, Kauer JMG. Carpal bone kinematics and ligament lengthening studied for the full range of joint movement. *J Biomech*. 1993;26(12):1389-1402. doi:10.1016/0021-9290(93)90090-2

23. L. K. Ruby, MD, W. P. Cooney III, MD, K. N. An, PhD, R. L. Linscheid, E. Y. S. Chao, PhD, Boston. Relative Motion of Selected Carpal Bones: A kinematic Analysis of the normal wrist. *J Hand Surg Am*. 1988;15(5):806-833. doi:http://dx.doi.org/10.1016/0363-5023(90)90163-L

24. Landsmeer JM. Studies in the anatomy of articulation. I. The equilibrium of the "intercalated" bone. *Acta Morphol Neerl Scand*. 1961;3:287-303.

25. Rainbow MJ, Wolff AL, Crisco JJ, Wolfe SW. Functional kinematics of the wrist. *J Hand Surg Eur Vol*. 2016;41(1):7-21. doi:10.1177/1753193415616939

26. Kaufmann R, Pfaeffle J, Blankenhorn B, Stabile K, Robertson D, Goitz R. Kinematics of the midcarpal and radiocarpal joints in radioulnar deviation: An in vitro study. *J Hand Surg Am*. 2005;30(5):937-942. doi:10.1016/j.jhsa.2005.05.016

27. Kamal RN, Chehata A, Rainbow MJ, Llusá M, Garcia-Elias M. The effect of the dorsal intercarpal ligament on lunate extension after distal scaphoid excision. *J Hand Surg Am*. 2012;37(11):2240-2245. doi:10.1016/j.jhsa.2012.07.029

28. Lichtman DM, Schneider JR, Swafford AR, Mack GR. Ulnar midcarpal instability—Clinical and laboratory analysis. *J Hand Surg Am*. 1981;6(5):515-523. doi:10.1016/S0363-5023(81)80115-3

29. Bain GI, Clitherow HDS, Millar S, et al. The effect of lunate morphology on the 3-

dimensional kinematics of the carpus. *J Hand Surg Am*. 2015;40(1):81-89.e1. doi:10.1016/j.jhsa.2014.09.019

30. Gupta A, Batra S, Jain P, Sharma SK. Carpal alignment in distal radial fractures. *BMC Musculoskelet Disord*. 2002;3:1-6. doi:10.1186/1471-2474-3-14

31. Stoesser H, Padmore C, Nishiwaki M, Gammon B, Langohr G, Johnson J. Biomechanical Evaluation of Carpal Kinematics during Simulated Wrist Motion. *J Wrist Surg*. 2016;06(02):113-119. doi:10.1055/s-0036-1588025

32. Morrey BF. *The Elbow and Its Disorders.* Philadelphia: W.B. Saunders Company; 2000.

33. Volz RG. Biomechanics of the Wrist. *J Hand Ther*. 1995;8(2):97-105. doi:10.1016/S0894-1130(12)80306-1

34. Short WH, Werner FW, Green JK, Masaoka S. Biomechanical Evaluation of the Ligamentous Stabilizers of the Scaphoid and Lunate: Part II. *J Hand Surg Am*. 2005;30(1):24-34. doi:10.1016/j.jhsa.2004.09.015

35. Crisco JJ, Heard WMR, Rich RR, Paller DJ, Wolfe SW. The mechanical axes of the wrist are oriented obliquely to the anatomical axes. *J Bone Jt Surg - Ser A*. 2011;93(2):169-177. doi:10.2106/JBJS.I.01222

36. Crisco JJ, Coburn JC, Moore DC, Akelman E, Weiss A-PPC, Wolfe SW. In vivo radiocarpal kinematics and the dart thrower's motion. *J Bone Jt Surg - Ser A*. 2005;87(12 I):2729-2740. doi:10.2106/JBJS.D.03058

37. Palmer AK, Werner FW, Murphy D, Glisson R. Functional wrist motion: A biomechanical study. *J Hand Surg Am*. 1985;10(1):39-46. doi:10.1016/S0363-5023(85)80246-X

38. Bergner JL, Farrar JQ, Coronado RA. Dart thrower's motion and the injured scapholunate interosseous ligament: A scoping review of studies examining motion, orthoses, and rehabilitation. *J Hand Ther*. 2019. doi:10.1016/j.jht.2018.09.005

39. Crisco JJ, Coburn JC, Moore DC, Akelman E, Weiss A-PC, Wolfe SW. In vivo radiocarpal kinematics and the dart thrower's motion. *J Bone Joint Surg Am*. 2005;87(12):2729-2740. doi:10.2106/JBJS.D.03058

40. Ishikawa JI, Cooney WP, Niebur G, An KN, Minami A, Kaneda K. The effects of wrist distraction on carpal kinematics. *J Hand Surg Am*. 1999;24(1):113-120. doi:10.1053/jhsu.1999.jhsu24a0113

41. Dimitris C, Werner FW, Joyce DA, Harley BJ. Force in the Scapholunate Interosseous Ligament During Active Wrist Motion. *J Hand Surg Am*. 2015;40(8):1525-1533. doi:10.1016/j.jhsa.2015.04.007

42. Patterson RM, Williams L, Andersen CR, Koh S, Viegas SF. Carpal Kinematics During Simulated Active and Passive Motion of the Wrist. *J Hand Surg Am*. 2007;32(7):1013-1019. doi:10.1016/j.jhsa.2007.05.004

43. Stromps JP, Eschweiler J, Knobe M, Rennekampff HO, Radermacher K, Pallua N. Impact of scapholunate dissociation on human wrist kinematics. *J Hand Surg (European Vol*. 2015:175319341560066. doi:10.1177/1753193415600669

44. Nishiwaki M, Welsh M, Gammon B, Ferreira LM, Johnson JA, King GJW. Distal radioulnar joint kinematics in simulated dorsally angulated distal radius fractures. *J Hand Surg Am*. 2014;39(4):656-663. doi:10.1016/j.jhsa.2014.01.013

45. Iglesias D. Development of an In-Vitro Passive and Active Motion Simulator for the Investigation of Wrist Function and Kinematics. 2015. http://ir.lib.uwo.ca/cgi/viewcontent.cgi?article=3380&context=etd.

46. Werner FW, Palmer AK, Somerset JH, et al. Wrist joint motion simulator. *J Orthop Res*. 1996;14(4):639-646. doi:10.1002/jor.1100140420

47. Shah DS, Kedgley AE. Control of a wrist joint motion simulator: A phantom study. *J Biomech*. 2016;49(13):3061-3068. doi:10.1016/j.jbiomech.2016.07.001

48. Erhart S, Schmoelz W, Lutz M. Clinical and biomechanical investigation of an increased articular cavity depth after distal radius fractures: Effect on range of motion,

osteoarthrosis and loading patterns. *Arch Orthop Trauma Surg*. 2013;133(9):1249-1255. doi:10.1007/s00402-013-1787-5

49. Shah DS, Middleton C, Gurdezi S, Horwitz MD, Kedgley AE. The effects of wrist motion and hand orientation on muscle forces: A physiologic wrist simulator study. *J Biomech*. 2017;60:232-237. doi:10.1016/j.jbiomech.2017.06.017

50. Gajdosik RL, Bohannon RW. Clinical measurement of range of motion. Review of goniometry emphasizing reliability and validity. *Phys Ther*. 1987;67(12):1867-1872. doi:10.1093/ptj/67.12.1867

51. Wu G, Van Der Helm FCT, Veeger HEJ, et al. ISB Recommendation on Definitions of Joint Coordinate Systems of Various Joints for the Reporting of Human Joint Motion - Part II: Shoulder, Elbow, Wrist and Hand. *J Biomech*. 2005;38(5):981-992. doi:10.1016/j.jbiomech.2004.05.042

52. Viegas SF, Tencer AF, Cantrell J, et al. Load transfer characteristics of the wrist. Part II. Perilunate instability. *J Hand Surg Am*. 1987;12(6):978-985. doi:10.1016/S0363-5023(87)80094-1

53. Nishiwaki M, T N, T N, Y T, Ikegami H. Ulnar-shortening effect on distal radioulnar joint pressure: a biomechanical study. *J Hand Surg Am*. 2008;33(2):198-205.

54. Lalone EA, McDonald CP, Ferreira LM, Peters TM, King GW, Johnson JA. Development of an image-based technique to examine joint congruency at the elbow. *Comput Methods Biomech Biomed Engin*. 2012;5842(January):37-41. doi:10.1080/10255842.2011.617006

55. Rainbow MJ, Kamal RN, Leventhal E, et al. In vivo kinematics of the scaphoid, lunate, capitate, and third metacarpal in extreme wrist flexion and extension. *J Hand Surg Am*. 2013;38(2):278-288. doi:10.1016/j.jhsa.2012.10.035

56. Rainbow MJ. An Examination of Carpal Function Using Kinematic Anylysis and Predictive Modeling. 2012.

57. Wolfe SW, Crisco JJ, Katz LD. A non-invasive method for studying in vivo carpal

kinematics. *J Hand Surg (British Eur Vol*. 1997;22(2):147-152. doi:10.1016/S0266-7681(97)80050-2

58. Akhbari B, Moore DC, Laidlaw DH, et al. Predicting Carpal Bone Kinematics Using an Expanded Digital Database of Wrist Carpal Bone Anatomy and Kinematics. *J Orthop Res*. 2019;37(12):2661-2670. doi:10.1002/jor.24435

59. Tay SC, Primak AN, Fletcher JG, et al. Four-dimensional computed tomographic imaging in the wrist: Proof of feasibility in a cadaveric model. *Skeletal Radiol*. 2007;36(12):1163-1169. doi:10.1007/s00256-007-0374-7

60. Kakar S, Breighner R, Leng S, et al. The Role of Dynamic (4D) CT in the Detection of Scapholunate Ligament Injury. *J Wrist Surg*. 2016;05(04):306-310. doi:10.1055/s-0035-1570463

61. Choi YS, Lee YH, Kim S, Cho HW, Song HT, Suh JS. Four-dimensional real-time cine images of wrist joint kinematics using dual source CT with minimal time increment scanning. *Yonsei Med J*. 2013;54(4):1026-1032. doi:10.3349/ymj.2013.54.4.1026

62. Dobbe JGG, De Roo MGA, Visschers JC, Strackee SD, Streekstra GJ. Evaluation of a Quantitative Method for Carpal Motion Analysis Using Clinical 3-D and 4-D CT Protocols. *IEEE Trans Med Imaging*. 2019;38(4):1048-1057. doi:10.1109/TMI.2018.2877503

63. Tischler BT, Diaz LE, Murakami AM, et al. Scapholunate advanced collapse: a pictorial review. *Insights Imaging*. 2014;5(4):407-417. doi:10.1007/s13244-014-0337-1

64. Watson HK, Ryu J. Evolution of arthritis of the wrist. *Clin Orthop Relat Res*. 1986;(202)(202):57-67. doi:10.1097/00003086-198601000-00008

Chapter 2

2 The Relative Contributions of the Radiocarpal and Midcarpal Joints to Wrist Motion: A Biomechanical Study

OVERVIEW

The motion from the midcarpal and radiocarpal joints have been previously investigated although previous studies have yet to report their contributions across the entire range of wrist motion. This chapter presents an in-vitro study that examines the relative motion of the radiocarpal and midcarpal joints during unconstrained planar wrist flexion and extension. This study also examined the effect of motion direction (i.e. flexion or extension) on radiocarpal and midcarpal joint contributions.[1]

---

[1] *A version of this work was presented at the 2016 Annual Meeting of the Orthopaedic Research Society, the 2016 Biennial Canadian Bone and Joint Conference, and at the 2016 Annual Meeting of the Canadian Orthopaedic Research Society. A version of this work study has been published in the Journal of Hand Surgery.*[16]

2.1 Introduction

As documented in Chapter 1 (Section 1.1), the wrist is a highly mobile, composite joint that links the bones of the forearm to the hand. It is characterized by its ability to sustain substantial load in all positions. In order to achieve this, there must be appropriate interactions between wrist tendons, soft tissue constraints, and articulating joint surfaces of the carpal bones. Most often the wrist is described as having a proximal and distal row of carpal bones, even though many theories exist to characterize the structure and function of the wrist. The tendons of the main flexors and extensors for the wrist attach distal to the distal row of carpal bones. As such, when motion is initiated, the distal row of carpal bones have been shown to move first, followed by the proximal row. This mechanism perhaps would suggest that the distal row would have greater contribution to motion than the proximal rows. However, there is still disagreement as to the relative contributions the proximal and distal rows throughout wrist motion.

In 1943 Gilford et al. popularized the longitudinal chain concept, where the distal carpal row, proximal carpal row and radius were the links. Central to that concept was the capitate-lunate-radius chain[1], with the scaphoid described as a stabilizing connecting bar bridging the intercarpal joint. The concept of a linked chain mechanism, initiated interest in the relative motion between those chain segments and their relative contribution to global wrist motion. In line with longitudinal chain concept, recent studies commonly quantified the relative contributions of the radiocarpal (motion of the proximal row to the radius), and midcarpal (motion between the distal and proximal row of carpal bones) joints (described in Section 1.1.4.1).

The majority of studies quantifying the relative contribution of the radiocarpal and midcarpal joints have examined the flexion-extension wrist motion. These studies generally fall within two categories, *in-vitro* cadaveric biomechanical studies (Section 1.3.1), or non-invasive studies (*i.e*. CT imaging, high speed cameras, etc.) (Section 1.4.2.1). Using high-speed video data acquisition in combination with imaging, Patterson *et al.* reported that during wrist motion the radiocarpal joint contributes more during wrist flexion, while the midcarpal joint contributes more during wrist extension.[2] Wolfe et al. used a non-invasive CT and body-mass-based algorithm to show that the rotation of the proximal row of carpal bones varied between

flexion and extension but varied linearly with capitate rotation. Sarrafian and colleagues agreed that proximal row rotation differs between wrist flexion and extension; however, reported that in flexion, the radiocarpal joint contributes 40% of motion while the midcarpal joint contributes 60%. Whereas in wrist extension, the radiocarpal joint contributes 66.5% while the midcarpal joint contributes 33.5%. Others have reported the opposite results,[3] or found that motion contribution was equal between the two joints.[4] The discrepancy in the current literature identifies a need for further research in this area.

A detailed understanding of the kinematics of carpal bones is essential to effectively diagnose and treat subtle injuries of the wrist. As such, this in vitro cadaver biomechanical study aims to build on previous literature and determine the radiocarpal and midcarpal contributions to global wrist motion, during continuous passive flexion-extension wrist motion (Section 1.7). We hypothesized that the radiocarpal and midcarpal joints would contribute equally to wrist motion across the flexion-extension motion arc.

2.2 Methods

2.2.1 Specimen Preparation

Six fresh-frozen cadaveric upper extremities (69±17yrs; 5 Male; 3 Right) were amputated at the mid-humerus and the fingers were disarticulated at the metacarpophalangeal joints. All specimens were screened with CT imaging and fluoroscopy to rule out wrist pathology; no history of trauma or wrist disease was present in any of the specimens. Optical tracking markers (Optotrak Certus; Northern Digital, Waterloo, Canada) were attached to the lunate and capitate under fluoroscopy using a 2.7 mm bone screw and a 1.6 mm Kirschner wire (K-wire) augmented by bone cement. To expose the lunate and capitate, a small transverse arthrotomy was performed. The lunate tracker was attached dorsal to palmar, 40º dorsal from the horizontal plane, while the capitate tracker was attached dorsal to palmar, 30º dorsal from the horizontal plane. Subsequently, the flexor and extensor tendons of the wrist including: extensor carpi radialis brevis (ECRB), extensor carpi radialis longus (ECRL), extensor carpi ulnaris (ECU), flexor carpi radialis (FCR) and flexor carpi ulnaris (FCU), had running Krakow sutures placed at their musculotendinous junctions and connected to actuators via stainless steel cables. A tracker marker was attached to the distal radius metaphysis, ensuring a similar line of sight as the carpal trackers to the optical tracking receiver. The specimen was then rigidly mounted to a previously described passive motion wrist simulator (Figure 2-1) by securing the humerus in a clamp.[5] The passive motion wrist simulator used pneumatic actuators to apply a constant force (10N) to the flexor and extensor tendons of the forearm. The ulna was secured using two parallel threaded pins to place the elbow at 90º flexion. A Steinmann pin was then inserted longitudinally into the third metacarpal and positioned into the passive motion arc (Figure 2-1), and used during testing as a guide for passive flexion-extension motion.

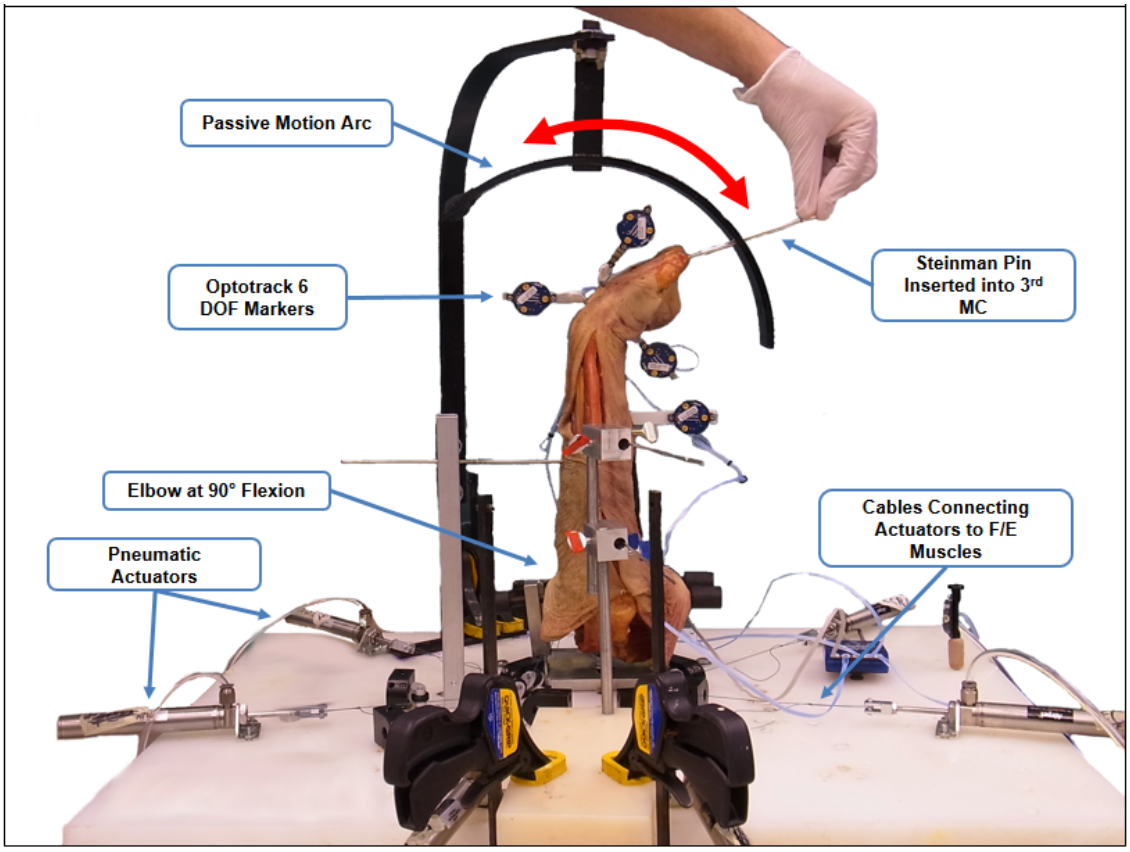

Figure 2-1: Passive motion wrist simulator.

Simulator with static restraint, capable of applying tone loads to wrist flexor and extensor muscles.

2.2.2 Testing Protocol

A constant 10N tone load was applied to each tendon, simulating native compressive force observed in the *in-vivo* wrist.[6] The Steinmann pin that had been previously inserted into the third metacarpal was guided through the passive motion arc at a rate of approximately 5º/sec simulating passive flexion-extension motion arc. Trials were defined as guiding the wrist from full flexion to full extension while a constant 10N tone load was applied to the ECRB, ECRL, ECU, FCR and FCU by pneumatic actuators. A total of five flexion-extension trials were completed in the native state and the final trial was used in the data analysis with the prior four performed to precondition the specimen. Following the testing protocol, the specimens were

denuded and the landmarks on the capitate, lunate, and radius were digitized to construct anatomic coordinate systems.

2.2.3 Outcome Variables and Data Analysis

Coordinate systems were defined for the lunate, capitate, third metacarpal, and distal radius (Figure 2-2). The origins of the lunate and capitate coordinate systems were located at their volumetric centroids, while the origin of the distal radius was located at the average of the radial styloid and dorsal and volar distal margins of the sigmoid notch. The volumetric centroids of the carpal bones were calculated by averaging the X, Y and Z coordinates from an evenly distributed point cloud representing the intact geometry of each bone. The point clouds were derived from intact CT scans, performed prior to the experimental protocol. The coordinate system of the capitate was translated to the adjacently positioned third metacarpal, as it is widely accepted that the capitate and third metacarpal move as rigid body.[2] The coordinate systems of the capitate, lunate and third metacarpal were aligned in parallel with that of the distal radius in neutral wrist position. Wrist position was defined as the angle between the long axis of the distal radius and the long axis of the third metacarpal, with neutral position specified by the International Society of Biomechanics (ISB) such that these two axes were aligned.[7] Radiocarpal joint motion was defined as the rotation of the lunate with respect to the distal radius in the flexion-extension plane. Midcarpal joint motion was defined as the rotation of the capitate with respect to the lunate in the flexion-extension plane. Radiocarpal and midcarpal joint motion were reported, in 5º increments across the captured wrist motion.

The third metacarpal and the capitate are thought to form a nearly rigid body.[2,8] Therefore, the rotation of the capitate relative to the long axis of the distal radius is indicative of total wrist motion and, as such, was used to report wrist angle. The cables sutured to the six flexor and extensor tendons of the wrist were attached to pneumatic actuators (Airport Corporation, Norwalk, CT) for tone loading during testing.

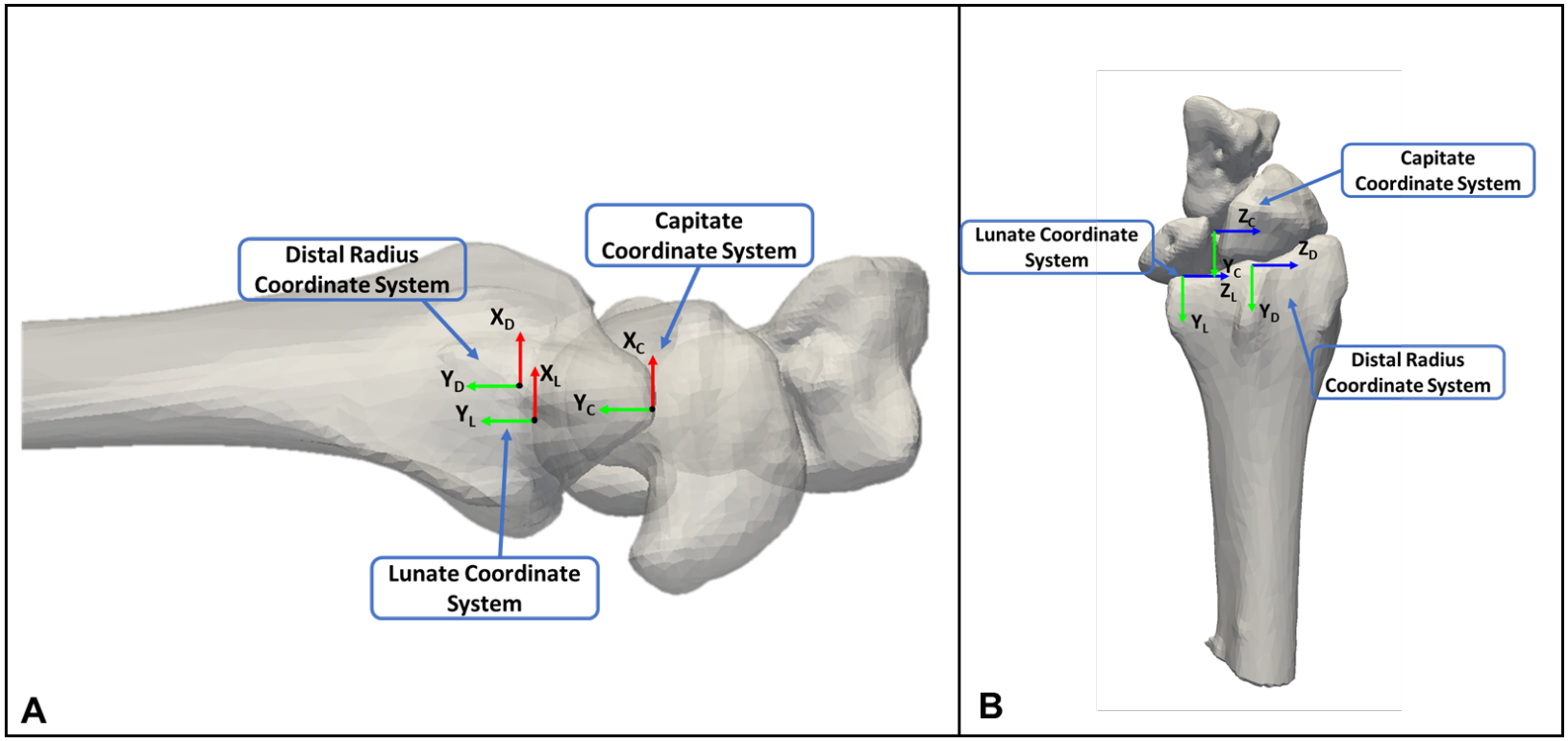

Figure 2-2: Radial and Carpal Coordinate Systems.

Depiction of the coordinate systems used in the present investigation. Define all the axes shown here. (+X-axis dorsal, +Y-axis proximal, +Z-axis radial). (A) A radial view of the coordinate systems. (B) A dorsal view of the coordinate systems used. The carpal coordinate systems were aligned with radial coordinate system in neutral wrist position (0° wrist angle)

2.2.4 Statistical Methods

Two two-way repeated-measures ANOVA analysis of variance (RM-ANOVA) with Greenhouse-Geisser correction were performed. The outcome variables (dependent) were intercarpal motion of the radiocarpal and midcarpal joints (Figure 2-2). The independent variables were direction of wrist motion (flexion or extension), and wrist angle (40º wrist flexion to 40º wrist extension in 5º increments). The first statistical test examined radiocarpal joint motion and the second examined midcarpal joint motion. This statistical test compared radiolunate and capitolunate joint motion in the native state across wrist motion. This analysis allowed for the comparison of the angular rotation between radiocarpal and midcarpal articulation in the native state to determine if the two articulations were moving synergistically. The arc of motion that was analyzed ranged from 40º of wrist flexion to 40º of wrist extension. Statistical significance was set at $p < 0.05$.

2.3 Results

During wrist extension, midcarpal joint motion had two distinct motion patterns Figure 2 3). The first occurred between 0-15º where the midcarpal and radiocarpal joints acted in unison, contributing almost equally (MC 51±9%; RC 49 ± 9%) to wrist motion. Past this point in wrist flexion (15-40º), the midcarpal joint contributed on average more to wrist motion (63±11%) compared to the radiolunate joint (37±11%). The midcarpal joint had a greater overall magnitude of angular rotation in wrist flexion compared to the radiocarpal joint (Figure 2 3; p=0.04). This trend was reversed in wrist extension (0-40º), whereby the radiocarpal joint's contribution (63±16%) was greater than that of the midcarpal joint's (37±16%). The radiocarpal joint had a greater magnitude of angular rotation in wrist extension compared to the midcarpal joint; however, this was not statically significant due to the large specimen variability (Fig. 4: p>0.05). Furthermore, the magnitude of rotation was different between wrist flexion and extension for both joints of interest. Radiocarpal joint rotation decreased in wrist flexion in comparison to wrist extension (p=0.03), whereas midcarpal joint rotation increased in wrist flexion compared to wrist extension (p=0.02).

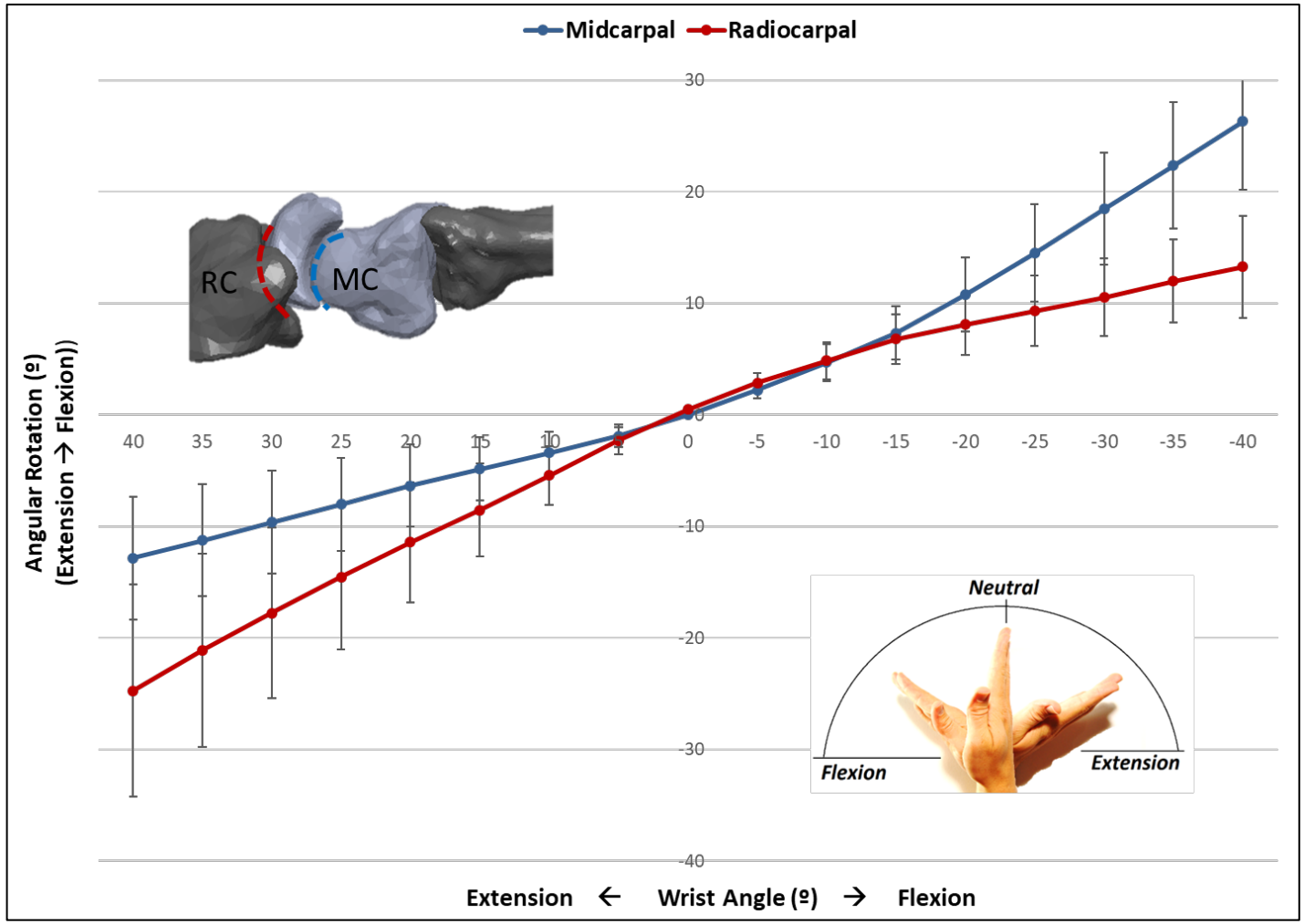

Figure 2-3: Angular rotation of the midcarpal and radiocarpal joints during wrist extension.

Angular rotation (mean ± SD) of the midcarpal (MC) and radiocarpal (RC) joints through wrist extension.

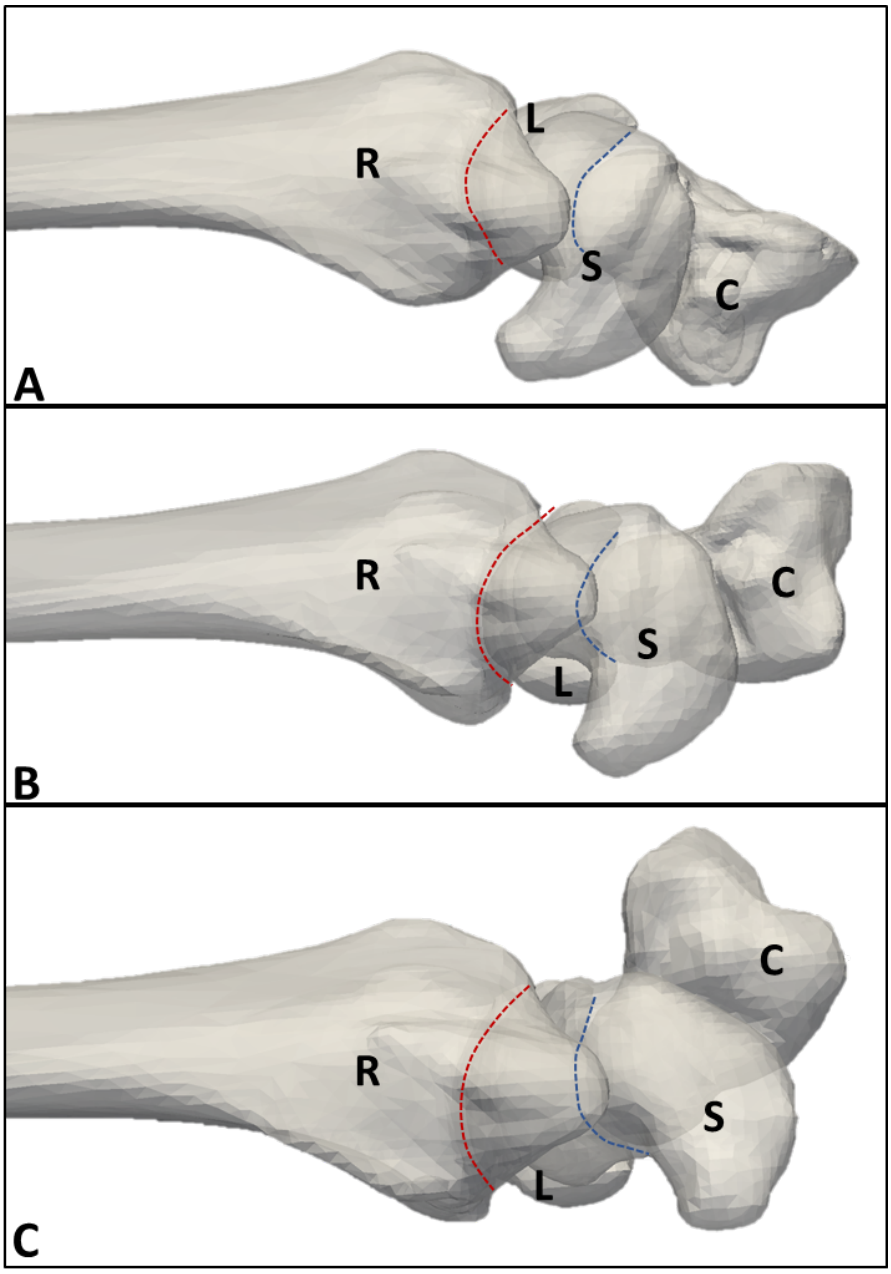

Figure 2-4: Carpal posture in wrist flexion, extension and neutral wrist position.

This is a representative specimen, and not a mean representation of carpal bone positioning. The radius (R), scaphoid (S), lunate (L), and capitate (C) are shown with the wrist in (A) flexion, (B) neutral, and (C) extension. In flexion, wrist motion primarily occurs at the radiocarpal joints, while in extension the midcarpal joint contributes more motion than the radiocarpal joint. The blue dotted line denoted the midcarpal joint, while the red dotted line denotes the radiocarpal joint.

2.4 Discussion

This study sought to examine radiocarpal and midcarpal joint motion contributions during wrist flexion-extension in the uninjured arm. The results of this study agrees with some of the previous literature, and reports that in the native wrist, the radiocarpal joint contributes more to wrist extension, and the midcarpal joint more to wrist flexion.[9] Previous literature has reported only average contribution of the radiocarpal and midcarpal joint motion in the flexion and extended wrist position, whereas this study reported the dynamic contribution throughout wrist motion. The study reports a novel finding that between 0-15º of wrist flexion, the midcarpal and radiocarpal joints acted in unison, contributing almost equally (MC 51±9%; RC 49%) to joints motion. Beyond this point in wrist flexion, the midcarpal joint contributed more to wrist motion (63±11%) compared to the radiocarpal joint (37±11%).[3,10,11] Furthermore, we found that the magnitude of rotation was different between wrist flexion and extension for both joints of interest. Radiocarpal joint rotation decreased in wrist flexion in comparison to wrist extension, whereas midcarpal joint rotation increased in wrist flexion compared to wrist extension ($p<0.05$).

The concept of a proximal row and distal row of carpal bones emerged in 1926 when Destot suggested the row theory to describe the structure of the carpus. The row theory suggests that there are two arched rows – one proximal and one distal. The proximal row is said to contain three bones, the scaphoid, lunate and triquetrum, and has been characterized as mobile. The distal row is composed of four bones, the trapezium, trapezoid, capitate and hamate. Destot suggested the head of the capitate was the centre of wrist motion, while the scaphoid acted as an external pillar that stabilizes the carpus in extension. The row theory introduced a systematic framework for further investigation of the carpus and since the proposal of the row theory, many investigators have sought to understand the contributions of the radiocarpal and midcarpal joints to global wrist motion.

Various investigators have examined the contributions of the radiocarpal and midcarpal joint in the framework of the row theory, and the results of these studies have been inconsistent. Using implanted staples and orthoradiography, Ruby et al concluded that wrist motion in flexion and extension was comprised of approximated 50% radiocarpal and 50% midcarpal motion.[12] They also documented just 24° of motion between the scaphoid and lunate during

global flexion/extension and concluded that it is justified to consider the wrist as composed of proximal and distal carpal rows. By simulating partial wrist fusion in a series of cadaver specimens, Gellmann et al similarly concluded that 63% of global wrist flexion and 53% of global wrist extension occurs at the radiolunate joint.[9] More recently Kobayashi et al measured carpal bone rotation in 3 dimensions using implanted metal markers and biplanar radiography on 22 cadaveric specimens while applying 100N load in each position to simulate physiologic loading. These investigators demonstrated that radiolunate motion comprised 50% of wrist extension but only 36% of wrist flexion. Patterson et al used a 3-dimensional CT analysis of 5 cadaveric wrist using implanted markers during passive wrist flexion/extension. They concluded that the wrist can be simplified into a 2-linkage system comprising the proximal and distal rows. Sarrafian et al. reported that during flexion, the midcarpal joint contributes 60% to motion, with the radiocarpal contributing 40%. While, in extension the midcarpal joint on average contributes 33.5% while the radiocarpal joint contributes 66.5%. Our findings suggest a greater contribution from the radiocarpal joint during wrist extension, while the midcarpal joint contributes more to wrist flexion, which is in agreement with the majority of previous literature. Interestingly, we also observed a period of motion from 0-15° where the radiocarpal joint and midcarpal joint rotated in unison and contributed equally to global wrist motion.

Recently, lunate morphology has been described as influencing the relative contributions from the radiocarpal and midcarpal joint.[13] Bain et al. described the effect of lunate morphology on 3-dimensional carpal kinematics during wrist flexion and extension. These investigators observed a greater magnitude of radiocarpal joint motion during wrist flexion-extension in type I lunate relative to type II lunate wrist. Additionally, the midcarpal articulation was relatively restricted during flexion and extension in the type II lunate wrist. Conversely, this study showed a greater degree of radiocarpal motion in both wrist flexion and extension in type II lunates in comparison to type I. While the midcarpal motion patterns were relatively similar between type I and type II lunate's in wrist flexion, however there was a greater degree of midcarpal rotation in type II in extension in comparison to type I lunates. However, our sample size was inadequate to assess for this important consideration, as our specimen cohort included only two type I lunates and four type II lunates. Further studies, either clinical or biomechanical will be needed to delineate this issue further. Previous studies have suggested that the additional facet of the lunate in type II morphology, acts as a restrictive mechanism limiting

motion, however this trend was not observed in this cohort of specimens. Morphology and individual ligamentous anatomy likely contribute in determining the motion pathway of each individual wrist. Further classification and examination of wrist morphology and overall soft tissue structures of the wrist would be beneficial to understanding the wrist complex motion and pathologies.

Conflicting results are not surprising as a wide range of experimental techniques have been used to investigate the relative contributions of the radiocarpal and midcarpal joints to global wrist motion. There are inherent difficulties simulating physiologic wrist motion. Some of those difficulties include applying appropriate *in-vivo* loads across wrist motion, executing physiologically relevant motion pathways (*i.e*. dart thrower motion, or circumduction), and lastly, testing applicable forearm positions that would be consistent with daily tasks. Apart from joint motion simulation approaches, coordinate system selection and application have the potential to bias results. Many studies apply an RM-ANOVA approach to data analysis, which compares results within subjects, and examines changes as opposed to the absolute magnitude of values, moving the potential for bias from coordinate system selection. However, a standardized wrist joint coordinate system definition would allow investigators to more freely make comparisons of results between studies.

This study had several limitations. A potential limitation of this study is the truncated range of motion used for analysis, ranging from 40º of wrist flexion to 40º of wrist extension. The range of motion was dictated by specimen variability in the form of reduce ability to achieve a larger motion arc by some specimens. As mean values were reported in this study, the range of motion analyzed was determined by the specimen with the smallest motion arc. Additionally, tracker impingement within the carpal bones could have affected carpal bone rotation. However, each tracker was checked fluoroscopically at the time of insertion and no impingement was evident within the arc of motion analyzed in this study. Tracking the carpal motion with 4D CT could have avoided potential tracker impingement.[14,15] However, the size of the joint motion simulator and accompanying control system did not allow this study to be performed with imaging. The passive nature of this study could have affected the results, as varying physiological loads were not applied during flexion-extension motion. However, we attempted to mitigate the differences that may be seen between active and passive motion by applying constant tone loads to the flexor and extensor muscles of the forearm.

2.5 Conclusions

This study shows that the radiocarpal joint plays a greater role in terms of contribution of motion to wrist extension, whereas the midcarpal joint contributes more motion than the radiocarpal joint to wrist flexion. The results of this study also revealed a novel finding that that there is a period near neutral wrist position, where the joints function in unison and contribute equally to global wrist motion.

These finding are of importance to furthering kinematic knowledge of the intact wrist. As we continue to seek to understand native biomechanics, further insight can be gained into how injury or disease alter biomechanics of the wrist. Additionally, the results and the experimental techniques applied in this chapter are of importance to the forthcoming chapters, as they seek to build on the experimental techniques applied in this chapter in an effort to better quantify wrist biomechanics and understand how study and apparatus design decisions influence results.

2.5.1 References

1. Kauer JMG. Functional anatomy of the wrist. *Clin Orthop Relat Res*. 1980;NO 149:9-20.

2. Patterson RM, Nicodemus CL, Viegas SF, Elder KW, Rosenblatt J. High-speed, three-dimensional kinematic analysis of the normal wrist. *J Hand Surg Am*. 1998;23(3):446-453. doi:10.1016/S0363-5023(05)80462-9

3. Sarrafian K, Melamed L, Goshgarian GM. Study of Wrist Motion in Flexion and Extension. *Clin Orthop Relat Res*. 1977;(126):153-159.

4. Sun JS, Shih TTF, Ko CM, Chang CH, Hang YS, Hou SM. In vivo kinematic study of normal wrist motion: An ultrafast computed tomographic study. *Clin Biomech*. 2000;15(3):212-216. doi:10.1016/S0268-0033(99)00064-9

5. Nishiwaki M, Welsh M, Gammon B, Ferreira LM, Johnson JA, King GJW. Distal radioulnar joint kinematics in simulated dorsally angulated distal radius fractures. *J Hand Surg Am*. 2014;39(4):656-663. doi:10.1016/j.jhsa.2014.01.013

6. Werner FW, Palmer AK, Somerset JH, et al. Wrist joint motion simulator. *J Orthop Res*. 1996;14(4):639-646. doi:10.1002/jor.1100140420

7. Wu G, Van Der Helm FCT, Veeger HEJ, et al. ISB Recommendation on Definitions of Joint Coordinate Systems of Various Joints for the Reporting of Human Joint Motion - Part II: Shoulder, Elbow, Wrist and Hand. *J Biomech*. 2005;38(5):981-992. doi:10.1016/j.jbiomech.2004.05.042

8. Rainbow MJ, Kamal RN, Leventhal E, et al. In vivo kinematics of the scaphoid, lunate, capitate, and third metacarpal in extreme wrist flexion and extension. *J Hand Surg Am*. 2013;38(2):278-288. doi:10.1016/j.jhsa.2012.10.035

9. Gellman H, Kauffman D, Lenihan M, Botte MJ, Sarmiento A. An in vitro analysis of wrist motion: The effect of limited intercarpal arthrodesis and the contributions of the radiocarpal and midcarpal joints. *J Hand Surg Am*. 1988;13(3):378-383. doi:10.1016/S0363-5023(88)80013-3

10. Volz RG. Biomechanics of the Wrist. *J Hand Ther*. 1995;8(2):97-105. doi:10.1016/S0894-1130(12)80306-1

11. Kaufmann RA, Pfaeffle HJ, Blankenhorn BD, Stabile K, Robertson D, Goitz R. Kinematics of the Midcarpal and Radiocarpal Joint in Flexion and Extension: An In Vitro Study. *J Hand Surg Am*. 2006;31(7):1142-1148. doi:10.1016/j.jhsa.2006.05.002

12. L. K. Ruby, MD, W. P. Cooney III, MD, K. N. An, PhD, R. L. Linscheid, E. Y. S. Chao, PhD, Boston. Relative Motion of Selected Carpal Bones: A kinematic Analysis of the normal wrist. *J Hand Surg Am*. 1988;15(5):806-833. doi:http://dx.doi.org/10.1016/0363-5023(90)90163-L

13. Bain GI, Clitherow HDS, Millar S, et al. The effect of lunate morphology on the 3-dimensional kinematics of the carpus. *J Hand Surg Am*. 2015;40(1):81-89.e1. doi:10.1016/j.jhsa.2014.09.019

14. Tay SC, Primak AN, Fletcher JG, et al. Four-dimensional computed tomographic imaging in the wrist: Proof of feasibility in a cadaveric model. *Skeletal Radiol*. 2007;36(12):1163-1169. doi:10.1007/s00256-007-0374-7

15. Mat Jais IS, Tay SC. Kinematic analysis of the scaphoid using gated four-dimensional CT. *Clin Radiol*. 2017;72(9):794.e1-794.e9. doi:10.1016/j.crad.2017.04.005

16. Padmore CE, Stoesser H, Nishiwaki M, et al. The Effect of Dorsally Angulated Distal Radius Deformities on Carpal Kinematics: An In Vitro Biomechanical Study. *J Hand Surg Am*. 2018;43(11):1036.e1-1036.e8. doi:10.1016/j.jhsa.2018.02.017

Chapter 3

3 The Effect of Coordinate System Selection on Wrist Kinematics

OVERVIEW

Three-dimensional motion analysis of the hand and wrist is common in in-vitro and in-vivo biomechanical research. However, all studies rely on post testing analysis, where anatomical joint coordinate systems (JCS) are created to generate clinically relevant data to describe wrist motion. The purpose of this study was to present a comparison of four JCSs that have been previously described in literature to ascertain which JCS provides the most reliable measurement of clinical wrist angle.[2]

[2] A version of this work was presented at the 2020 Annual Meeting of the Orthopaedic Research Society and is in second revision for the Journal of Biomechanics

3.1 Introduction

Three-dimensional motion analysis of the wrist is common in *in-vitro* and *in-vivo* biomechanical research (as discussed in Chapter 1). These studies have played a critical role in advancing knowledge in wrist surgery as well as rehabilitation [1–5]. Novel soft tissue reconstruction methods, insight into fracture management, and improved post-operative rehabilitation protocols have been positively affected by this body of literature [3,6,7]. These studies rely on the generation of anatomical joint coordinate systems (JCS), which are used to describe the relative motion between two segment/bodies; with each of those bodies having their own coordinate systems (Body Coordinate System (BCS)). Wrist JCSs describe the relative motion of the hand (hand BCS) to the radius (radius BCS) as described in Chapter 1 (Section 1.3.3)

The identification and selection of accurate and repeatable anatomic landmarks are imperative to create physiologically relevant JCSs. *In-vitro* (or cadaveric) studies often have the advantage of digitizing non-palpable anatomical landmarks found on the surface of the bone. In the case of the wrist JCS, anatomical landmarks on the radius and on the third metacarpal are digitized to create a body coordinate system on each bone. The relationship between these two body coordinate systems are then in turn used to define wrist joint angle [8–11]; whereas, *in-vivo* (or clinical) studies are limited to digitizing palpable points (on the surface of the skin) to generate these same JCSs [12,13]. Both *in-vitro* and *in-vivo* studies have stated that a limitation of the current body of literature for wrist and carpal biomechanical studies is a lack of a standardized wrist JCS that would be suitable for both *in-vivo* and *in-vitro* studies.

The International Society of Biomechanics (ISB) has previously proposed JCS guidelines for the wrist and hand [14]; however few investigators have adopted their methodology and have instead used alternative methods to define wrist joint angle [9,12,15–17]. Chapter 2 of this body of work does employ the ISB standards, however, several drawbacks of ISB were noted during the data analysis in chapter 2. Other authors have also drawn attention to the limitations of ISB standards. A limitation that has been previously noted is the recommended origin of the radial coordinate system, located at the midpoint of the radial shaft, which is often difficult to access.

In view of the foregoing, it is important to determine which currently used wrist JCS affords the most, accurate and repeatable characterization of wrist motion. A standardized definition

of wrist joint angle is imperative as this angle is used as the independent variable to which results from different studies are compared. Therefore, the purpose of this study was to assess current methodologies for generating wrist coordinate systems and compare how coordinate system selection effects the calculation of global wrist joint angle.

3.2 Methods

3.2.1 Specimen Preparation and Experimental Setup

Five fresh frozen cadaver upper extremities (70.4 ± 16.4yrs, 5 left male) were amputated at the mid-humerus level. All soft tissues were left intact to preserve natural function and avoid tissue desiccation. Similar to Chapter 2, Krackow sutures were placed at the distal musculotendinous junctions of the flexor carpi radialis (FCR), flexor carpi ulnaris (FCU), extensor carpi radialis longus (ECRL), extensor carpi radialis brevis (ECRB), extensor carpi ulnaris (ECU), biceps brachii (Bi), and pronator teres (PT). Sutures were then passed under the skin adjacent to the muscle belly to guide blocks at their respective origins (where applicable) on the lateral/medial epicondyles of the humerus to maintain anatomical lines of action. A Steinmann pin inserted into the third metacarpal along its longitudinal axis. Active optical tracking markers (Optotrak Certus; Northern Digital, Waterloo, Canada) were fixed, as previously described by Padmore et al. (2019), to the third metacarpal, radius and ulna to capture 3-dimensional motion of each during testing. The camera of the optical tracking system was placed perpendicular to the wrist motion simulator at approximately 2.5m. All active optical tracking markers were oriented to maintain an optimal line of sight with the camera during motion trials to ensure continuous data collection.

Each specimen was mounted rigidly to the custom motion simulator using a humeral clamp along with two Steinmann pins inserted into the proximal ulna to maintain 90 degrees of elbow flexion (Figure 3-1). The Steinmann pin that had been previously inserted into the third metacarpal, was then slotted into the guide rail (Figure 3-1). The purpose of the guide rail was threefold. First, the guide served as a tool to physically measure wrist angle during motion testing. To measure wrist angle a goniometer (with a scale in 10-degree increments) was employed to measure 50° of wrist flexion and 50° of wrist extension; each specimen was hand guided to these wrist positions. The end points of motion were marked on the guide rail. This same procedure was then executed for radial-ulnar deviation by rotating the guide rail 90 degrees from the flexion-extension position. Second, the planar motion guide rail was equipped with LED lights along the rails surface which illuminated at 5°/sec, giving the investigator visual cues as to how quickly to proceed with wrist motion when passively guiding each specimen though the predetermined motion pathways. The LEDs ensured that all specimens

were guided by the investigator through wrist motion at the same rate. Third, the guide rail was used to restrict out of plane motion, ensuring the achievement of planar flexion-extension and radial-ulnar deviation. All skin incisions were sutured closed to preserve specimen hydration during testing.

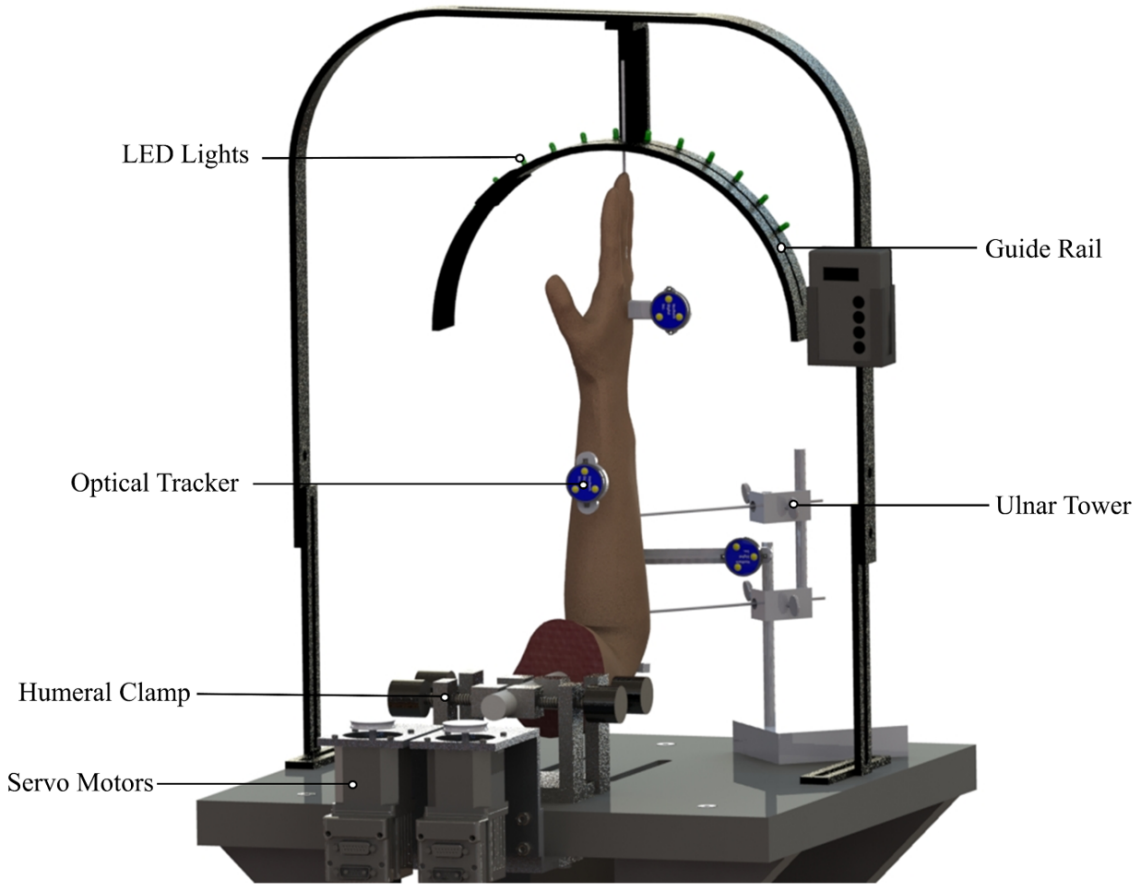

Figure 3-1: Wrist motion simulator platform.

The wrist motion simulator shown with optical tracking markers attached to the radius, ulnar and third metacarpal. The simulator is also equipped with a passive motion guide rail to ensure planar and repeatable wrist motion.

3.2.2 Experimental Protocol

As shown in Figure 3-1, the simulator was oriented in a gravity neutral position similar to the experimental approaches of others, and the experimental technique used in Chapter 2.[5,11,18] Passive flexion-extension (FEM) and radioulnar deviation (RUD) motion trials were executed. The Steinmann pin inserted into the third metacarpal was used to hand guide each specimen through two predetermined motion pathways at 5°/s, to simulate the quasi-static condition. This was done to eliminate the need to consider dynamic motion variables in the data analysis. The first motion pathway was flexion-extension, where the wrist was hand guided from 50° of extension to 50° of flexion. The second motion pathway was radial-ulnar deviation, where the specimen was hand guided from 20° of ulnar deviation to 20° of radial deviation, again using the guide rail to limit out-of-plane motion in the flexion-extension axis and the pronation-supination axis. For each motion pathway, four pre-conditioning trials followed by the definitive trial were conducted. During the passive motion trials, a constant load of 10N was applied to each of the flexors and extensors of the wrist [11]. The constant loads did not contribute to actuation of the wrist, but rather served to simulate physiologic compressive load at the wrist as a result of muscle tone.

3.2.3 Landmark Digitization

Following testing, anatomical landmark digitization was performed using an optical tracking stylus. First, palpable anatomical landmarks were digitized using the optical tracking stylus. Subsequently, the specimens were denuded of all soft tissue while leaving the optical tracking markers attached. Anatomical landmarks, on the surface of radius and third metacarpal required for data analysis, as well as surface traces of each bone were digitized using an active optical tracker stylus. The digitizations were collected with respect to each bone's optical tracking marker. This allowed for the transformation of the motion data collected by the optical trackers with respect to the camera, to anatomical JCSs during post processing.

3.2.4 Coordinate Systems Assessed and Outcome Variables

Four separate JCSs to describe global wrist angle were generated (Figure 3-2). Global wrist angle describes the relative motion between the body coordinate system (BCS) of the third metacarpal and the BCS of the radius. Wrist angle for both flexion-extension and radial-ulnar

deviation is described by the relative motion between the body coordinate system (BCS) of the third metacarpal and the BCS of radius. Whereas wrist pronation-supination angle is described by the relative motion between the radius and the ulna. In this study wrist flexion-extension, radial-ulnar deviation and pronation-supination angles are reported.

A variety of methods exist in the literature to generate a BCS for the radius, which in turn contributes to the description of global wrist angle. The right-hand rule is followed during coordinate systems generation to specific orientation and direction of the X, Y and Z axes. In this study, four different methods were used to generate a BCS for the radius (Figure 3-2); the description of those coordinate systems are as follows:

BCS_A[9]

BCS_A uses palpable anatomical landmarks to generate CS.

O_r: The origin is located at the interval of the distal radius and distal ulna (distal radioulnar joint, DRUJ) on the dorsal aspect of wrist

$\overrightarrow{X_R}$: The common line perpendicular to the $\overrightarrow{v_1}$ ($\overrightarrow{Y_{AXIS}}$) and $\overrightarrow{v_2}$

$\overrightarrow{Y_R}$: A line the length of the long shaft of the radius originating from the Origin (O_r, located at the interval of the distal radius and distal ulna) directed towards a point at the proximal radioulnar joint (PRUJ)

$\overrightarrow{Z_R}$: The line perpendicular to the $\overrightarrow{Y_{AXIS}}$, and in a plane defined by the tip of the radial styloid and the O_r

BCS_B[8]

$\overrightarrow{X_R}$: A line fit through the centroids of the radial diaphysis (shaft). Simply, the axis coincides with the radial long axis ($+\overrightarrow{X_R}$ was proximal)

$\overrightarrow{Y_R}$: Directed through the radial styloid and defined perpendicular to the $\overrightarrow{X_R}$. Flexion ($+\overrightarrow{Y_R}$) and extension ($-\overrightarrow{Y_R}$) rotations were measured around this axis.

$\overrightarrow{Z_R}$: Directed volarly and calculated from the cross product of $\overrightarrow{X_R}$ and $\overrightarrow{Y_R}$. Ulnar (+Z_r) and radial (-$\overrightarrow{Z_R}$:) deviation was measured around this axis.

O_r: Defined by the intersection of $\overrightarrow{X_R}$ and the distal radial articular surface.

BCS$_C$[14]

$\overrightarrow{X_R}$: The common line perpendicular to the $\overrightarrow{Y_R}$ and $\overrightarrow{Z_R}$ axis.

$\overrightarrow{Y_R}$: The line parallel to the long shaft of the radius from Origin (O_r) to intersect with the ridge between the radioscaphoid fossa and the radiolunate fossa (midway dorsally and volarly along the ridge).

$\overrightarrow{Z_R}$: The line perpendicular to the $\overrightarrow{Y_R}$ axis, and in a plane defined by the tip of the radial styloid (RS), the base of the concavity of the sigmoid notch (SN) and the specified origin.

O_r: The origin is located midway between the distal radius at the level of the ridge between the radioscaphoid fossa and the radiolunate fossa, and the proximal radius at the level of the depression in the proximal radial head. If the distance to the ridge between the radioscaphoid and radiolunate fossas varies, then the location halfway between the dorsal and volar extremes of the ridge will be used to define the distal landmark on the radius. In the transverse plane it will be at the approximate centre of the tubular bone (along its principal axis of inertia).

BCS$_D$[12]

$\overrightarrow{Y_R}$: Vector between V_{MR} [Midpoint along the vector between V_{RH} and V_{RB} (Perpendicular projection from P_{RR} (Lister's Tubercle) to vector between P_{RS} (radial styloid) and P_{US} (ulnar styloid))] and V_{RH} (Point 20% the distance along the vector between P_{LH} (Lateral Humeral Epicondyle) and P_{HM} (Medial Humeral Epicondyle), proximal is positive

$\overrightarrow{X_R}$: Vector normal to plane containing V_{RB}, V_{MR} and P_{RS}, dorsal is positive

$\overrightarrow{Z_R}$: Common perpendicular to $\overrightarrow{X_R}$ and $\overrightarrow{Y_R}$ (Cross product of $\overrightarrow{X_R}$ and $\overrightarrow{Y_R}$)

O_r: Midpoint along the vector between V_{RH} and V_{RB}

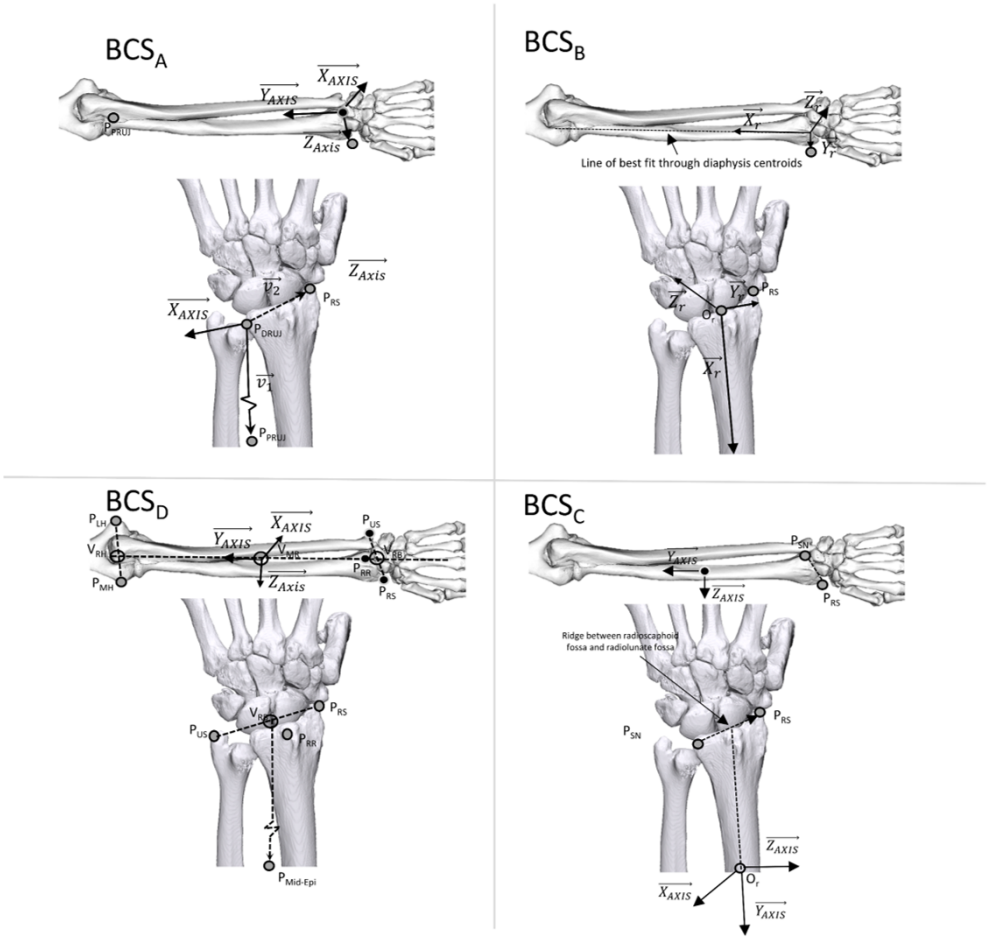

Figure 3-2: Illustration of four assessed radial body coordinate systems (BCS).

BCS_A and BCS_D use palpable anatomical points to define the axes of their coordinate systems, while BCS_B and BCS_C denude the specimen's following testing and digitize boney anatomical landmarks to generate their axes. The digitized anatomical landmarks are denoted by circles, while the dotted lines indicate vectors, and solid lines are the final unitized vectors of the coordinate systems.

Following the construction of the four different radial BCSs, as per the definitions above, the relationship between the radial BCS and the third metacarpal BCS was calculated to describe global wrist motion, also known as wrist joint coordinate system (JCS_A-JCS_D). Custom LabVIEW software was developed to calculate the outcome measure of global wrist motion in all three axes of rotation (The axes are clinically referred to as: flexion-extension (Z-axis), radial-ulnar deviation (Y-axis), and pronation-supination (X-axis) in the context of the wrist) to examine the performance of the wrist JCSs in each axis. The performance of each CS was

compared to each other in terms of mean difference across all wrist angles ± standard deviation (SD). In addition to comparing calculated wrist joint angles from each of the four methods described above to each other, the calculated wrist from each method was compared to the measured goniometric value from test day and reported as the deviation from measured wrist angle ± SD.

3.2.5 Statistical Methods

To examine the performance of each JCS, flexion-extension motion trials in addition to radial-ulnar deviation trials were analyzed. First, the performance of each JCS was evaluated in all three axes for wrist flexion-extension motion. To examine the differences in the description of global wrist angle in each axis, a 2-way repeated-measures ANOVA (RM-ANOVA) was performed. Furthermore, the same method of statistical analysis was employed to examine the performance of all four JCSs during radial-ulnar deviation motion. For each RM-ANOVA, the factors included joint coordinate system (JCSA-JCSD), and calculated wrist angle (5° increments). The independent variable for each of the RM-ANOVA statistical tests was the measured wrist angle. Statistical significance was set at $P < 0.05$.

3.3 Results

3.3.1 Flexion-Extension Motion

Wrist angle derived from each of the four CS generation methods (JCSA-JCSD) were evaluated in three axes of rotations (flexion-extension, radial-ulnar, and pronation-supination) for data collected during planar wrist flexion and extension wrist motion. The data presented are the mean differences ± SD between the calculated wrist angle of each analyzed JCS, across wrist motion (50° of wrist flexion to 50° of wrist extension). During wrist flexion-extension motion, there were significant mean differences in calculated wrist angle between JCSA and JCSB ($p=.003$), as well as JCSB and JCSD ($p=.045$) in the flexion-extension axis (Figure 3-3). However, during flexion-extension motion, the calculated angle in the radial-ulnar deviation axis and pronation supination axis were not significantly different.

In addition to comparing the performance of each JCS to each other in terms of the global wrist angle, the wrist angle determined by each JCS was also compared to the goniometric measurement of wrist angle on the day of testing (Figure 3-4). The only significant deviation

from the goniometric measurement of wrist angle was found in the calculated flexion-extension axis of JCSA. All other deviations from the goniometric measurement of wrist angle were less than 2° in the three analyzed axes of wrist angle.

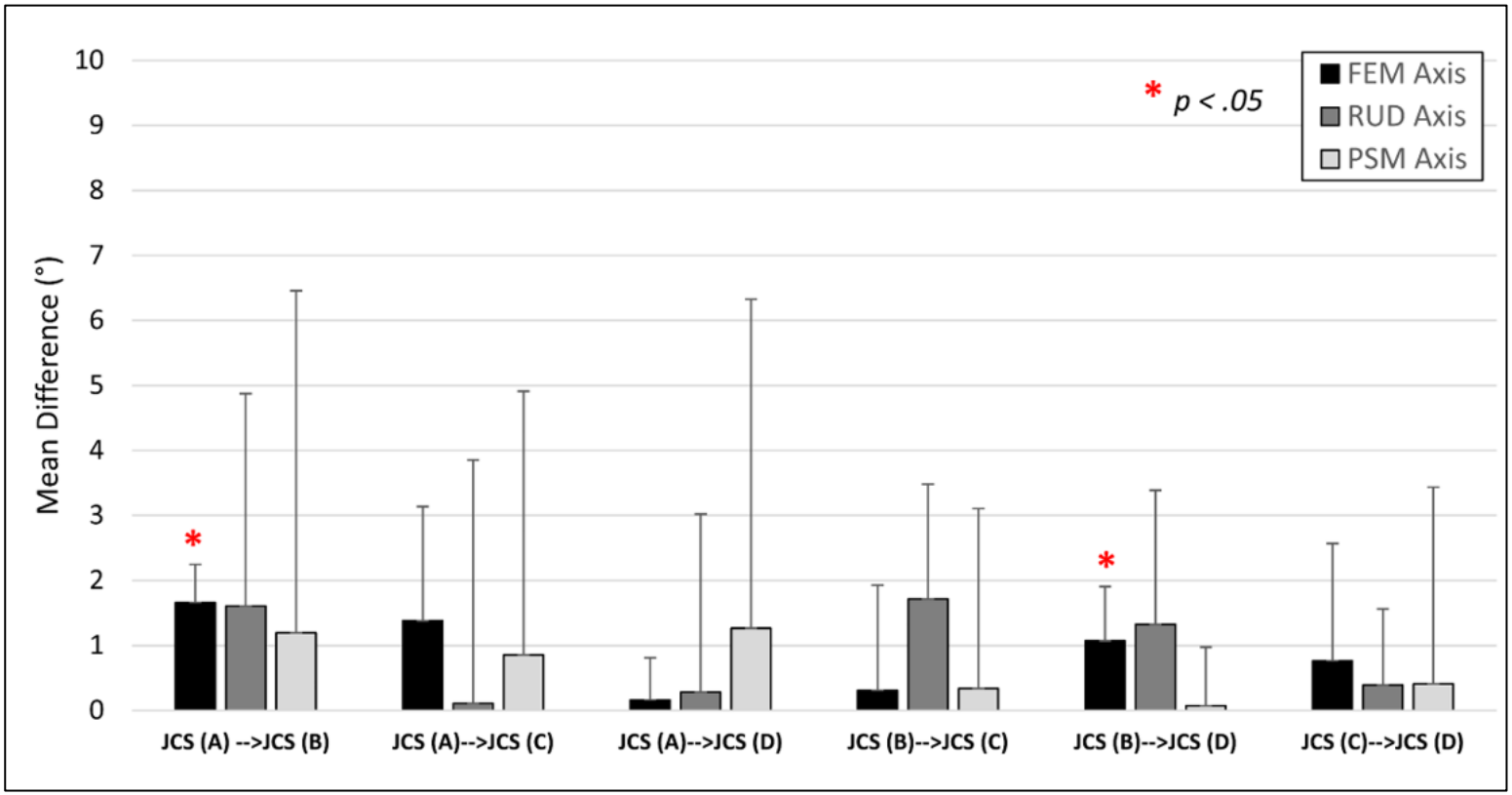

Figure 3-3 Mean ± SD difference between the four analyzed wrist joint coordinate systems (JCS) across a flexion-extension motion pathway.

The mean (+1 standard deviation) differences were calculated for each axis (flexion-extension, radial-ulnar deviation and pronation supination) of rotation, which was defined as the rotation of the third metacarpal with respect to the radius.

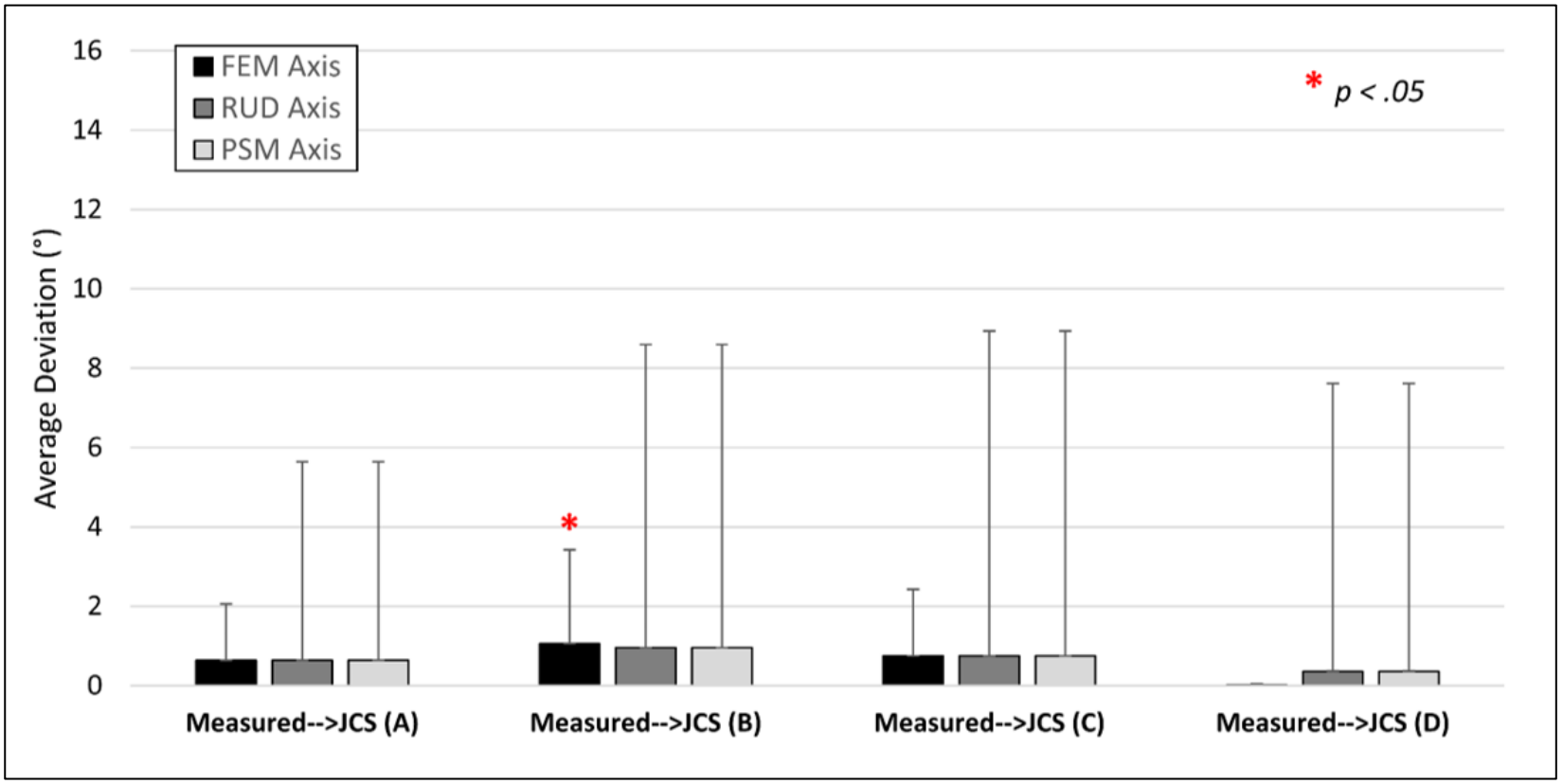

Figure 3-4 Mean ± SD of the calculated wrist angle from each analyzed wrist joint coordinate systems (JCS) and the measured wrist joint angle, across a flexion-extension motion pathway.

The mean (+1 standard deviation) deviation was reported for each axis of rotation, which was defined as the rotation of the third metacarpal with respect to the radius. The axes of rotation are clinically named flexion-extension, radial-ulnar deviation and pronation supination.

3.3.2 Radial-Ulnar Deviation Motion

Wrist angle derived from each of the four JCS generation methods (JCS_A-JCS_D) were evaluated in three axes of rotations (flexion-extension, radial-ulnar, and pronation-supination) for data collected during planar radial-ulnar deviation motion. The data presented are the mean differences ± SD between the calculated wrist angle of each analyzed JCS, across the motion pathway (20° of ulnar deviation to 20° of radial deviation). There were significant differences observed in the calculated wrist angle between JCS_A and JCS_B ($p=.005$), as well as JCS_B and JCS_D ($p=.044$) in the flexion-extension axis (Figure 3-5). Additionally, there were significant differences in the radial-ulnar deviation axis between JCS_B and JCS_C ($p=.004$), and JCS_B and JCS_D ($p=.047$).

In addition to comparing the performance of each JCS to each other in terms of global wrist angle, the wrist angle reported by each JCS was also compared to the goniometric measurement of wrist angle on the day of testing (Figure 3-6). There were no significant differences between the measured wrist angle the calculated wrist angle for any of the JCSs; however, the standard deviations were substantial for the pronation-supination axis for all CSs analyzed during radial-ulnar deviation motion.

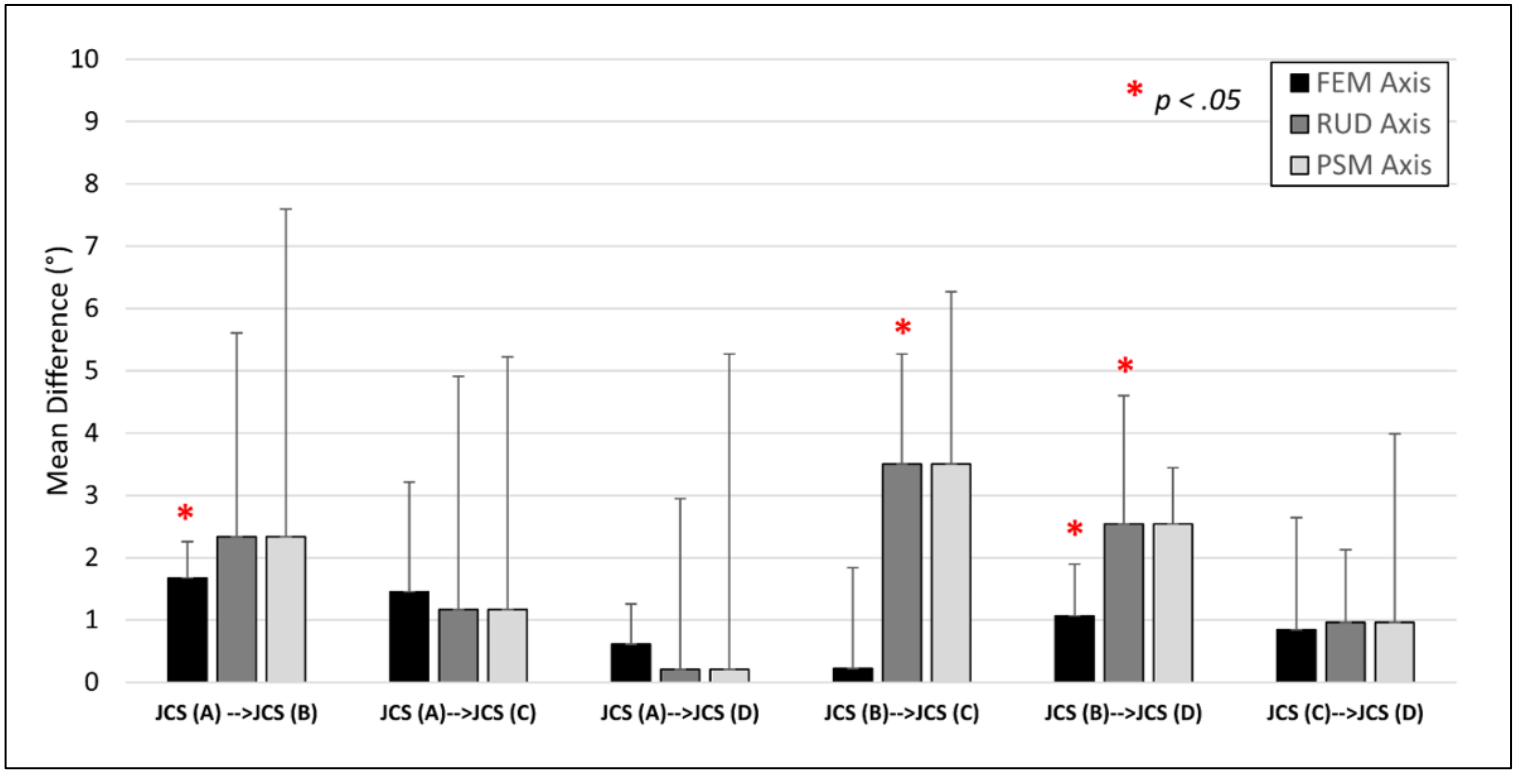

Figure 3-5 Mean ± SD between the four analyzed wrist joint coordinate systems (JCS) across a radial-ulnar deviation motion pathway.

The mean (+ 1 standard deviation) deviation was reported for each axis of rotation, which was defined as the rotation of the third metacarpal with respect to the radius. The axes of rotation are flexion-extension (FEM), radial-ulnar deviation (RUD) and pronation supination (PSM).

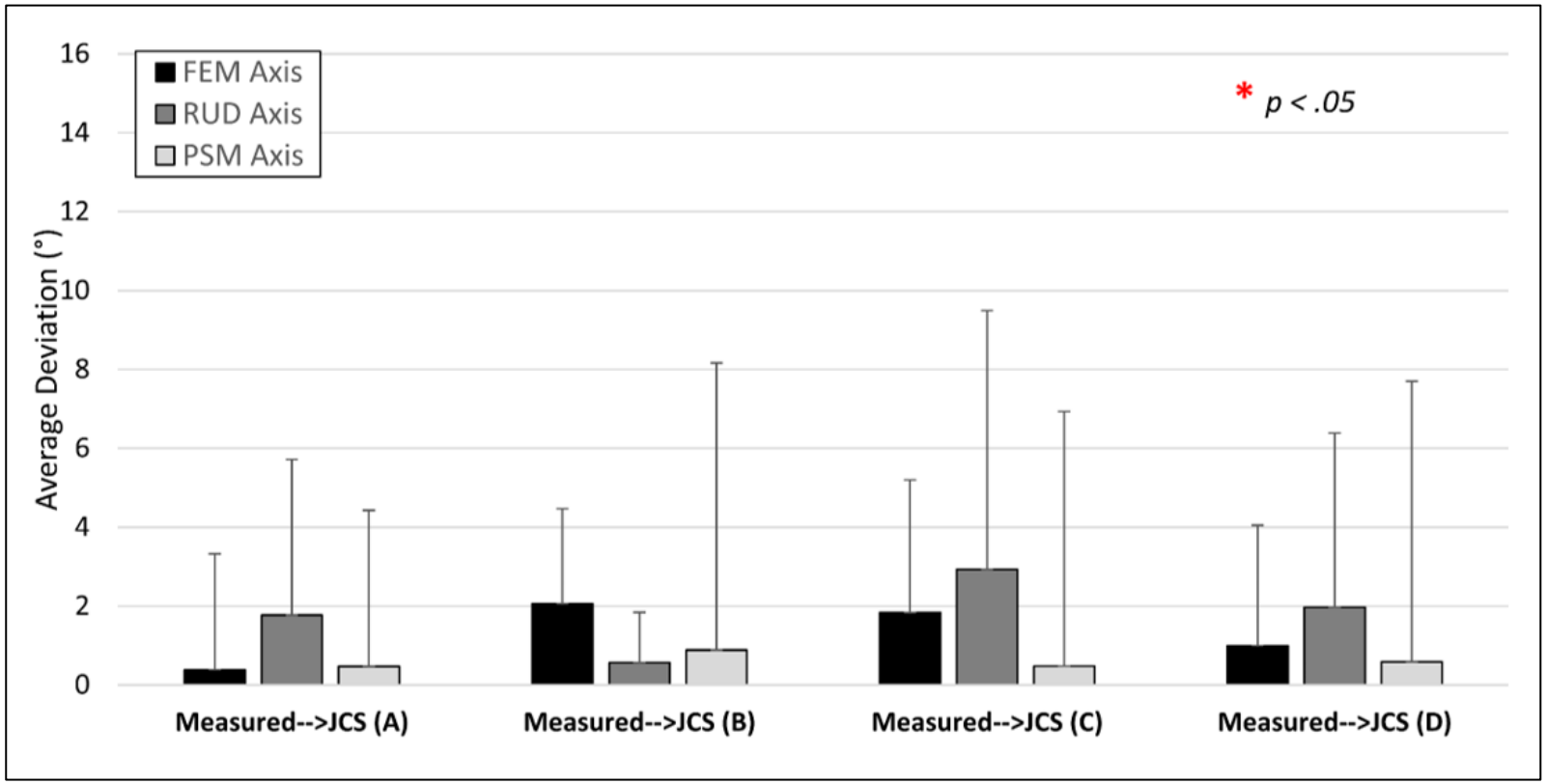

Figure 3-6 Mean ± SD of the calculated wrist angle from each analyzed wrist joint coordinate systems (JCS) and the measured wrist joint angle, across a radial-ulnar deviation motion pathway.

The mean (+ 1 standard deviation) deviation was reported for each axis of rotation, which was defined as the rotation of the third metacarpal with respect to the radius. The axes of rotation are clinically named flexion-extension, radial-ulnar deviation and pronation supination.

3.4 Discussion

The aim of this study was to compare the four-alternative radial BCS generation methods in the literature, which contribute to describing wrist joint motion in biomechanical studies. The four radial BCSs use different anatomical landmarks and approaches to define their axes. Even though the results of this study found statistically significant differences between the four analyzed coordinate systems methods, the differences were subtle and are likely not clinically significant. Furthermore, this study examined the magnitude by which the calculated JCS wrist angle deviated from the clinically measured wrist angle. Again, the differences were subtle; however, the scatter (*i.e*. standard deviations) of the mean calculated wrist angles were greater for some of the analyzed JCSs. Certain JCSs had greater mean differences, but with higher standard deviations. This combination of results suggests greater variance in calculated wrist angle by some JCSs, and the reduced consistency in measurement may help to explain the lack of statistical difference in those cases.

Previous literature has identified limitations with current radial BCS standards offered by the ISB (BCS_C), such as its proximally located origin which is centered at the midway point between the distal radius and proximal radial head. The location of the origin is specifically problematic for studies that employ specimens amputated at the mid-forearm in cadaveric studies, or *in-vivo* CT based studies that only scan the distal end of the radial and hand to reduce radiation dose for patients[15,19,20]. Additionally, the standard set forth by ISB for the radial BCS require access to anatomical landmarks such as the center of the radial dish on the radial head which requires significant dissection and disarticulation. These limitations have driven some researchers away from using the ISB standard and instead developed their own radial BCSs. Regarding performance of the ISB JCS, in this study we found that the IBS JCS performed similarly to the other JCSs analyzed. However, a difference was noted between JCS_B and the ISB JCS (JCS_C) during radial-ulnar deviation motion. Although the noted difference was statically different ($p=.004$), it was relatively small (mean dif. = 3.5 ± 1.3°). Furthermore, when compared to the other analyzed wrist JCSs, the ISB JCS had greater standard deviation from the mean measured wrist angle. Large standard deviations may be an indication that the ISB JCS definition may be susceptible to error due to point selection.

The standardization of JCS definition is important to permit inter-study comparisons. Landmark selection to define JCSs should be defined without ambiguity and they should be possible to digitize repeatably to reduce error. The use of palpable landmarks may yield different results, as it may be difficult to repeatably select the same point. Landmarks found on the bony surface, may be subject to less error in terms of repeatability as they are often easier to visually locate following the soft tissue removal subsequent to cadaveric testing. In this study, JCS_A and JCS_D both used palpable landmarks to define their wrist JCSs, whereas JCS_B and JCS_C used non-palpable landmarks. In agreement with previous studies, we did note differences in global wrist angle between the JCS that used palpable landmarks compared those that used non-palpable landmarks. However, all JCSs analyzed appear to report wrist joint angles relatively close to clinically measured wrist angle.

Another consideration with respect to selecting an appropriate JCS would be the setting of pathological specimens where erosion of bony structures due to conditions such as arthritis or acute injuries may destroy or alter the location of anatomical landmarks. The alteration of location of anatomical landmarks may bias the axes in a resulting wrist JCS making the calculated wrist angle deviate substantially from clinical wrist angle. Repeatable point selection is imperative for a reliable coordinate system, and therefore in pathological wrist, considerations should be made to account for the altered location of anatomical landmarks. Often wrist pathology which would alter bony geometry manifests in similar patterns, for example SLAC or SNAC wrist. Selecting anatomical landmarks which are often not altered by common pathologies may be a strategy for creating consistent JCS which will be less likely to be affected by wrist pathology.

Potential limitations exist in this study, which the authors have attempted to minimize. The generation and calculation of wrist angle of the assessed JCSs were based on the interpretation of previously described methodologies. Anatomical points and methodologies were replicated to the best of the authors abilities based on the descriptions in previous publications. Furthermore, this study only examined planar motion pathways, as opposed to complex composite motion such as the dart thrower motion. Simplified planar motion was simulated as it allowed for a highly standardized experimental setup. Additionally, complex motions are more difficult to measure clinically and as such, it would have been difficult to repeatably measure wrist angle to use as our independent variable. Lastly, the performance of these JCSs

were not analyzed during a pronation-supination motion pathway but the authors believe this would be of interest to analyze in the future.

3.5 Conclusions

The results of this JCS comparison do not favor one JCS generation method over another, as all were found to be similar and differences are not thought to be clinically significant. These findings support the use of any of the currently analyzed JCS generation methods; however, a practical advantage of using certain methods including the methods developed by Padmore et al, and Hillstrom et al. are that the required digitized points to form the JCSs are palpable. Due to the findings of this chapter, a JCS_A that employs palpable landmarks along the dorsal surface of the forearm and hand will be used in the forthcoming chapters.

3.6 References

1. Wang Q, Markopoulos P, Yu B, Chen W, Timmermans A. Interactive wearable systems for upper body rehabilitation: A systematic review. *J Neuroeng Rehabil*. 2017;14(1):1-21. doi:10.1186/s12984-017-0229-y

2. Isa AD, Mcgregor ME, Padmore CE, et al. An In Vitro Study to Determine the Effect of Ulnar Shortening on Distal Forearm Loading During Wrist and Forearm Motion: Implications in the Treatment of Ulnocarpal Impaction. *J Hand Surg Am*. 2019;44(8):669-679. doi:10.1016/j.jhsa.2019.04.007

3. Padmore CE, Stoesser H, Nishiwaki M, et al. The Effect of Dorsally Angulated Distal Radius Deformities on Carpal Kinematics: An In Vitro Biomechanical Study. *J Hand Surg Am*. 2018;43(11):1036.e1-1036.e8. doi:10.1016/j.jhsa.2018.02.017

4. Short WH, Werner FW, Green JK, Masaoka S, Walter H. Short, MD, Frederick W. Werner, MME, Jason K. Green, BS, and Shunji Masaoka, MD P. Biomechanical Evaluation of Ligamentous Stabilizers of the Scaphoid and Lunate. *J hand surg am*. 2002;27(6):991-1002. doi:10.1053/jhsu.2002.35878.Biomechanical

5. Stoesser H, Padmore C, Nishiwaki M, Gammon B, Langohr G, Johnson J. Biomechanical Evaluation of Carpal Kinematics during Simulated Wrist Motion. *J Wrist Surg*. 2016;06(02):113-119. doi:10.1055/s-0036-1588025

6. Garcia-Elias M, Cooney WP, An KN, Linscheid RL, Chao EYS. Wrist kinematics after limited intercarpal arthrodesis. *J Hand Surg Am*. 1989. doi:10.1016/S0363-5023(89)80077-2

7. Short WH, Palmer AK, Werner FW, Murphy DJ. A biomechanical study of distal radial fractures. *J Hand Surg Am*. 1987. doi:10.1016/S0363-5023(87)80202-2

8. Coburn JC, Upal MA, Crisco JJ. Coordinate systems for the carpal bones of the wrist. *J Biomech*. 2007;40(1):203-209. doi:10.1016/j.jbiomech.2005.11.015

9. Padmore C, Stoesser H, Langohr GD, Johnson J, Suh N. Carpal Kinematics following Sequential Scapholunate Ligament Sectioning. *J Wrist Surg*. 2019;08(02):124-131.

doi:10.1055/s-0038-1676865

10. Nishiwaki M, Welsh M, Gammon B, Ferreira LM, Johnson JA, King GJW. Distal radioulnar joint kinematics in simulated dorsally angulated distal radius fractures. *J Hand Surg Am*. 2014;39(4):656-663. doi:10.1016/j.jhsa.2014.01.013

11. Werner FW, Palmer AK, Somerset JH, et al. Wrist joint motion simulator. *J Orthop Res*. 1996;14(4):639-646. doi:10.1002/jor.1100140420

12. Hillstrom HJ, Garg R, Kraszewski A, et al. Development of an anatomical wrist joint coordinate system to quantify motion during functional tasks. *J Appl Biomech*. 2014;30(4):586-593. doi:10.1123/jab.2011-0094

13. Rainbow MJ, Kamal RN, Leventhal E, et al. In vivo kinematics of the scaphoid, lunate, capitate, and third metacarpal in extreme wrist flexion and extension. *J Hand Surg Am*. 2013;38(2):278-288. doi:10.1016/j.jhsa.2012.10.035

14. Wu G, Van Der Helm FCT, Veeger HEJ, et al. ISB Recommendation on Definitions of Joint Coordinate Systems of Various Joints for the Reporting of Human Joint Motion - Part II: Shoulder, Elbow, Wrist and Hand. *J Biomech*. 2005;38(5):981-992. doi:10.1016/j.jbiomech.2004.05.042

15. Moojen TM, Snel JG, Ritt MJPF, Venema HW, Kauer JMG, Bos KE. In vivo analysis of carpal kinematics and comparative review of the literature. *J Hand Surg Am*. 2003;28(1):81-87. doi:10.1053/jhsu.2003.50009

16. Snel JG, Venema HW, Moojen TM, Ritt MJPF, Grimbergen CA, Den Heeten GJ. Quantitative in vivo analysis of the kinematics of carpal bones from three-dimensional CT images using a deformable surface model and a three-dimensional matching technique. *Med Phys*. 2000;27(9):2037-2047. doi:10.1118/1.1289896

17. Crisco JJ, Pike S, Hulsizer-Galvin DL, Akelman E, Weiss APC, Wolfe SW. Carpal Bone Postures and Motions Are Abnormal in Both Wrists of Patients with Unilateral Scapholunate Interosseous Ligament Tears. *J Hand Surg Am*. 2003;28(6):926-937. doi:10.1016/S0363-5023(03)00422-2

18. Shah DS, Kedgley AE. Control of a wrist joint motion simulator: A phantom study. *J Biomech*. 2016;49(13):3061-3068. doi:10.1016/j.jbiomech.2016.07.001

19. Belsole RJ, Hilbelink DR, Llewellyn JA, Stenzler S, Greene TL, Dale M. Mathematical analysis of computed carpal models. *J Orthop Res*. 1988;6(1):116-122. doi:10.1002/jor.1100060115

20. Feipel V, Rooze M. Three-dimensional motion patterns of the carpal bones: An in vivo study using three-dimensional computed tomography and clinical applications. *Surg Radiol Anat*. 1999. doi:10.1007/s00276-999-0125-7

Chapter 4

4 Comparison of a CT-Based Joint Congruency Method for Assessing Joint Contact Mechanics of the Wrist

OVERVIEW

The investigation of articular contact patterns has been useful in examining disease progression mechanisms at the hip, knee, shoulder and elbow. However, due to the small size and variable curvature of the wrist articulations, contact has been difficult to previously quantify using traditional direct approaches. Due to the difficulties in measuring articular joint contact at the wrist, few studies have been able to examine joint contact across a motion arc; and this study looks to build on those previous few that have been able to quantify joint contact across a motion arc. The objective of this chapter is to use a non-invasive CT-based technique to measure articular contact at the wrist. The secondary objective of this study is to use Tekscan® to validate this CT-based technique for measuring contact at the wrist.

4.1 Introduction

In the investigation of joint biomechanics, knowledge of joint contact is useful in identifying normal and pathologic mechanics. As described in detail in Chapter 1 (Section 1.4) a variety of *in-vitro* methods have been employed to gain information regarding joint contact including various casting[1], and pressure-sensitive films.[2–4] More recently, as discussed (Section 1.4.2.1), imaging based techniques have been used to examine joint contact mechanics at the wrist including CT[5] and MRI based[6,7] methods. However, except for those including dynamic CT[8,9]as an imaging modality, studies have not quantified wrist contact mechanics throughout motion to date.

Cadaver studies have used pressure-sensitive film to determine contact and load distribution patterns in the radiocarpal and midcarpal joints under static loading. [2,3,10] However, it should be noted that pressure sensitive film cannot sufficiently address the complex *in-vivo* conditions, particularly when looking to assess the effectiveness of surgical techniques. Additionally, these methods employ partial or complete joint exposure, thereby potentially altering the joint kinematics by disturbing soft tissue stabilizers. Moreover, the interposition of the transducer is invasive and may affect the joint contact measurement.

Novel indirect methods of assessing joint contact have also been developed.[11–13] Indirect methods have the advantage of being non-invasive and use 3D imaging modalities (*i.e.* CT), or magnetic resonance imaging) in conjunction with computational means to evaluate the relative position and interaction between adjacent articular surfaces. MRI studies have the advantage of excellent soft tissue contrast but exhibit poor bone contrast and have rather involved experimental scanning protocols to capture an entire range of motion. In contrast, CT based studies have excellent bony distinction; however, in some studies that employ scanning intact specimens, cartilage thickness must be estimated and applied in post processing. In order to eliminate this assumption in cadaveric studies, specimens can be denuded of all soft tissue following experimental protocols, and accurate cartilage thickness can be ascertained by scanning denuded bones and using air as a contrast to delineate articular cartilage from bone.[14,15] Indirect methods have been used to investigate larger joints such as the hip, knee,

shoulder and elbow; however, they have yet to be used and validated in smaller joints such as the wrist.

More recently, a novel indirect technique of assessing joint contact mechanics, Inter-Cartilage Distance (ICD), was developed by Lalone and co-workers.[16,17] ICD has been validated in the elbow and applied to the distal radioulnar joint (DRUJ); however, it has yet to be applied to the wrist. Compared with other indirect techniques which rely on distances between osseous structures, ICD relies on the use of cartilage models. The cartilage morphology is derived from CT scans performed with air as the contrast. These models incorporate regional variations in cartilage thickness and have been shown to be highly accurate to within ±0.3 mm.[14] The cartilage bearing models are then registered to kinematic data that has been collected using an optical tracking system. This method allows for the visualization of 3D cartilage bearing models throughout a motion arc. The interaction between the cartilage bearing models can then be evaluated, and isocontoured colour maps are used to display the degree of proximity between adjacent articulating surfaces. However, due to cartilage thickness variation between joints, threshold values should be tailored to the joint of investigation to reliably predict joint contact area. As this indirect technique has yet to be used at the wrist, a reliable threshold value has yet to be identified.

Prior to the use of indirect methods and computational model, validation of these models should be performed to evaluate their validity and agreement with current gold standard experimental studies. Previous literature can be useful in providing overall trends and establish confidence in indirect methods, however direct validation to experimental outcomes is imperative. *Tekscan*® or Fuji film are often the direct modalities used at the wrist to quantify contact mechanics. Johnson et al.[18] used *Tekscan*® as the gold standard to validate an indirect MRI based joint contact technique, as the reliability of the direct contact area measurement has also been shown in a previous validation study examining wrist joint contract.[19]

In this study, we sought modified a current non-invasive joint congruency (ICD) methodology to make it suitable for use at the wrist. Secondly, we sought to validate the non-invasive joint congruency method at the wrist using *Tekscan*®. The joints assessed in this chapter to validate ICD were the radioscaphoid and radiolunate joints.

4.2 Methods

4.2.1 Specimen Preparation

One cadaveric previously frozen upper extremity (right arm, male, 67 years) was surgically prepared for mounting to a wrist simulator, as described in Chapter 2 (Section 2.2.1) (Figure 4-1). Optical tracking markers (Optotrak Certus; Northern Digital, Waterloo, Canada) were attached to the lunate, scaphoid, third metacarpal, and radius using a 2.7 mm bone screw. To expose the lunate, a small transverse arthrotomy was performed. The lunate tracker was attached dorsal to volar, 40º dorsal from the horizontal plane, while the third metacarpal tracker was attached dorsal to palmar, perpendicular from the horizontal plane. To expose the scaphoid, a small arthrotomy was performed on the volar aspect of the wrist. The scaphoid tracker was attached volar to palmar, 50° from the horizontal plane. To expose the radius and the extensor tendons, an incision was made along the dorsal aspect of the forearm. The radial tracker was secured in the distal 1/3 of the radius in line with the first metacarpal in the neutral wrist position. Subsequently, the flexor and extensor tendons of the wrist including: extensor carpi radialis brevis (ECRB), extensor carpi radialis longus (ECRL), extensor carpi ulnaris (ECU), flexor carpi radialis (FCR) and flexor carpi ulnaris (FCU), had Krackow locking sutures placed at their musculotendinous junctions and connected to pneumatic actuators via 100-lbs braided fishing line. A nylon threaded rod was then inserted longitudinally into the third metacarpal. The specimen was mounted to the passive motion simulator (Figure 4-1) via a humeral clamp. The nylon threaded rod that had been previously inserted into the third metacarpal was positioned in the guide rail. The guide rail was used to hold static wrist positions during the testing protocol and restrict out of plane motion. A dorsal incision exposing the radiocarpal joint was performed and a Tekscan® sensor was inserted.

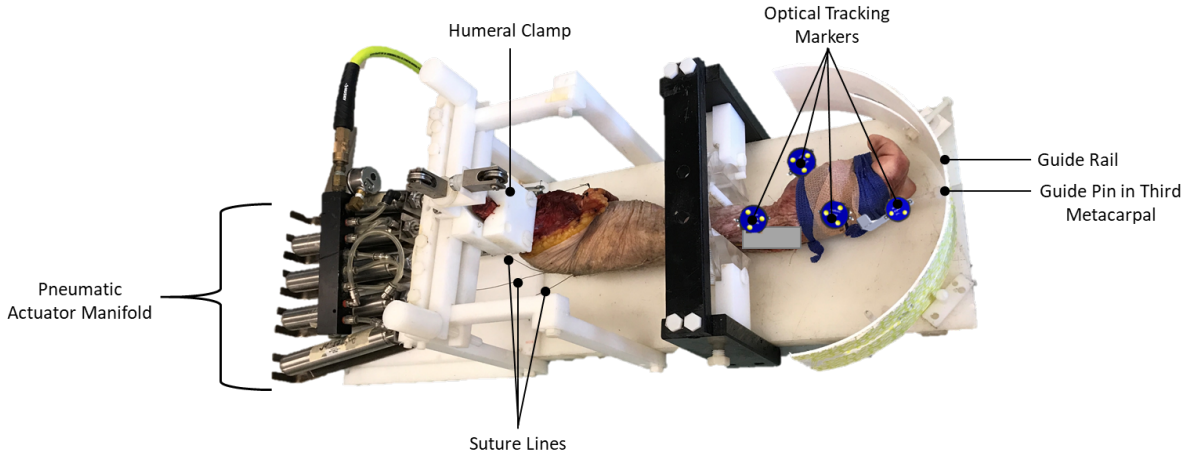

Figure 4-1 Passive Wrist Joint Motion Simulator.

The cadaveric specimen was surgically prepared and then mounted to the simulator using the humeral clamp. The tendons of the relevant muscles involved in wrist flexion and extension were attached to braided fishing line and then attached to the pneumatic actuators.

4.2.2 Experimental Protocol

Three static wrist positions (50° wrist flexion, neutral, and 50° wrist extension) were simulated using the simulator. While the static positions were simulated, tone loads of ~10N were applied to each flexor and extensor tendons of the forearm to simulate the *in-vivo* compressive loading of the wrist. Optical tracking was used to collect positional and rotational data of the bones of interest (Optotrak Certus®, NDI, Waterloo, ON, Canada). The previously inserted Tekscan® (Medical Sensor 4201) sensors were initially positioned in the scaphoid fossa to collect radioscaphoid contact data and then subsequently repositioned to the radiolunate fossa to collect radiolunate contact data. This process was repeated three times at each static position. As some variability existed within *Tekscan*® experimental data collection, the average of the three trials was used.

Subsequent to testing, all soft tissues were removed, and the wrist was disarticulated. Four fiducial markers (4.7mm optically reflective nylon spheres attached to threaded screws) were secured to the denuded bones (Figure 4-2). The fiducial markers were placed in an optimal configuration based on previous literature.[14] Care was taken to ensure that a pair of fiducials were placed distally and two proximally as well as radially and ulnarly, as this was found to produce the least registration error. The surface of each bone along with all four fiducial

markers were digitized with a calibrated stylus. A post-testing CT scan of the denuded bones with the fiducial markers affixed was acquired. The cartilage covered bones of interest were scanned in air to ascertain the specimens' cartilage thickness. The CT scans were performed using a GE Discovery CT750 HD scanner (GE Healthcare, Pewaukee, WI) at 120 kv and 292 mAs with a slice thickness of 0.625 mm.

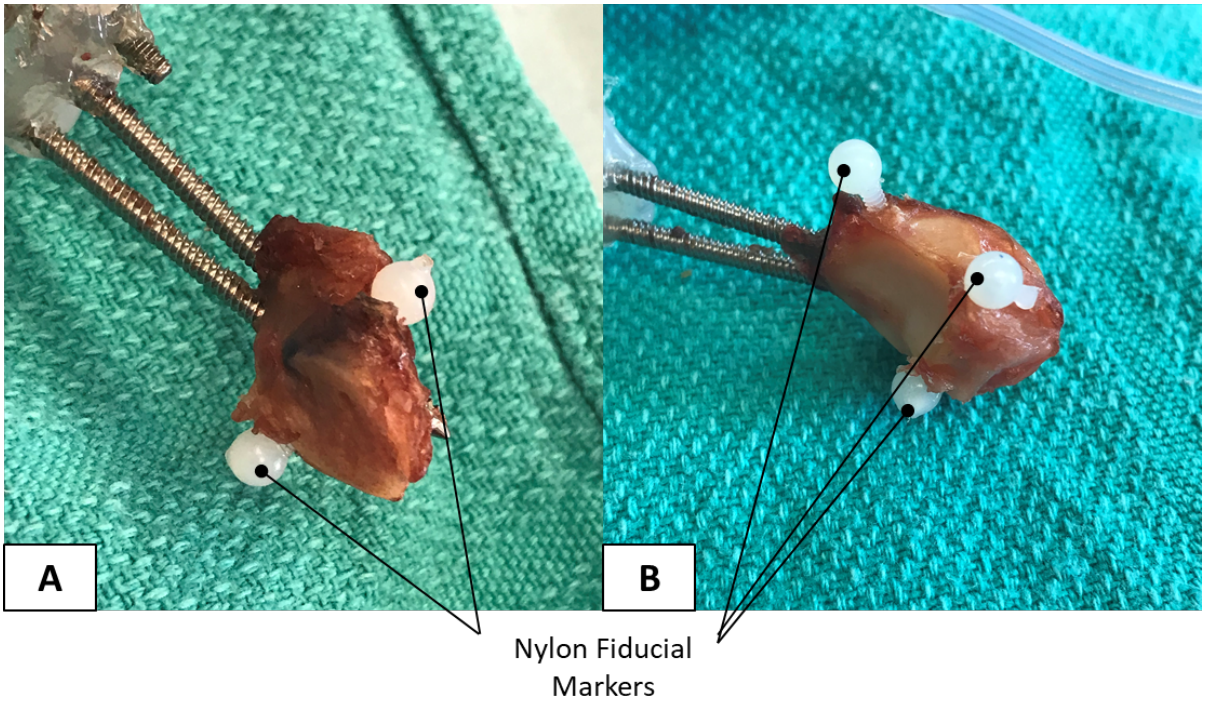

Figure 4-2 Nylon Fiducial Markers.

Four fiducial markers (4.7mm optically reflective nylon spheres attached to threaded screws) were secured to the denuded (A) scaphoid and (B) lunate.

4.2.3 Inter-Cartilage Distance Analysis

The CT image data was imported into Mimics Research (version 21.0, Materialise, Leuven, Belgium). Three-dimensional (3D) reconstructed surface models of the scaphoid, lunate, radius (+250 HU), and cartilage (-700HU) were created using semi-automated segmentation. Models were then processed to create sealed hollow-shell models that were exported as sterolithography format. A homologous paired-point registration was employed to render the 3D models into their respective position based on the collected optical tracking data and

subsequent digitization of the bones' surface and fiducial markers. The registration protocol employing fiducial markers has been previously described.[20]

Cartilage models of the scaphoid, lunate and radius were reassembled using kinematic data over the arc of active wrist motion. An inter-cartilage distance algorithm was applied and visualized in Paraview VTK toolkit (Paraview 4.4.1 Parallel Visualization Application; open source). Contact was defined as the cartilage-cartilage overlap between the radius and scaphoid (radioscaphoid contact), or radius and lunate (radiolunate contact). Contact area was calculated for the specified location by integration of the triangular mesh of the contact patch. The contact area was visualized on the surface of the distal radius. Visualization of the inter-cartilage radioscaphoid distances were displayed using an isocontoured proximity map (assigning distances a unique colour) that was then projected onto the surface of the radius' articular surface.

4.2.4 Validation

Following quantification of the contact area from *Tekscan*® and ICD, the two modalities were compared quantitatively. If the model data fell within two times the accuracy of the experimental measure, then the validation criteria was met.[21] The accuracy of *Tekscan*® sensors has been previously accessed and found to be depended on the specific sensor used and its resolution. Previous literature has reported *Tekscan*® error as low as 4-12%.[19,22] Using this error level, we set the validation criteria for specimen-specific model outcome data within two times the expected experimental error (within 25%).

In addition to the validation criteria above, we evaluated the threshold level used when defining articular contact. In the development of the ICD technique, any degree of cartilage-cartilage overlap was defined as articular contact. To evaluate the agreement of this chief assumption varying threshold levels between -2mm and +4mm of proximity were plotted against their resulting contact area magnitude and a polynomial line of best fit was added. The contact area

obtained from *Tekscan*® was added to each figure and the intercept between the *Tekscan*® contact magnitude and the line of best fit was determined (Figure 4-3).

4.2.5 Statistical Analysis

To understand the repeatability in the ICD and *Tekscan*® measurements, and determine if their measurement variance was similar, a F-Test was performed for each wrist position. Statistical significance was set at $p<.05$.

4.3 Results

Contact area of the radioscaphoid and radiolunate joints was quantified using *Tekscan*® and ICD. Data presented is the mean radioscaphoid and radiolunate contact area ± standard deviation of the three trials executed at each wrist angle (wrist flexion, neutral and wrist extension) unless otherwise specified.

4.3.1 Validity of Threshold Value

The intercept values for all six three wrist positions from the two joints, for a total of six cases, were averaged. This averaged value of 0.1± 0.3 mm was deemed a reliable threshold value which would accurately predict joint contact area (Figure 4-3).

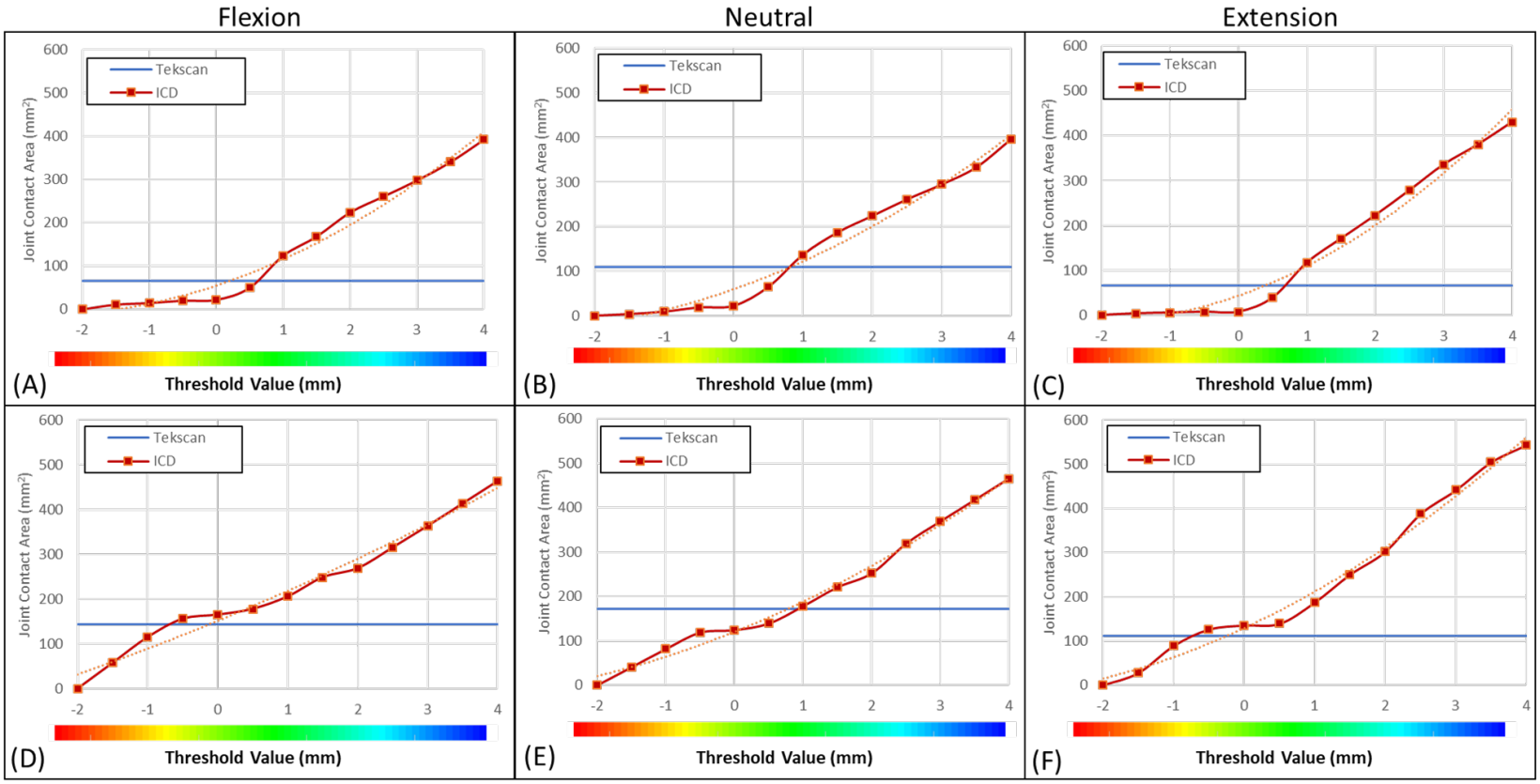

Figure 4-3: Threshold level determination based on *Tekscan*®.

The relationship between threshold value and joint contact area for ICD is shown. This relationship was investigated 6 times (3 joints positions and 2 joints) (A-C) Radiolunate joint (D-F) Radioscaphoid joint contact area. Varying threshold levels between -2mm and +4mm of proximity were plotted against their resulting contact area magnitude, and a polynomial line of best fit was added to the ICD calculated joint contact area. The intercept of the joint contact area calculated by Tekscan® (solid blue line), and the line of best fit of the ICD calculated joint contact area was identified. The intercept values for all six trials cases were averaged, and this averaged value of 0.14mm was deemed a reliable threshold value which would accurately predict joint contact area.

4.3.2 Radiolunate Joint Contact Area

With the wrist flexed to 50°, contact area of radiolunate joint was measured as 64 mm^2 using *Tekscan*®, and 45 mm^2 using ICD (Figure 4-4). In neutral wrist position, radiolunate contact area was 112 mm^2 using *Tekscan*®, and 76 mm^2 with ICD. At 50° of wrist extension, radiolunate joint contact area was measured as 67 mm^2 using Tekscan and 56 mm^2 with ICD. The agreement of the ICD value to the experimental *Tekscan*® values were 17%, 37%, and 30%, respectively for wrist extension, neutral wrist position and wrist flexion. The variance in measurement for the three trials was also found to be similar between *Tekscan*® and ICD at all three wrist positions ($p>.05$).

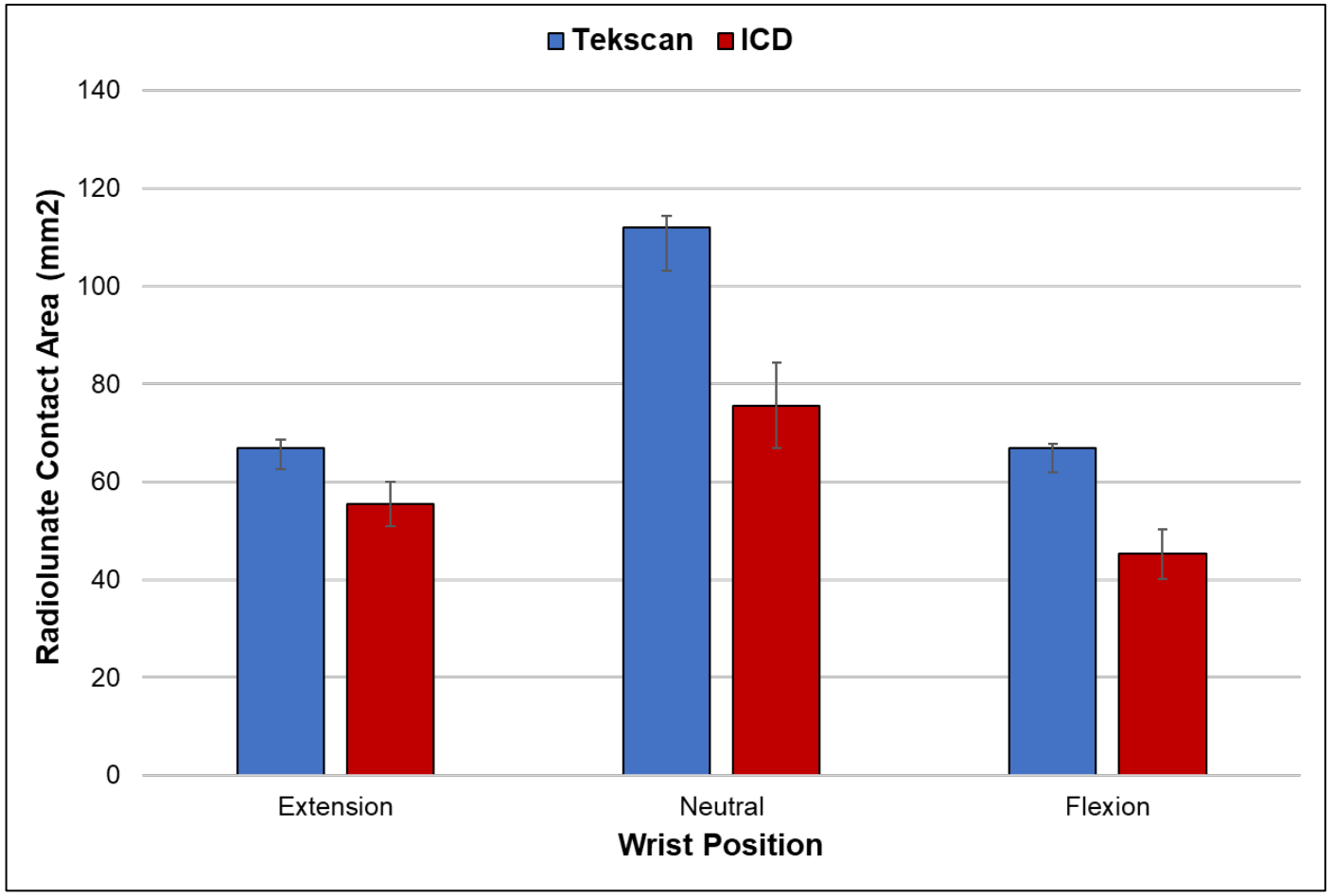

Figure 4-4 Mean radiolunate joint contact area measured by Tekscan® and calculated by ICD.

The mean contact area for the radiolunate joint measured by Tekscan® and ICD.

4.3.3 Radioscaphoid Joint Contact Area

With the wrist flexed to 50°, contact area of radioscaphoid joint was measured as 115 mm2 using Tekscan®, and 132 mm^2 using ICD (Figure 4-5). In neutral wrist position, radioscaphoid contact area was measured as 163 mm^2 using Tekscan®, and 145 mm^2 with ICD. At 50° of wrist extension, radioscaphoid joint contact area was measured as 163 mm^2 using Tekscan® and 132 mm^2 with ICD. The agreement of the ICD value to the experimental Tekscan® values were 11%, 11%, and 13% respectively for wrist extension, neutral wrist position and wrist flexion. The variance in measurement for the three trials was also found to be similar between Tekscan® and ICD at all three wrist positions ($p>.05$).

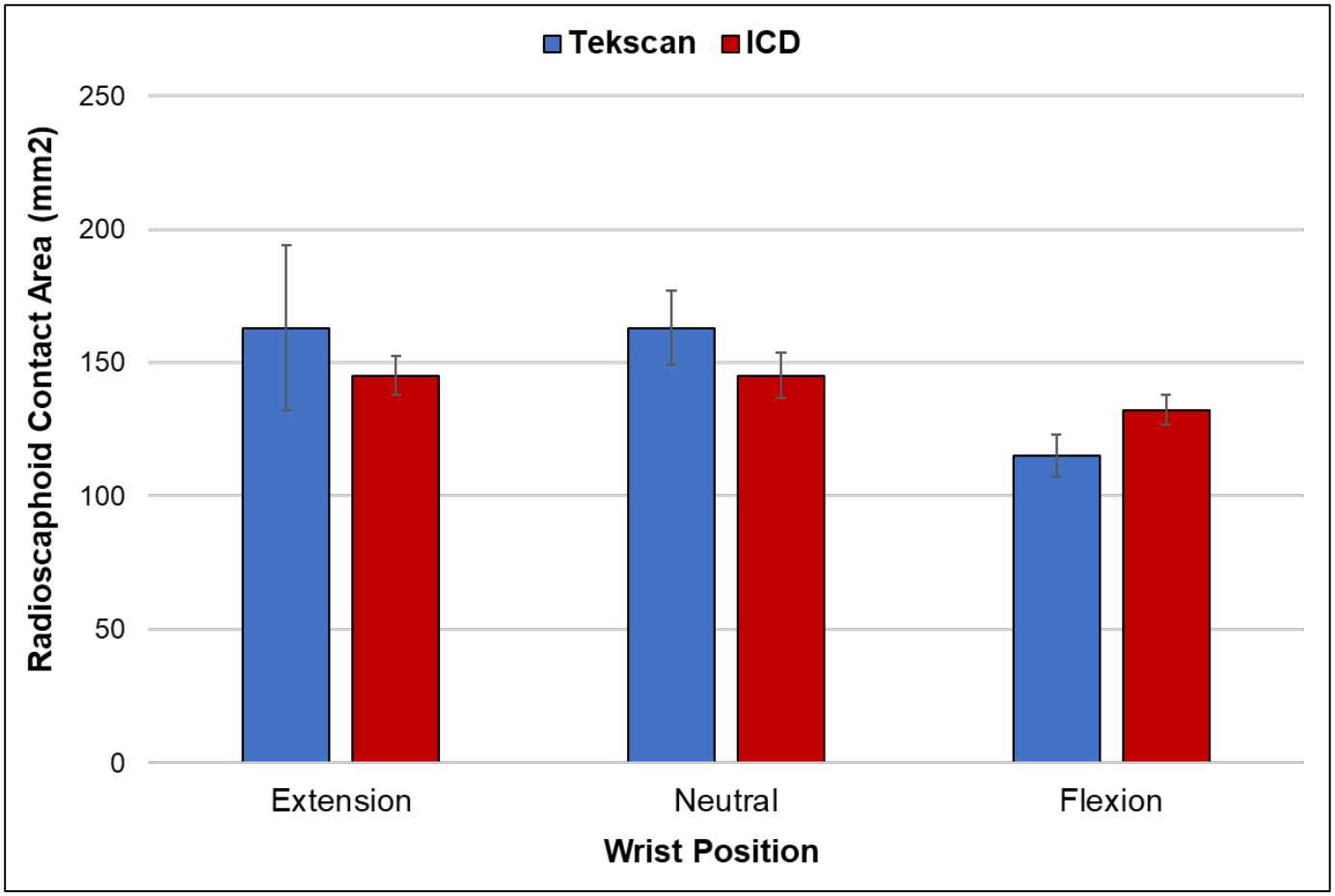

Figure 4-5 Radioscaphoid joint contact area measured by Tekscan® and calculated by a CT-based joint congruency method.

The contact area measurements presented are an average of three trial

4.4 Discussion

The current study presents the application of ICD for modeling joint congruency in the wrist and compares the contact area magnitude from ICD to Tekscan®. Similar trends in the magnitude of contact area were observed when comparing ICD to Tekscan®. This was in contrast to previous work which compared ICD to Tekscan® at the DRUJ and reported notably larger contact area measurements with the ICD measurement technique. Furthermore, our validity criteria was such that ICD measurements were required to be within 25% of those of Tekscan® to be deemed valid; ICD contact are was within 12% for the radioscaphoid joint, while 30% for the radiolunate joint in comparison to the Tekscan® measurements. Furthermore, this study performed an evaluation of the threshold value used in ICD to define contact area. The threshold value found was near zero (0.1 ± 0.3mm), representing that all regions of cartilage-cartilage overlap should be considered in contact area measurements at the wrist.

In contrast to work performed by Gammon et al. who reported ICD contact area values three times larger than Tekscan®, this study found similar trends between the two techniques.23 The large difference in calculated joint contact area observed by Gammon et al may be attributed to an unreliable threshold level, as they used a value of 2.8 mm, that was based on previous ICD work in the elbow. In this study radioscaphoid joint contact area measured from ICD was much closer to the Tekscan® measurements at only 12% difference, whereas ICD radiolunate joint contact area measurements differed by 30% in comparison to Tekscan®. The large difference may be attributed to the difficult data collection process of Tekscan®. Reliable insertion and positioning of the Tekscan® film into radiolunate joint was vastly more difficult due to difficulties with visualization and access.

Figure 4-3 shows the relationship between threshold value and calculated contact area. As the threshold value increases, so does the number of recruited points. Identifying a suitable threshold value which accurately predicts joint contact area is imperative. This study found a threshold value of 0.1 ± 0.3 mm reliably predicts joint contact area at the wrist. This value is significantly smaller than the value used in previous work by Lalone et al.16 The results of this study showed that ICD is a viable technique to investigate joint mechanics at the wrist, however, details such as threshold value need to be tailored for the specific joint.

Presently, a gold standard to validate computational models does not exist as direct measurement techniques are prone to variability.[21]. Tekscan® specifically has inherent limitations. Measurements are prone to variability within and across specimen trials. For example, in this study, the contact area measurement for the radiolunate joint was very repeatable resulting in small deviations between trials. However, the measurement of radioscaphoid joint contact area was less repeatable, causing higher deviations between trials. The difference in repeatability was most likely due to the difficultly we had at accessing and placing the Tekscan® in the radioscaphoid articulation. The sectioning of capsuloligamentous structures to introduce the Tekscan® film may alter the joint mechanics and in turn the measured joint contact area. Moreover, the introduction of material into the joint with an inherent stiffness and thickness may distract the articular surfaces apart, again leading to an altered measurements of joint contact area. Lastly, Tekscan® is prone to other aspects which affect its reliability as well, including incorrect calibration, liquid saturation, migration of the sensor position, and shear stress across the film causing deformation.[24] Even with direct measurement limitations, experiments can provide a reasonable idea of model performance.

There are some limitations of the ICD technique. ICD relies are CT scans to generate cartilage bearing models for the bones of interest. The CT scans that were captured for this study, used a clinical CT scanner with a slice thickness 0.625 mm. A slice thickness of 0.625 mm has the potential to introduce volume averaging artifact at the periphery of the joint surfaces, which may in turn cause model size discrepancies. The accuracy of cartilage models is reported to be 0.3 mm at the elbow joint, however this accuracy may differ at the wrist.[14] Additionally, ICD accuracy is contingent upon the optical tracking system used for characterizing the position and orientation of the radius and ulna in vitro. If a direct line of sight between the camera and the position sensors is maintained and kept within 2.5 m, then reported accuracy is up to 0.1 mm. Error may be higher, however, if conditions vary from this scenario.

4.5 Conclusions

Modifications to a previously developed approach for examining joint contact mechanics were performed to optimize the ICD technique for the wrist joint. The ICD technique will be employed in the studies described in forthcoming chapters (Chapters 5 & 6) to examine joint contact mechanics during dynamic wrist motion.

4.6 References

1. Momose T. Cartilage degeneration and measurement of the contact area of the trapeziometacarpal joint: Morphological observation. *J Japanese Orthop Assoc*. 1994;68(5):426-434.

2. Pogue DJ, SF V, RM P, et al. Effects of distal radius fracture malunion on wrist joint mechanics. *J Hand Surg Am*. 1990;15(5):721-727.

3. Viegas SF, Patterson RM. Load Mechanics of the Wrist. *Hand Clin Clin*. 1997;13(1):109-128.

4. McNary SM, Heyrani N, Volk I, Szabo RM, Bayne CO. The Effect of Radioscapholunate Fusion With and Without Distal Scaphoid and Triquetrum Excision on Capitolunate Contact Pressures. *J Hand Surg Am*. 2019;44(5):420.e1-420.e7. doi:10.1016/j.jhsa.2018.07.009

5. Rainbow MJ, Kamal RN, Leventhal E, et al. In vivo kinematics of the scaphoid, lunate, capitate, and third metacarpal in extreme wrist flexion and extension. *J Hand Surg Am*. 2013;38(2):278-288. doi:10.1016/j.jhsa.2012.10.035

6. Johnson JE, Lee P, McIff TE, Toby EB, Fischer KJ. Scapholunate ligament injury adversely alters in vivo wrist joint mechanics: An MRI-based modeling study. *J Orthop Res*. 2013;31(9):1455-1460. doi:10.1002/jor.22365

7. Johnson JE, Lee P, McIff TE, Toby EB, Fischer KJ. Effectiveness of surgical reconstruction to restore radiocarpal joint mechanics after scapholunate ligament injury: An in vivo modeling study. *J Biomech*. 2013;46(9):1548-1553. doi:10.1016/j.jbiomech.2013.03.020

8. Foumani M, Strackee SD, Van De Giessen M, Jonges R, Blankevoort L, Streekstra GJ. In-vivo dynamic and static three-dimensional joint space distance maps for assessment of cartilage thickness in the radiocarpal joint. *Clin Biomech*. 2013;28(2):151-156. doi:10.1016/j.clinbiomech.2012.11.005

9. Foumani M, Strackee SD, Stekelenburg CM, Blankevoort L, Streekstra GJ. Dynamic

in vivo evaluation of radiocarpal contact after a 4-corner arthrodesis. *J Hand Surg Am*. 2015;40(4):759-766. doi:10.1016/j.jhsa.2014.11.028

10. Tang P, Gauvin J, Muriuki M, Pfaeffle JH, Imbriglia JE, Goitz RJ. Comparison of the "Contact Biomechanics" of the Intact and Proximal Row Carpectomy Wrist. *J Hand Surg Am*. 2009;34(4):660-670. doi:10.1016/j.jhsa.2008.12.004

11. Omori S, Moritomo H, Omokawa S, Murase T, Sugamoto K, Yoshikawa H. In vivo 3-dimensional analysis of dorsal intercalated segment instability deformity secondary to scapholunate dissociation: A preliminary report. *J Hand Surg Am*. 2013;38(7):1346-1355. doi:10.1016/j.jhsa.2013.04.004

12. Kawanishi Y, Moritomo H, Omokawa S, Murase T, Sugamoto K, Yoshikawa H. In vivo 3-dimensional analysis of stage III kienböck disease: Pattern of carpal deformity and radioscaphoid joint congruity. *J Hand Surg Am*. 2015;40(1):74-80. doi:10.1016/j.jhsa.2014.10.035

13. Ateshian GA, Kwak SD, Soslowsky LJ, Mow VC. A stereophotogrammetric method for determining in situ contact areas in diarthrodial joints, and a comparison with other methods. *J Biomech*. 1994;27(1):111-124. doi:10.1016/0021-9290(94)90038-8

14. Lalone EA, Willing RT, Shannon HL, King GJW, Johnson JA. Accuracy assessment of 3D bone reconstructions using CT: an intro comparison. *Med Eng Phys*. 2015;37(8):729-738. doi:10.1016/j.medengphy.2015.04.010

15. Willing R, Lapner M, Lalone EA, King GJW, Johnson JA. Development of a computational technique to measure cartilage contact area. *J Biomech*. 2014;47(5):1193-1197. doi:10.1016/j.jbiomech.2014.01.047

16. Lalone E a., Giles JW, Alolabi B, Peters TM, Johnson J a., King GJW. Utility of an image-based technique to detect changes in joint congruency following simulated joint injury and repair: An in vitro study of the elbow. *J Biomech*. 2013;46(4):677-682. doi:10.1016/j.jbiomech.2012.11.047

17. Lalone EA, McDonald CP, Ferreira LM, Peters TM, King GW, Johnson JA.

Development of an image-based technique to examine joint congruency at the elbow. *Comput Methods Biomech Biomed Engin*. 2012;5842(January):37-41. doi:10.1080/10255842.2011.617006

18. Johnson JE, McIff TE, Lee P, Toby EB, Fischer KJ. Validation of radiocarpal joint contact models based on images from a clinical MRI scanner. *Comput Methods Biomech Biomed Engin*. 2014;17(4):378-387. doi:10.1080/10255842.2012.684446

19. Fischer KJ, Johnson JE, Waller AJ, McIff TE, Bruce Toby E, Bilgen M. MRI-based modeling for radiocarpal joint mechanics: Validation criteria and results for four specimen-specific models. *J Biomech Eng*. 2011;133(10):1-7. doi:10.1115/1.4005171

20. Lalone EA, Peters TM, King GW, Johnson JA. Accuracy assessment of an imaging technique to examine ulnohumeral joint congruency during elbow flexion. *Comput Aided Surg*. 2012;17(3):142-152. doi:10.3109/10929088.2012.673638

21. Henninger HB, Reese SP, Anderson AE, Weiss JA. Validation of computational models in biomechanics. *Proc Inst Mech Eng Part H J Eng Med*. 2010;224(7):801-812. doi:10.1243/09544119JEIM649

22. Wilson DC, Niosi CA, Zhu QA, Oxland TR, Wilson DR. Accuracy and repeatability of a new method for measuring facet loads in the lumbar spine. *J Biomech*. 2006;39(2):348-353. doi:10.1016/j.jbiomech.2004.12.011

23. Gammon B. Arthrokinematics of the Distal Radioulnar Joint in the Normal Wrist and Following Distal Radius Malunion. 2016. doi:Electronic Thesis and Dissertation Repository. 3713. https://ir.lib.uwo.ca/etd/3713

24. Wilharm A, Hurschler C, Dermitas T, Bohnsack M. Use of Tekscan K-scan sensors for retropatellar pressure measurement avoiding errors during implantation and the effects of shear forces on the measurement precision. *Biomed Res Int*. 2013;2013. doi:10.1155/2013/829171

Wrist Joint Kinematics is Affected by Forearm Position during Active Flexion and Extension

1. Momose T. Cartilage degeneration and measurement of the contact area of the

trapeziometacarpal joint: Morphological observation. *J Japanese Orthop Assoc*. 1994;68(5):426-434.

2. Pogue DJ, SF V, RM P, et al. Effects of distal radius fracture malunion on wrist joint mechanics. *J Hand Surg Am*. 1990;15(5):721-727.

3. Viegas SF, Patterson RM. Load Mechanics of the Wrist. *Hand Clin Clin*. 1997;13(1):109-128.

4. McNary SM, Heyrani N, Volk I, Szabo RM, Bayne CO. The Effect of Radioscapholunate Fusion With and Without Distal Scaphoid and Triquetrum Excision on Capitolunate Contact Pressures. *J Hand Surg Am*. 2019;44(5):420.e1-420.e7. doi:10.1016/j.jhsa.2018.07.009

5. Rainbow MJ, Kamal RN, Leventhal E, et al. In vivo kinematics of the scaphoid, lunate, capitate, and third metacarpal in extreme wrist flexion and extension. *J Hand Surg Am*. 2013;38(2):278-288. doi:10.1016/j.jhsa.2012.10.035

6. Johnson JE, Lee P, McIff TE, Toby EB, Fischer KJ. Scapholunate ligament injury adversely alters in vivo wrist joint mechanics: An MRI-based modeling study. *J Orthop Res*. 2013;31(9):1455-1460. doi:10.1002/jor.22365

7. Johnson JE, Lee P, McIff TE, Toby EB, Fischer KJ. Effectiveness of surgical reconstruction to restore radiocarpal joint mechanics after scapholunate ligament injury: An in vivo modeling study. *J Biomech*. 2013;46(9):1548-1553. doi:10.1016/j.jbiomech.2013.03.020

8. Foumani M, Strackee SD, Van De Giessen M, Jonges R, Blankevoort L, Streekstra GJ. In-vivo dynamic and static three-dimensional joint space distance maps for assessment of cartilage thickness in the radiocarpal joint. *Clin Biomech*. 2013;28(2):151-156. doi:10.1016/j.clinbiomech.2012.11.005

9. Foumani M, Strackee SD, Stekelenburg CM, Blankevoort L, Streekstra GJ. Dynamic in vivo evaluation of radiocarpal contact after a 4-corner arthrodesis. *J Hand Surg Am*. 2015;40(4):759-766. doi:10.1016/j.jhsa.2014.11.028

10. Tang P, Gauvin J, Muriuki M, Pfaeffle JH, Imbriglia JE, Goitz RJ. Comparison of the "Contact Biomechanics" of the Intact and Proximal Row Carpectomy Wrist. *J Hand Surg Am*. 2009;34(4):660-670. doi:10.1016/j.jhsa.2008.12.004

11. Omori S, Moritomo H, Omokawa S, Murase T, Sugamoto K, Yoshikawa H. In vivo 3-dimensional analysis of dorsal intercalated segment instability deformity secondary to scapholunate dissociation: A preliminary report. *J Hand Surg Am*. 2013;38(7):1346-1355. doi:10.1016/j.jhsa.2013.04.004

12. Kawanishi Y, Moritomo H, Omokawa S, Murase T, Sugamoto K, Yoshikawa H. In vivo 3-dimensional analysis of stage III kienböck disease: Pattern of carpal deformity and radioscaphoid joint congruity. *J Hand Surg Am*. 2015;40(1):74-80. doi:10.1016/j.jhsa.2014.10.035

13. Ateshian GA, Kwak SD, Soslowsky LJ, Mow VC. A stereophotogrammetric method for determining in situ contact areas in diarthrodial joints, and a comparison with other methods. *J Biomech*. 1994;27(1):111-124. doi:10.1016/0021-9290(94)90038-8

14. Lalone EA, Willing RT, Shannon HL, King GJW, Johnson JA. Accuracy assessment of 3D bone reconstructions using CT: an intro comparison. *Med Eng Phys*. 2015;37(8):729-738. doi:10.1016/j.medengphy.2015.04.010

15. Willing R, Lapner M, Lalone EA, King GJW, Johnson JA. Development of a computational technique to measure cartilage contact area. *J Biomech*. 2014;47(5):1193-1197. doi:10.1016/j.jbiomech.2014.01.047

16. Lalone E a., Giles JW, Alolabi B, Peters TM, Johnson J a., King GJW. Utility of an image-based technique to detect changes in joint congruency following simulated joint injury and repair: An in vitro study of the elbow. *J Biomech*. 2013;46(4):677-682. doi:10.1016/j.jbiomech.2012.11.047

17. Lalone EA, McDonald CP, Ferreira LM, Peters TM, King GW, Johnson JA. Development of an image-based technique to examine joint congruency at the elbow. *Comput Methods Biomech Biomed Engin*. 2012;5842(January):37-41. doi:10.1080/10255842.2011.617006

18. Johnson JE, McIff TE, Lee P, Toby EB, Fischer KJ. Validation of radiocarpal joint contact models based on images from a clinical MRI scanner. *Comput Methods Biomech Biomed Engin*. 2014;17(4):378-387. doi:10.1080/10255842.2012.684446

19. Fischer KJ, Johnson JE, Waller AJ, McIff TE, Bruce Toby E, Bilgen M. MRI-based modeling for radiocarpal joint mechanics: Validation criteria and results for four specimen-specific models. *J Biomech Eng*. 2011;133(10):1-7. doi:10.1115/1.4005171

20. Lalone EA, Peters TM, King GW, Johnson JA. Accuracy assessment of an imaging technique to examine ulnohumeral joint congruency during elbow flexion. *Comput Aided Surg*. 2012;17(3):142-152. doi:10.3109/10929088.2012.673638

21. Henninger HB, Reese SP, Anderson AE, Weiss JA. Validation of computational models in biomechanics. *Proc Inst Mech Eng Part H J Eng Med*. 2010;224(7):801-812. doi:10.1243/09544119JEIM649

22. Wilson DC, Niosi CA, Zhu QA, Oxland TR, Wilson DR. Accuracy and repeatability of a new method for measuring facet loads in the lumbar spine. *J Biomech*. 2006;39(2):348-353. doi:10.1016/j.jbiomech.2004.12.011

23. Gammon B. Arthrokinematics of the Distal Radioulnar Joint in the Normal Wrist and Following Distal Radius Malunion. 2016. doi:Electronic Thesis and Dissertation Repository. 3713. https://ir.lib.uwo.ca/etd/3713

24. Wilharm A, Hurschler C, Dermitas T, Bohnsack M. Use of Tekscan K-scan sensors for retropatellar pressure measurement avoiding errors during implantation and the effects of shear forces on the measurement precision. *Biomed Res Int*. 2013;2013. doi:10.1155/2013/829171

Chapter 5

5 Wrist Joint Kinematics is Affected by Forearm Position during Active Flexion and Extension

OVERVIEW

Active motion wrist joint simulators have been designed to simulate physiologic wrist motion; however, a main difference amongst studies has been the orientation of the forearm (viz. horizontal or vertical with respect to gravity). Gaining a better understanding of the effect of forearm position and the role of gravity on wrist motion is of clinical interest for rehabilitation protocols and post-operative care. Furthermore, investigators have freely compared the results from studies using different experimental techniques without taking into consideration the influence of forearm position. This in-vitro biomechanical study aims to determine whether gravity alters wrist kinematics and contact mechanics during active flexion-extension wrist motion, using an active motion wrist simulator, with the capacity to simulate wrist motion with the forearm in different orientations.[3]

[3] A version of this work was presented at the 2019, Annual Meeting of the Canadian Orthopaedic Research Society, 2020 American Society for Surgery of the Hand Annual Meeting. A version of this in second revision for the Journal of Hand Surgery.

5.1 Introduction

Joint motion simulators are commonly employed to perform *in-vitro* wrist joint motion studies (as discussed in Chapter 1) capturing both native and injured states. The majority of these devices apply tensile loads to the flexors and extensors of the forearm to actuate the wrist through a range of motion, including but not limited to flexion-extension, radial-ulnar deviation, and dart-thrower motions. Although the position of the forearm (*viz.* horizontal or vertical with respect to gravity) during testing can vary between different simulators, the results of these studies are often compared. However, the effect of forearm orientation on wrist contact mechanics may be an important variable to consider when comparing results between studies. This has significant clinical relevance to hand surgeons as it examines the correctness of prior biomechanical studies and their conclusions regarding carpal kinematics and effectiveness of surgical interventions. It is also relevant to surgical repair and reconstruction, and rehabilitation protocols.

The effect of forearm orientation on forearm muscle forces has been previously investigated. Shah et al. reported that the horizontal forearm positions (palm facing down, with elbow at 90° elbow flexion), results in an increase to muscle forces in the flexors and extensors of the forearm.[1]The increase in muscle forces is likely due to the influence of gravity on the center of mass of the wrist and perhaps may cause higher joint contact forces and area at the radiocarpal joint.

As documented in the previous chapters of this treatise, the radiocarpal and midcarpal joints play key roles in wrist flexion and extension [2], and soft tissue structures in conjunction with the osseous anatomy act to stabilize the radiocarpal joint.[3] With the arm in the horizontal orientation, loading of wrist muscle groups to generate motion may not function to stabilize these joints and may contribute to instability. It may be preferable for biomechanical testing to be performed in positions that simulate consistent forearm orientation with activities of daily living as well as rehabilitation protocols to understand the effect on the wrist joints.

In view of the foregoing, the purpose of this study was to determine the effect of forearm orientation on wrist kinematics and contact mechanics, with special interest in advancing wrist biomechanics research and to aid in the development of novel surgical reconstruction techniques and rehabilitation protocols.

5.2 Methods

5.2.1 Specimen Preparation and Experimental Setup

Testing was performed on 7 fresh-frozen cadaveric right upper limbs (mean age: 68 ± 8.3 years) with no CT evidence of pathology. Specimens were thawed for 18 hours at room temperature and all soft tissues were left intact.

A longitudinal dorso-central wrist incision was performed, followed by an extensor retinacular step-cut through the third compartment to expose the carpus. Optical tracking markers (Optotrak Certus; Northern Digital, Waterloo, Canada) were indirectly secured to the scaphoid, lunate, third metacarpal, radius and ulna via 3D printed mounts to capture 3D motion of each carpal bone during testing. Under fluoroscopic guidance, two 2.7-mm screws were placed in both the volar scaphoid tuberosity and into the dorsal lunate, in positions to avoid bony impingement with wrist flexion and extension (Figure 5-1). Meanwhile, the third metacarpal tracker was placed on the dorsal surface, the ulnar tracker was placed on the proximal third subcutaneous border and the radial tracker was placed on the middle third shaft using two 3.5-mm cortical screws, respectively. All trackers were oriented to maintain an optimal line of sight with the optical tracking camera, which was the reference for all the mounted trackers.

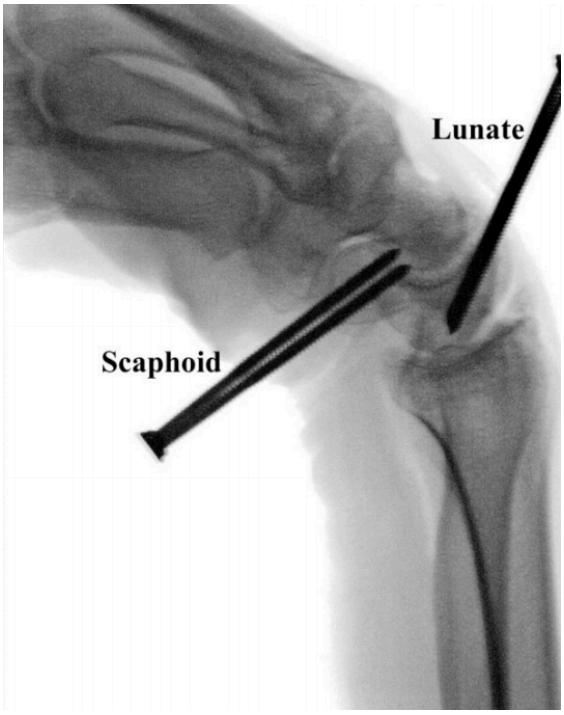

Figure 5-1: Scaphoid and Lunate Tracker Placement.

Two cortical screws (2.7mm) inserted into the scaphoid and lunate showing no impingement in full flexion.

Following a similar protocol described in Chapter 3, tendons of the flexor carpi radialis (FCR), flexor carpi ulnaris (FCU), extensor carpi radialis longus (ECRL), extensor carpi radialis brevis (ECRB), extensor carpi ulnaris (ECU), and pronator teres (PT) and Biceps (BI) were isolated at the musculo-tendinous junction and a running Krackow locking stitch was placed using 100-pound braided fishing line (Shimano Canada Ltd. Reel Support Services, Peterborough, Canada). Blocks were fixed to the lateral and medial epicondyles via 3.5-mm cortical screws to guide the suture lines and maintain appropriate tendon line of action. Subsequently, the specimen was mounted on a custom wrist active motion simulator by rigidly securing the humerus using a clamp and securing the ulna using threaded Steinmann pins connected to a support tower maintaining the elbow at 90° flexion (Figure 5-2). Each suture was routed to individual servomotors (SM2316D-PLS2, SMI Animatics Corp., CA) fitted with a load cell to provide force feedback and to permit closed loop control of muscle forces.

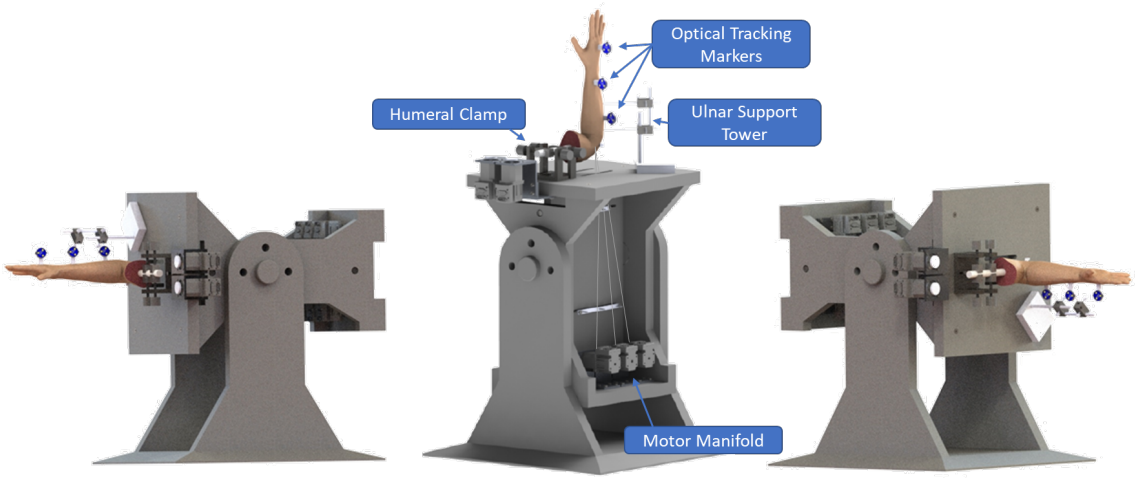

Figure 5-2: Active motion simulation platform.

Allows for three attainable positions: gravity flexion (left), gravity neutral (middle), and gravity extension (right). Optical tracking markers are shown on the radius, ulna and third metacarpal. (Iglesias, 2015).

After specimen mounting with the forearm held in neutral pronation-supination, palpable anatomical landmarks on the radius, ulna and third metacarpal were digitized to create relevant coordinate systems that were required for the simulation of anatomical motions. These coordinate systems were used to give real-time wrist position feedback during the motion trials. Neutral position of the wrist was defined as collinear alignment of the 3rd metacarpal with the long axis of the radius and changes from this neutral position defined the wrist angle during motion.

5.2.2 Simulation of Motion

The previously described motion simulator utilized in this study simulates *in-vivo* behavior. [4,5] This was achieved by the application of loads to antagonistic muscle pairs at their musculotendons junction to more accurately simulate an *in-vivo* wrist with a minimum tone load applied to the groups resisting motion (8.9 N to FCU, FCR, ECRL, ECRB, and ECU and 15 N to BI and PT). Each specimen was subjected to five cyclic active motion trial of planar wrist flexion-extension motion (FEM; 50° flexion to 50° extension), and DTM (to 30° wrist

extension with 15° radial deviation to 30° wrist flexion with 15° ulnar deviation) at a rate of 5°/sec, in the gravity neutral, gravity flexion, and gravity extension positions (Figure 5-2).

5.2.3 Inter-Cartilage Distance Measurement

This study employed the modified inter-cartilage distance (ICD) as described in Chapter 4 (Figure 5-3). At the conclusion of the testing protocol, the forearm was denuded of soft tissue. Landmarks on the distal radius, scaphoid, and lunate were digitized relative to the attached motion trackers. This permitted the creation of a 3D anatomic coordinate systems to be applied to the radius, scaphoid, and lunate enabling the transformation of optical tracker kinematic data to clinically relevant osseous anatomy. The position of the scaphoid and lunate relative to the radius could then be described.

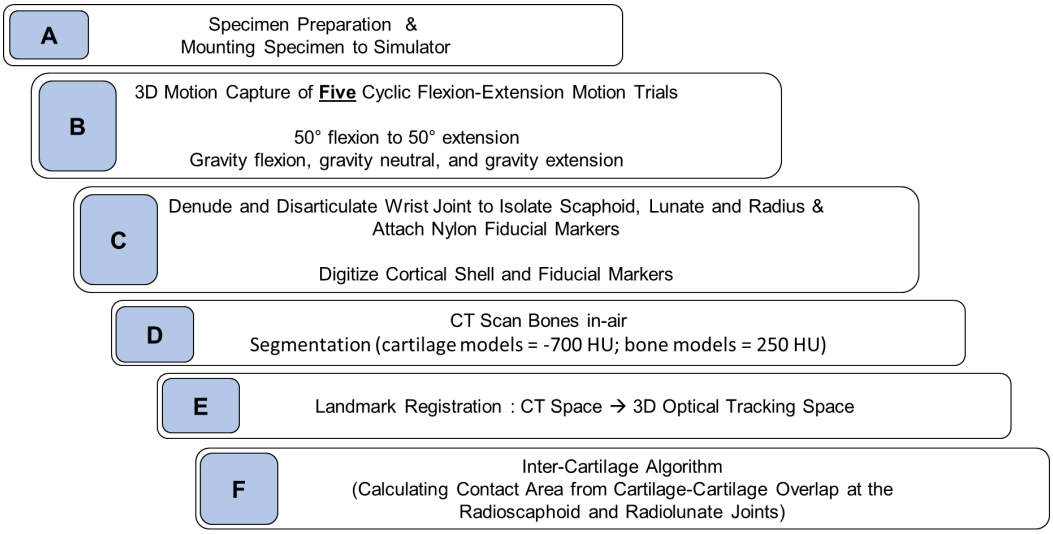

Figure 5-3: Overview of Experimental Protocol.

(A–H) Experimental protocol. (A) Optical tracking markers attached and specimens mounted to the active motion wrist simulator, (B) 3D motion was captured of lunate, scaphoid and radius for flexion-extension and dart thrower motion in all three forearm orientations, (C) Each specimen was then denuded and disarticulated, nylon fiducial markers were attached and the bones of interest were digitized (D) CT scans in-air were acquired for each specimen, from which 3D models of the bones of interest were created ('air' was used as a contrast agent to visualize the cartilage), (E) The 3D cartilage covered models of the bones of interest were then registered using a landmark based registration technique to the test day kinematic dataset, (F) An inter-cartilage distance (ICD) algorithm was then applied to each registered model at each wrist angle tested in all three forearm orientations, from which contact area was ascertained.

Once digitization of these landmarks was complete, 4 spherical nylon fiducial markers were attached to each bone. Their locations were digitized with respect to each bone's corresponding optical motion tracker using a stylus. The optical trackers were then removed from each bone and all bones were then CT scanned in air to ascertain the specimen cartilage thickness and allow for the creation of 3D models. [6,7]

CT scanning was performed using a GE Discovery CT750 HD scanner (GE Healthcare, Pewaukee, WI) at 120 kV and 292 mAs with a slice thickness of 0.625 mm (in-plane pixel size, 0.320 mm). The CT image data of the denuded bones with fiducials was imported into Mimics for manipulation (version 15.1, Materialise, Leuven, Belgium). Bone and cartilage geometries were determined using minimum threshold-based segmentation (cartilage models = -700 HU; bone models = 250 HU). Models were processed to create sealed hollow-shell objects that were exported in the stereolithography format. The models were repositioned from CT images to anatomic-based coordinate systems using a rigid-body registration algorithm. This registration procedure used the fiducials digitized during the experiment and imaged using CT as homologous points.

The 3D models were positioned and animated using the 3-dimensional kinematic data over the arc of simulated active FEM and DTM. The ICD mathematical algorithm (Section 4.2.3), was applied using custom software[8] and Paraview's VTK toolkit (Paraview 4.0.1 Parallel Visualization Application; open source) (Figure 5-4). To describe the interaction between the contacting surfaces, isometric-colour contact maps for the radioscaphoid (scaphoid fossa) and radiolunate (lunate fossa) joints were generated for 10° interval of wrist flexion-extension for all three gravity positions, resulting in a total of 66 (33 radioscaphoid maps; 33 radiolunate maps) different contact maps for each specimen. A local coordinate system was then generated for each specimen on the distal radius using the following anatomical landmarks: radial styloid, dorsal mid-ridge (dorsal interval between the lunate fossa and lunate fossa), volar mid-ridge, and distal radioulnar joint (Figure 5-5). The midpoint between the dorsal mid-ridge and the volar mid-ridge was designated as the origin of the coordinate system. The centroid of each joint contact area was then determined by first identifying the area of contact, and then averaging the location of that contact area. The location of the joint contact centroid location was described relative to the origin of local radial coordinate system. Centroid location was described in both the dorsal-volar plane, as well as the radial-ulnar plane.

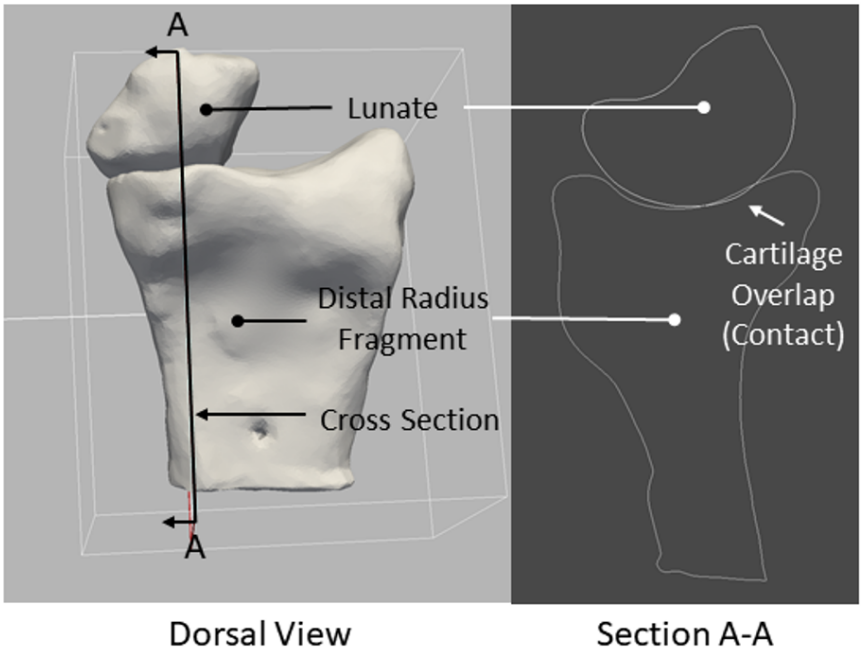

Figure 5-4: Distal radius and lunate cartilage models.

These were reassembled using fiducial-based registration to their original position and orientation. Note the cartilage-cartilage overlap between models in the cross section. This area of overlap is designated as the contact area.

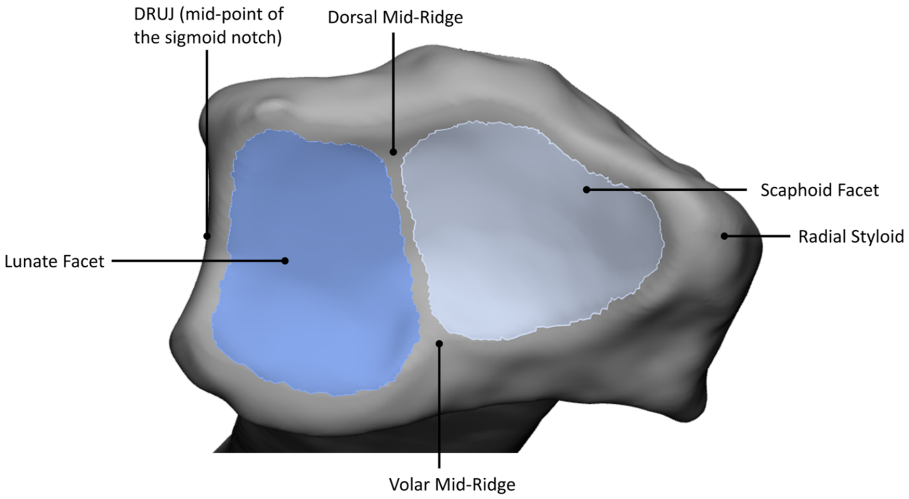

Figure 5-5: Anatomical landmarks used to generate the local coordinate system on the articular surface of the distal radius.

5.2.4 Statistical Methods

The effects of wrist motion (flexion-extension and DTM) and forearm orientation on the radiocarpal contact area of both the radioscaphoid and radiolunate fossas were examined using 2-way repeated-measures analysis of variation (RM-ANOVA) for the independent variables of wrist position and testing position for both FEM and DTM. The effect of forearm orientation on the location of the radioscaphoid and radiolunate contact centroid was assessed also using 2-way RM-ANOVA for both flexion-extension motion and DTM. A Greenhouse-Geisser correction was applied. Statistical significance was set at $p < .05$.

5.3 Results

5.3.1 Flexion-Extension Motion Joint Contact Area

We compared radioscaphoid and radiolunate contact area in the gravity neutral, gravity flexion, and gravity extension forearm positions (Figure 5-2). The data presented are the mean radioscaphoid and radiolunate contact area ± SD unless otherwise specified. The greatest radioscaphoid contact area across wrist motion was observed in the gravity extension position (compared to gravity neutral: mean difference = 35 mm^2, $p<.05$; gravity flexion: mean difference = 47 mm^2, $p<.05$) (Figure 5-6). There was a statistically significant difference in radioscaphoid contact area between forearm orientation at the extremes of wrist motion. The mean contact area during extreme extension in the gravity extension position was 234 ± 94 mm^2, compared to 185.6 ±85.8 mm^2 in the gravity flexion orientation and 224 ± 93 mm^2 in the gravity neutral orientation ($p<.05$). This trend was similar to extreme wrist flexion, where the greatest contact area was again in the gravity extension orientation, with a mean area of 179 ± 37 mm^2, compared to 144 ± 52 mm^2 in the gravity flexion orientation and 143 ± 40 mm^2 in the gravity neutral orientation ($p<.05$; Figure 5-6). Conversely, there was a noticeable increase in radiolunate contact area in the gravity flexion and extension orientations compared to the gravity neutral orientation; however, there was no statistical significance ($p<.05$, Figure 5-7). The mean radiolunate contact area across wrist motion was relatively consistent for all three orientations. The mean radiolunate contact area in the gravity flexion position was 224 ± 75 mm^2, compared to 258 ± 94 mm^2 in the gravity flexion orientation and 256 ± 87 mm^2 in the gravity extension orientation.

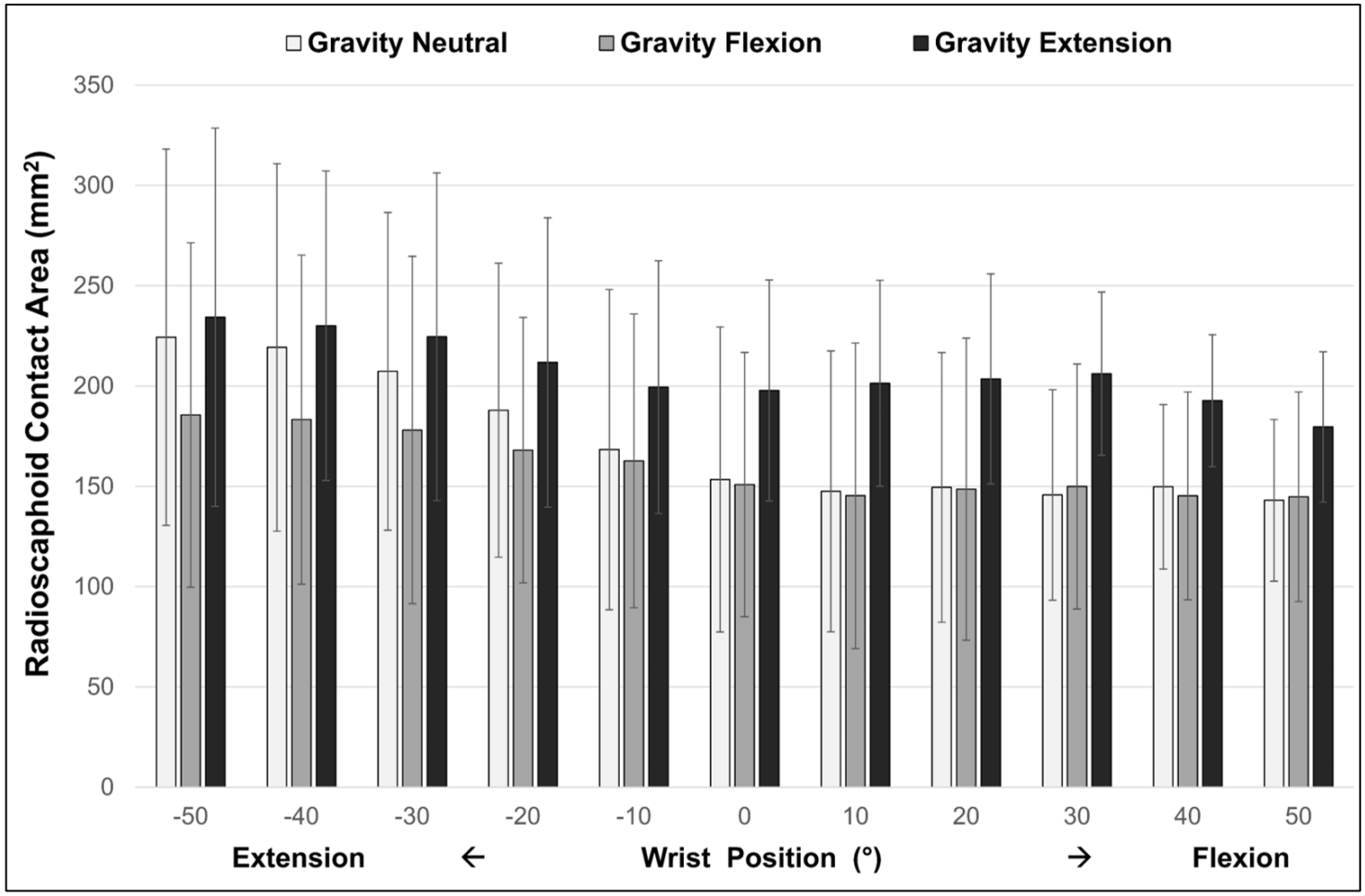

Figure 5-6: Radioscaphoid Joint Contact Area across FEM.

Mean (± 1 standard deviation) contact area measured in mm² of the radioscaphoid joint in the gravity flexion, gravity extension and gravity neutral positions.

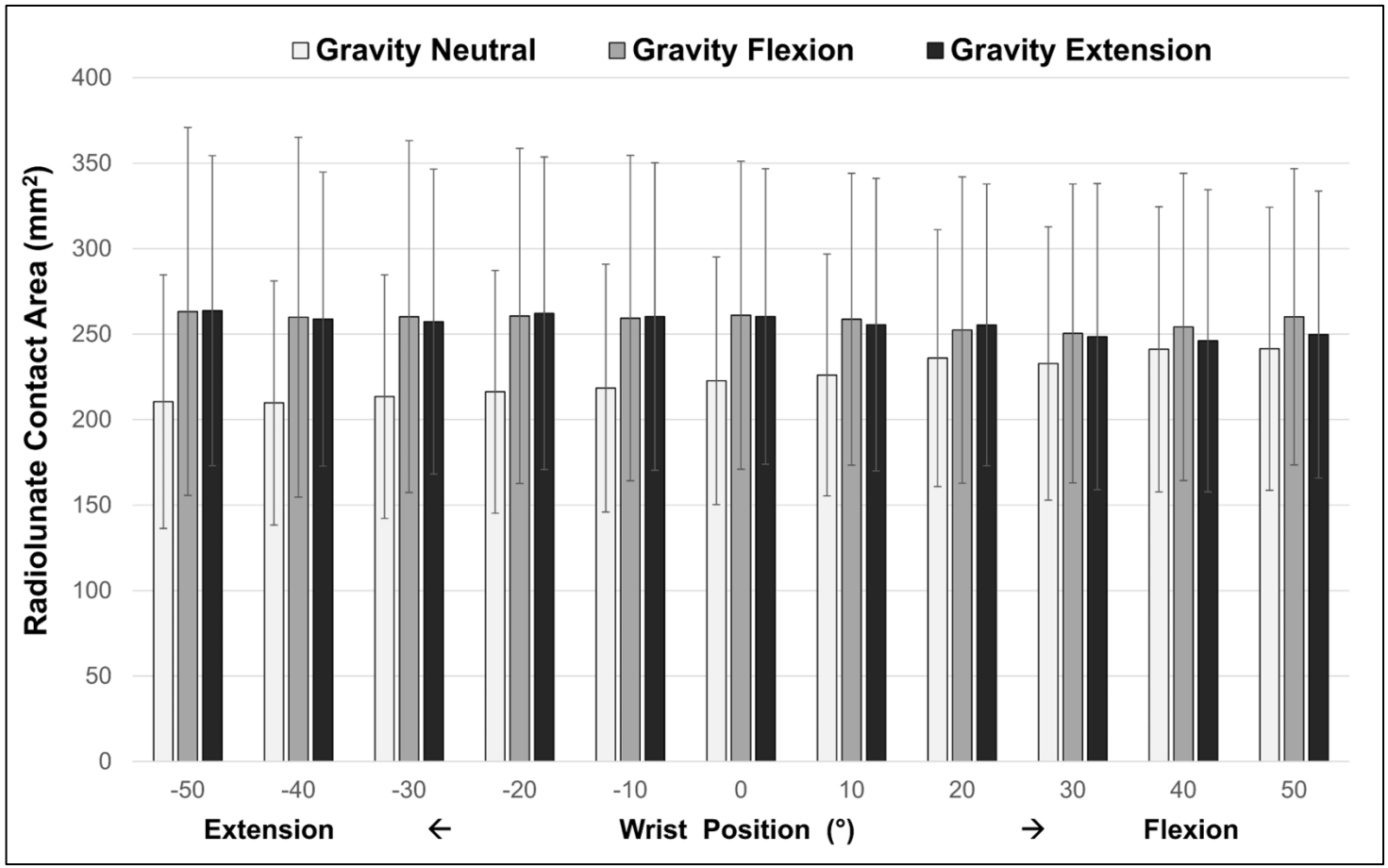

Figure 5-7: Radiolunate Joint Contact Area across FEM.

Mean (± 1 standard deviation) contact area measured in mm^2 of the radiolunate joint in the gravity flexion, gravity extension and gravity neutral positions.

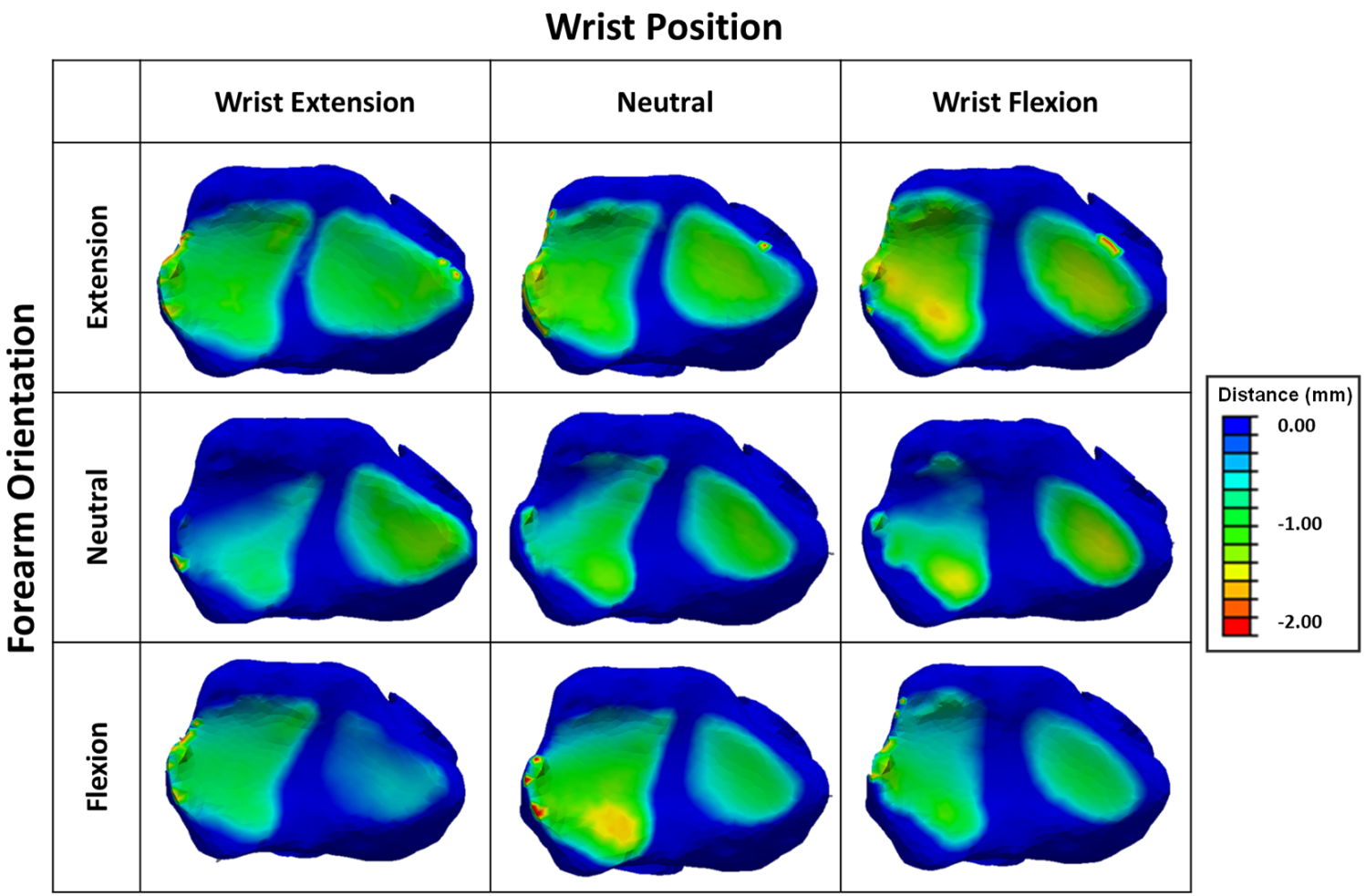

Figure 5-8: Representative Joint Contact of the Radioscaphoid and Radiolunate Joints during FEM.

The carpus is removed and the scaphoid fossa on the distal radius' articular surface is in view, with a typical radioscaphoid and radiolunate joint contact map output shown at three wrist angles (neutral, extreme flexion, and extreme extension), in addition to three forearm orientations (gravity flexion, gravity neutral and gravity extension). The contact patch is represented by a scalar color map (Paraview, v4.4.1, Parallel Visualization Application, New York), which delineates the degree of overlap between cartilage models.

5.3.2 Dart Thrower Motion Joint Contact Area

We compared radioscaphoid and radiolunate contact area in the gravity neutral, gravity flexion, and gravity extension forearm positions. The data presented are the mean radioscaphoid and radiolunate contact area ± SD unless otherwise specified. Forearm orientation cause significant differences in radioscaphoid joint contact area ($p=0.01$, Figure 5-9), while radiolunate joint contact area was similar between all three tested forearm orientations ($p>.05$, Figure 5-10). The greatest radioscaphoid contact area across DTM was observed in the gravity extension position (compared to gravity neutral: mean difference = 78mm^2, $p=0.01$; gravity flexion: mean difference = 22 mm^2, $p=0.02$) (Figure 5-9). In all three forearm orientations, there was a trend towards decreasing radioscaphoid joint contact area as the wrist progressed towards an extended and ulnarly deviation wrist position.

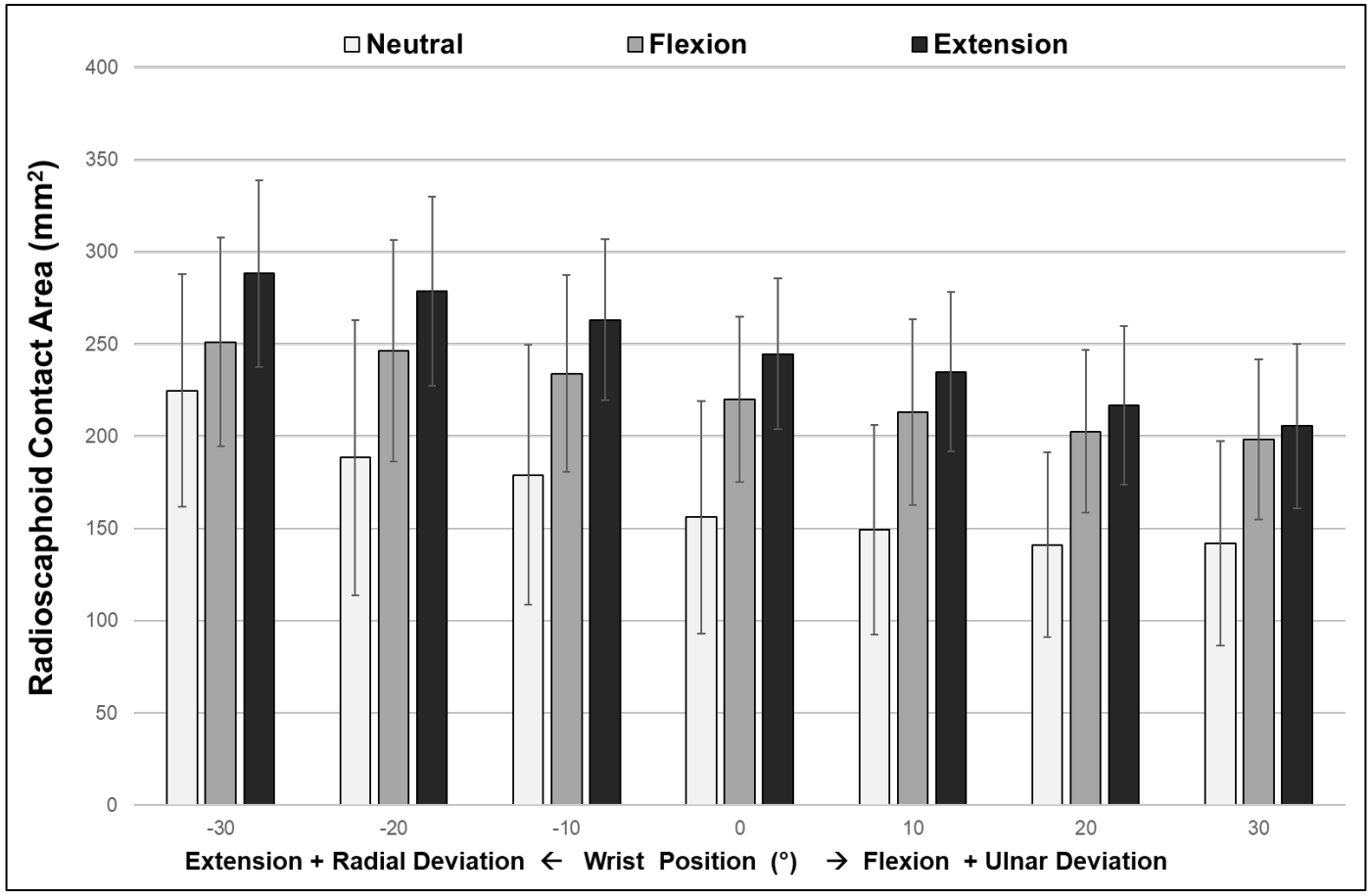

Figure 5-9: Radioscaphoid Joint Contact Area across DTM.

Mean (± 1 standard deviation) contact area measured in mm^2 of the radioscpahoid joint in the gravity flexion, gravity extension and gravity neutral positions during DTM.

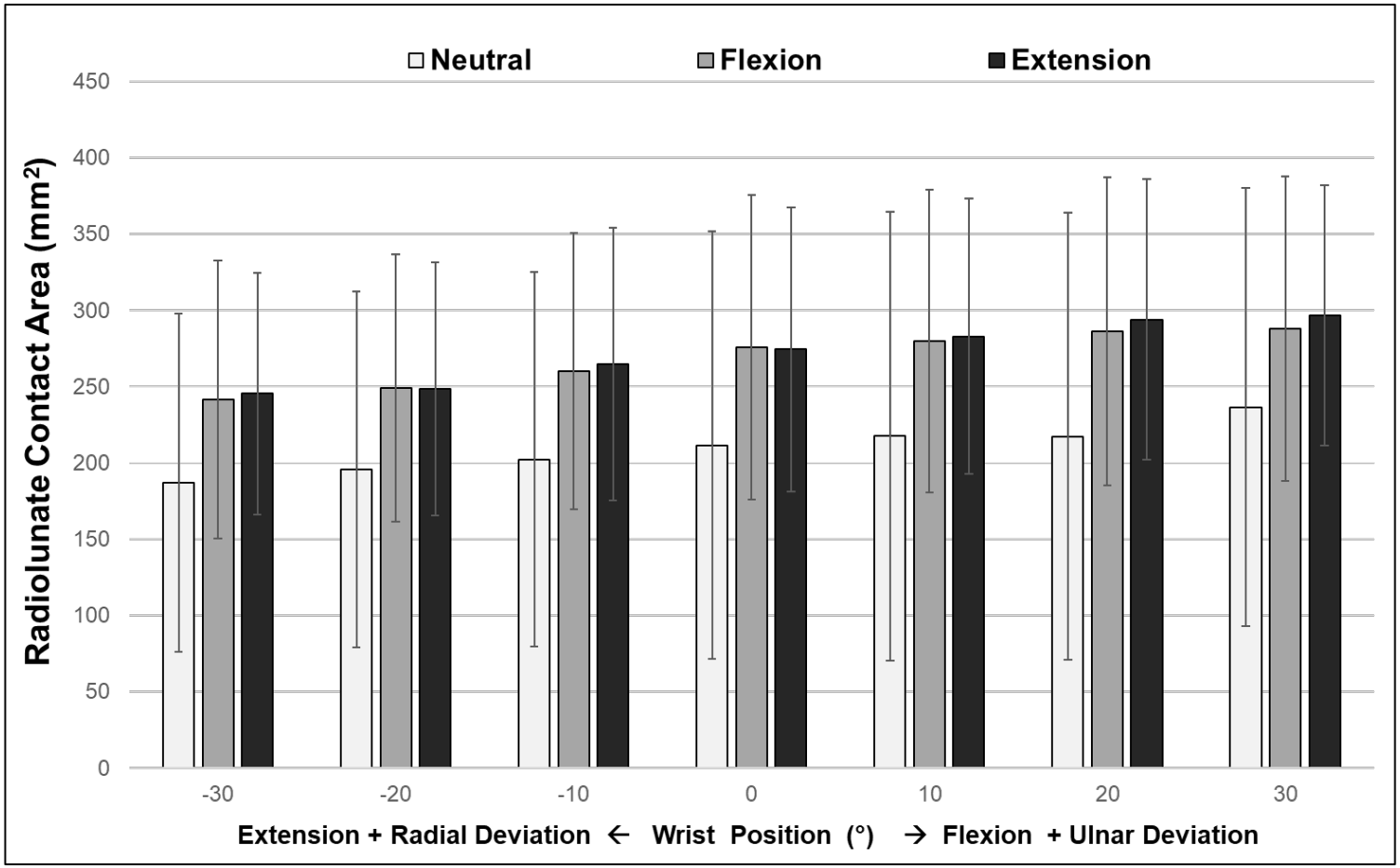

Figure 5-10: Radiolunate Joint Contact Area across DTM.

Mean (± 1 standard deviation) contact area measured in mm^2 of the radiolunate joint in the gravity flexion, gravity extension and gravity neutral positions during DTM.

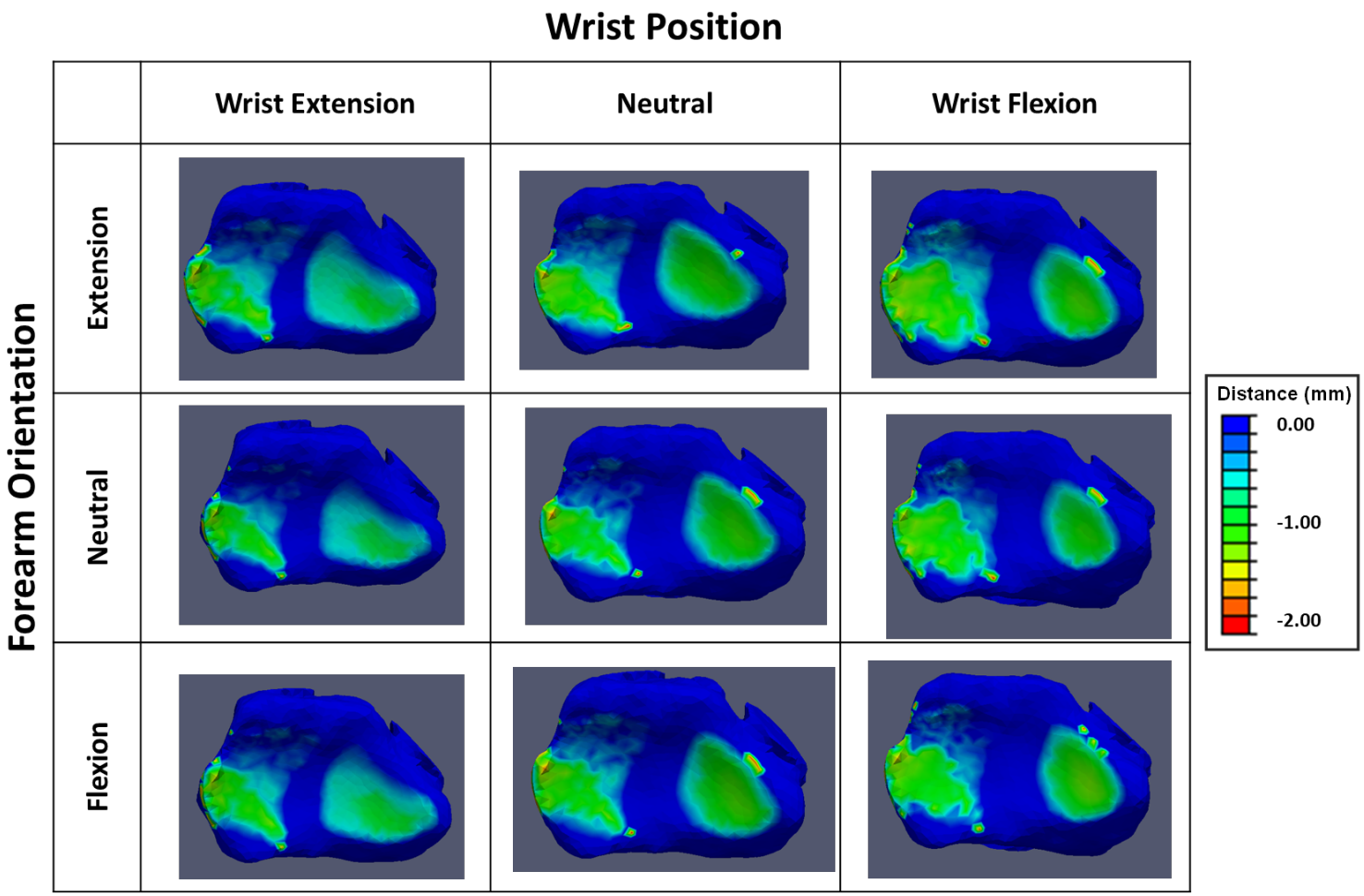

Figure 5-11: Representative Joint Contact of the Radioscaphoid and Radiolunate Joints during DTM.

The carpus is removed and the scaphoid fossa on the distal radius' articular surface is in view, with a typical radioscaphoid and radiolunate joint contact map output shown at three wrist angles (neutral, extreme flexion with ulnar deviation, and extreme extension with radial deviation), in addition to three forearm orientations (gravity flexion, gravity neutral and gravity extension). The contact patch is represented by a scalar color map (Paraview, v4.4.1, Parallel Visualization Application, New York), which delineates the degree of overlap between cartilage models.

5.3.3 Flexion-Extension Motion Joint Contact Centroid Translation

We compared radioscaphoid and radiolunate joint contact centroid position in the gravity neutral, gravity flexion, and gravity extension forearm positions. The data presented are the mean radioscaphoid and radiolunate joint contract centroid positions ± SD unless otherwise specified. The radioscaphoid position of the contact centroid was relatively consistent between the three tested positions with the wrist in neutral position (0°) (Figure 5-12). In contrast, the radioscaphoid contact centroid was significantly translated radially in the gravity neutral position relative to the gravity flexion position in extreme extension (mean difference = 1.2 mm, $p<.05$) (Figure 5-12). There were no other significant radioscaphoid centroid translations when comparing the three forearm orientations. Moreover, there were no significant differences in radiolunate centroid contact position in the three forearm orientations at extreme flexion, extreme extension or neutral wrist positions ($p>.05$) (Figure 5-12).

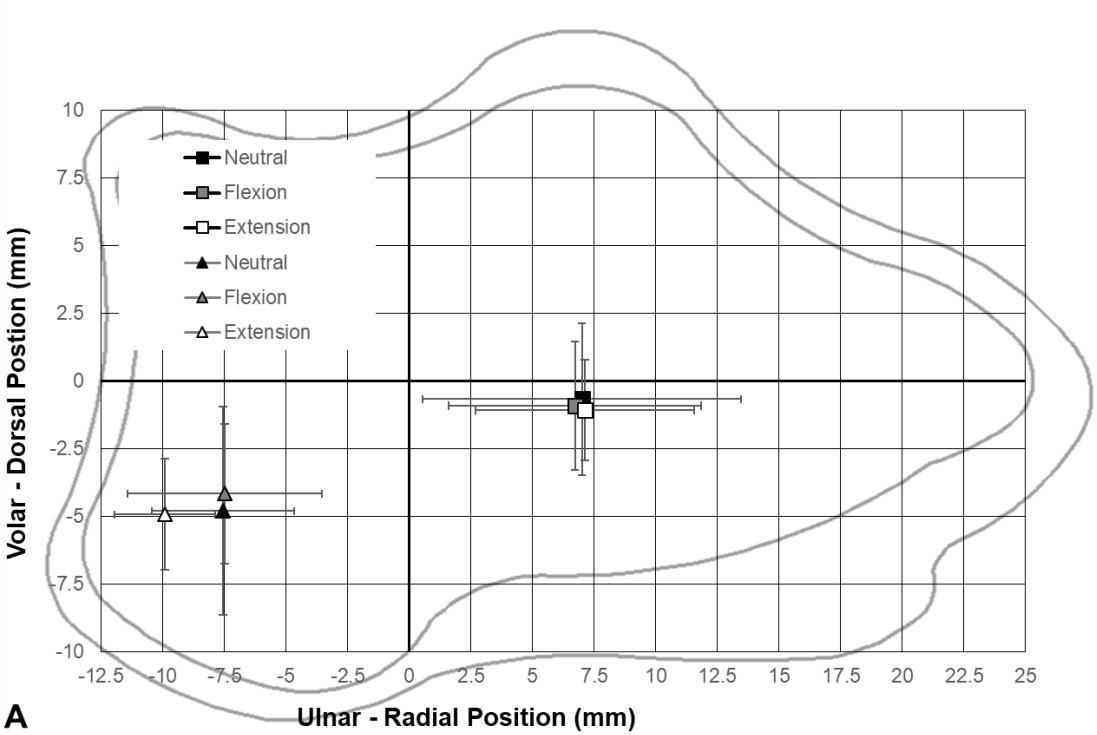
Neutral
Flexion
Extension
Neutral
Flexion
Extension
Volar - Dorsal Postion (mm)
Ulnar - Radial Position (mm)
A

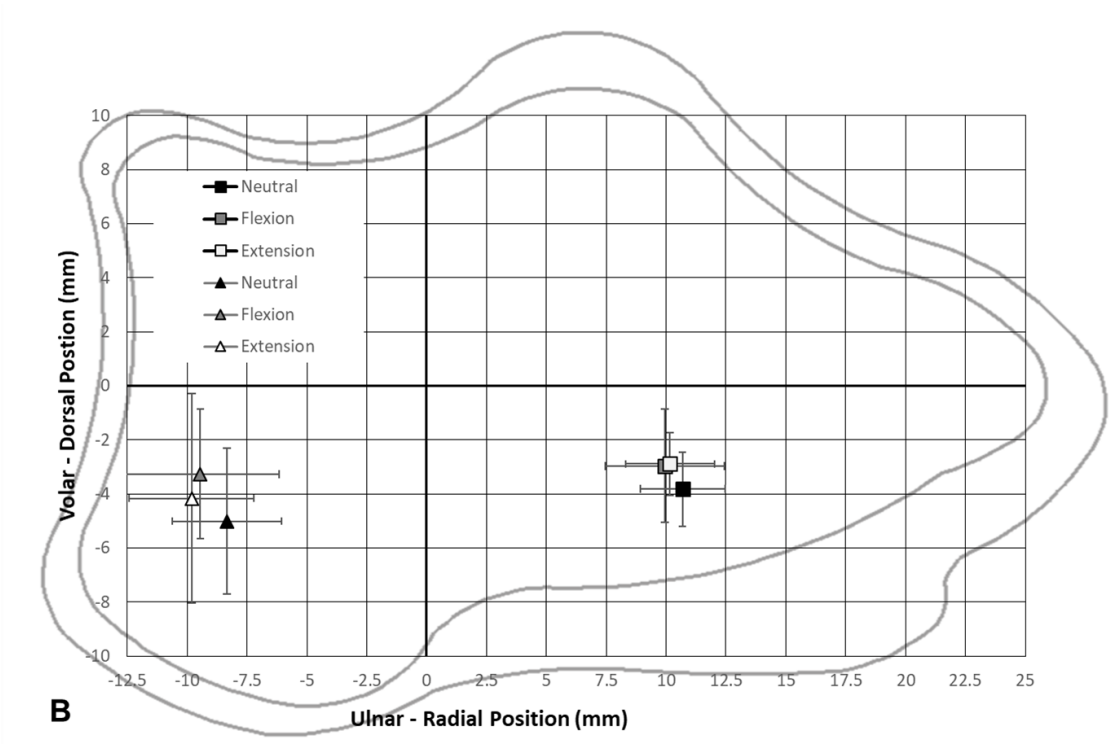
Neutral
Flexion
Extension
Neutral
Flexion
Extension
Volar - Dorsal Postion (mm)
Ulnar - Radial Position (mm)
B

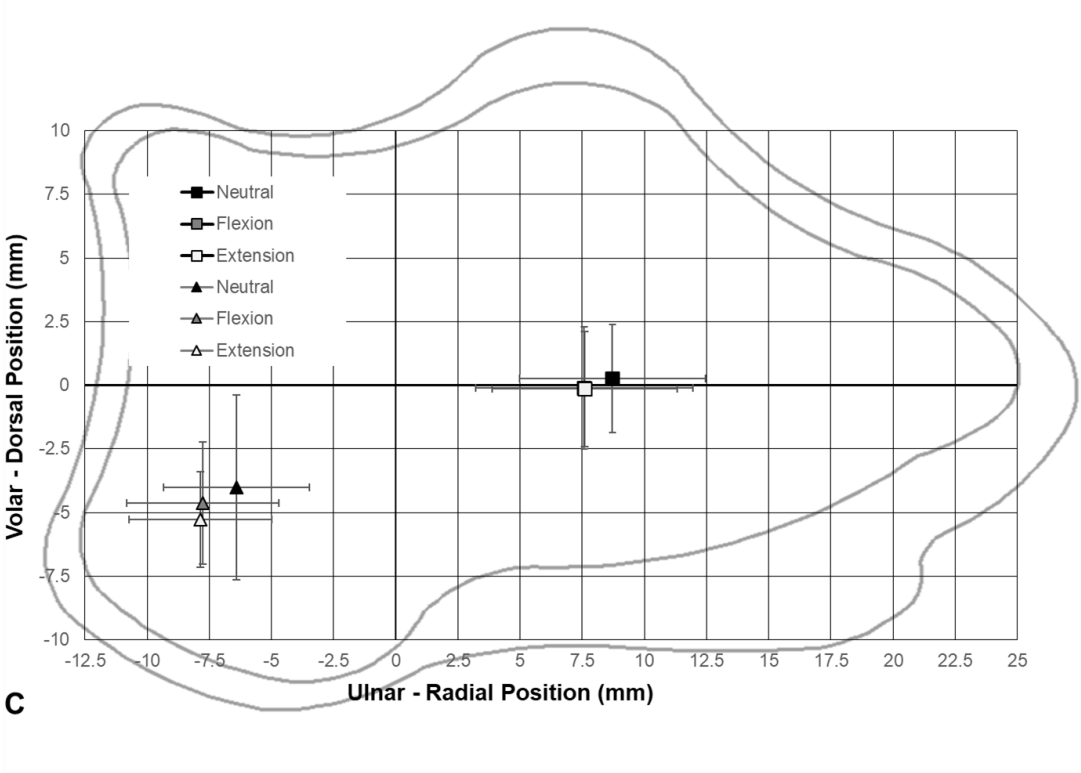

Figure 5-12: Radioscpahoid and Radiolunate Joint Contact Centroid Translation.

Mean (± 1 standard deviation) centroid location in local radial coordinate system. Effect of forearm orientation on the contact centroid location of the radioscaphoid and radiolunate contact area in the (A) neutral wrist (B) 50° wrist flexion and (C) 50° wrist extension. Articular surface of distal radius is illustrated with the origin of the coordinate system located at the intersection between the midpoint of the volar mid-ridge and the dorsal mid-ridge and the midpoint of the radial styloid and distal radial-ulnar joint. The centroid of articular contact of the scaphoid (squares) and lunate (triangles) is shown for the gravity neutral orientation as well as the gravity flexion and gravity extension orientation.

5.3.4 Dart Thrower Motion Joint Contact Centroid Translation

We compared radioscaphoid and radiolunate joint contact centroid position in the gravity neutral, gravity flexion, and gravity extension forearm positions. The data presented are the mean radioscaphoid and radiolunate joint contract centroid positions ± SD unless otherwise specified. There was no significant difference in joint contact centroid location between forearm orientations for both the radioscaphoid and radiolunate joints ($p>.05$, Figure 5-13)

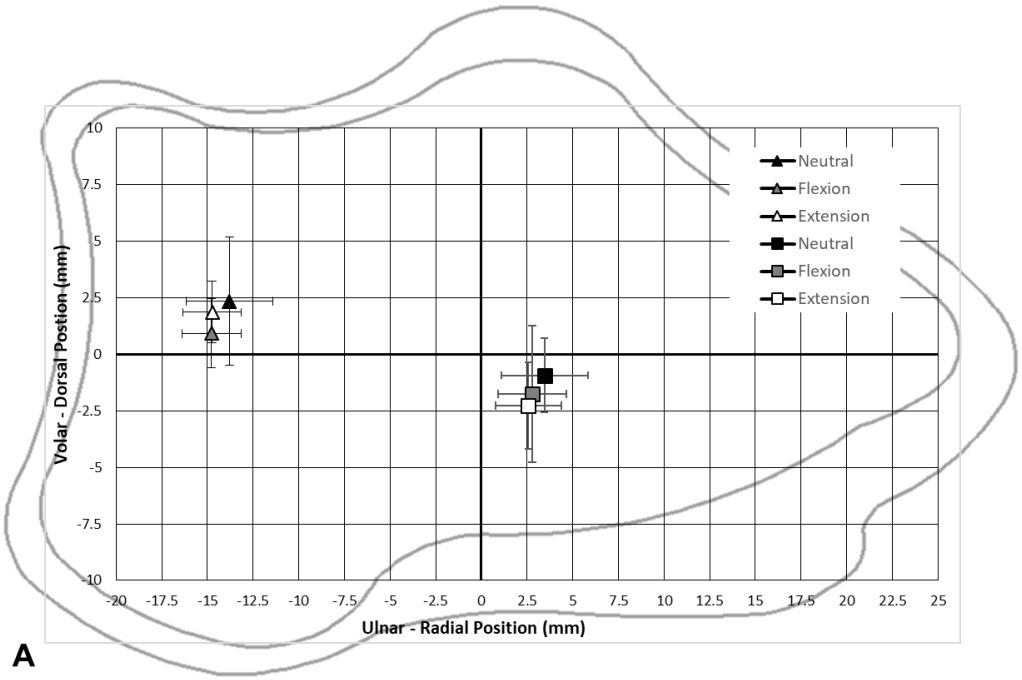
Neutral
Flexion
Extension
Neutral
Flexion
Extension
Volar - Dorsal Postion (mm)
Ulnar - Radial Position (mm)
10
7.5
5
2.5
0
-2.5
-5
-7.5
-10
-20
-17.5
-15
-12.5
-10
-7.5
-5
-2.5
0
2.5
5
7.5
10
12.5
15
17.5
20
22.5
25

A

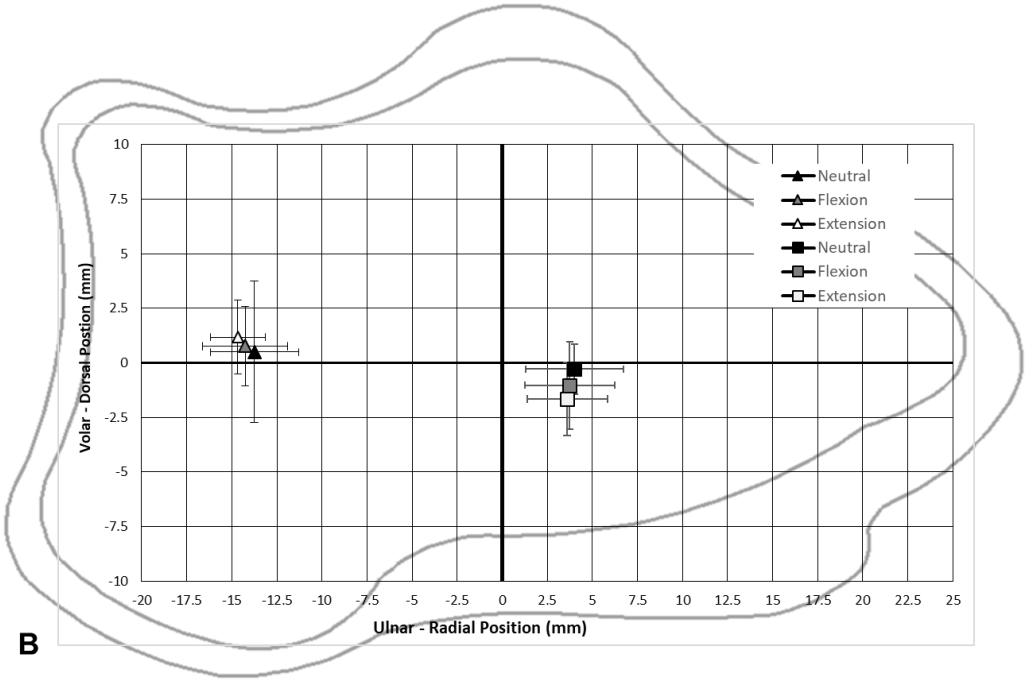
Neutral
Flexion
Extension
Neutral
Flexion
Extension
Volar - Dorsal Postion (mm)
Ulnar - Radial Position (mm)
10
7.5
5
2.5
0
-2.5
-5
-7.5
-10
-20
-17.5
-15
-12.5
-10
-7.5
-5
-2.5
0
2.5
5
7.5
10
12.5
15
17.5
20
22.5
25

B

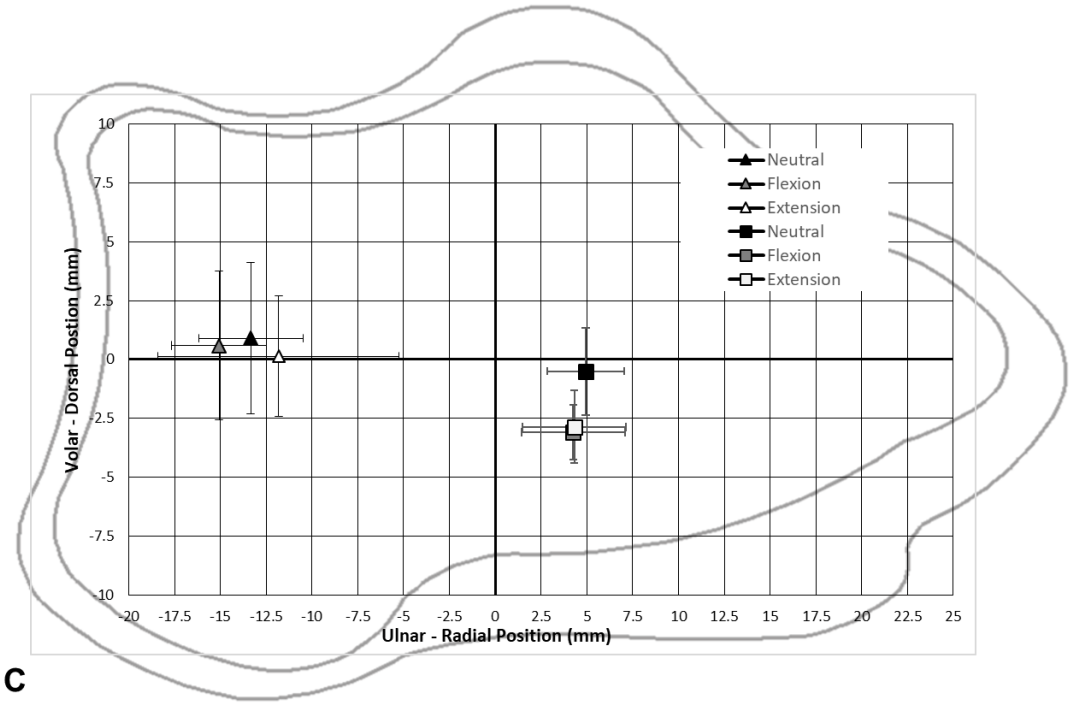

Figure 5-13: Radioscpahoid and Radiolunate Joint Contact Centroid Translation during DTM.

Mean (± 1 standard deviation) centroid location in local radial coordinate system. Effect of forearm orientation on the contact centroid location of the radioscaphoid and radiolunate contact area in the (A) neutral wrist (B) 30° wrist flexion with 15° ulnar deviation and (C) 30° wrist extension with 15° radial deviation. Articular surface of distal radius is illustrated with the origin of the coordinate system located at the intersection between the midpoint of the volar mid-ridge and the dorsal mid-ridge and the midpoint of the radial styloid and distal radial-ulnar joint. The centroid of articular contact of the scaphoid (squares) and lunate (triangles) is shown for the gravity neutral orientation as well as the gravity flexion and gravity extension orientation.

5.3.5 Flexion-Extension Motion Carpal Kinematics

Forearm orientations (gravity flexion, gravity neutral, and gravity extension) did not affect scaphoid rotation relative to distal radius (Figure 5-14, $p>.05$). Lunate rotation relative to the distal radius, was also not affected by forearm orientation (Figure 5-15, $p>.05$). However, an interaction was observed between forearm orientation and wrist angle when examining lunate rotation relative to the distal radius. In the gravity neutral orientation, the lunate's rotational arc was greater than the other two forearm orientations. In the gravity neutral orientation, the mean lunate flexion at 45° of wrist flexion was greater than the other two forearm orientations ($p<.05$). The mean lunate flexion at 45° wrist flexion in the gravity neutral forearm rotation was 36.7 ± 7.4°, while it was only 26.6 ± 8.8° in the gravity flexion orientation and 24.7 ± 10.2° in the gravity extension orientation. The mean lunate extension at 45° of wrist extension in the gravity neutral orientation was also greater than the other two gravity forearm positions ($p<.05$). The mean lunate extension at 45° wrist extension in the gravity neutral forearm rotation was the 40.8 ± 5.9°, while it was only 24.8 ± 16.0° in the gravity flexion orientation and 24.6 ± 14.1° in the gravity extension orientation.

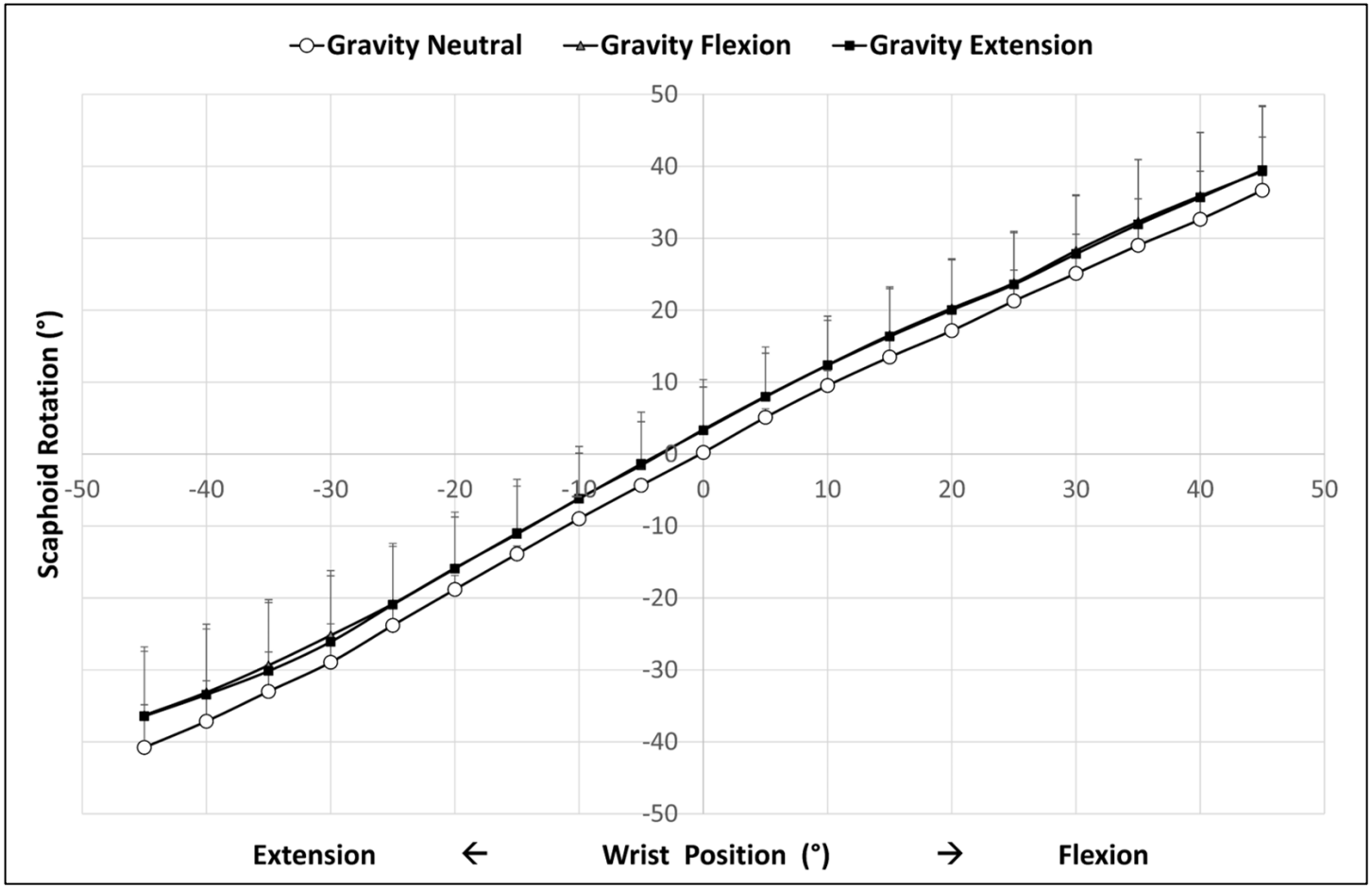

Figure 5-14: Angular Scaphoid Rotation in Three Forearm Orientations across FEM.

Mean angular rotation (mean ± 1 Standard Deviation) of the scaphoid in the neutral, gravity flexion and gravity extension forearm orientations during a flexion-extension wrist motion.

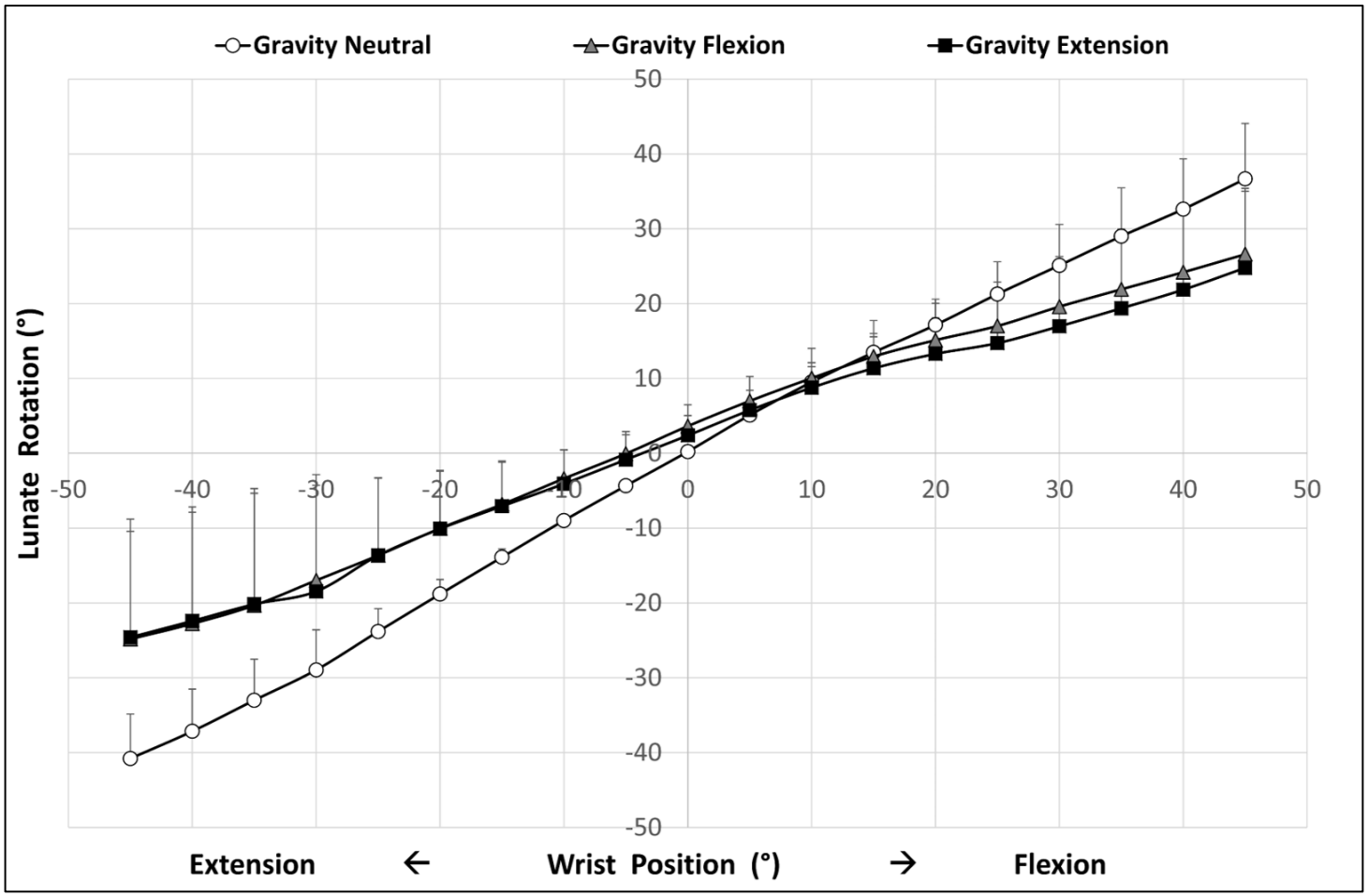

Figure 5-15: Angular Lunate Rotation in Three Forearm Orientations across FEM.

Mean angular rotation (mean ± 1 Standard Deviation) of the lunate in the neutral, gravity flexion and gravity extension forearm orientations during a flexion-extension wrist motion.

5.3.6 Dart Thrower Motion Carpal Kinematics

Forearm orientations (gravity flexion, gravity neutral, and gravity extension) did not affect scaphoid rotation relative to distal radius during DTM (Figure 5-16, $p>.05$). Lunate rotation relative to the distal radius, was also not affected by forearm orientation during DTM (Figure 5-17, $p>.05$).

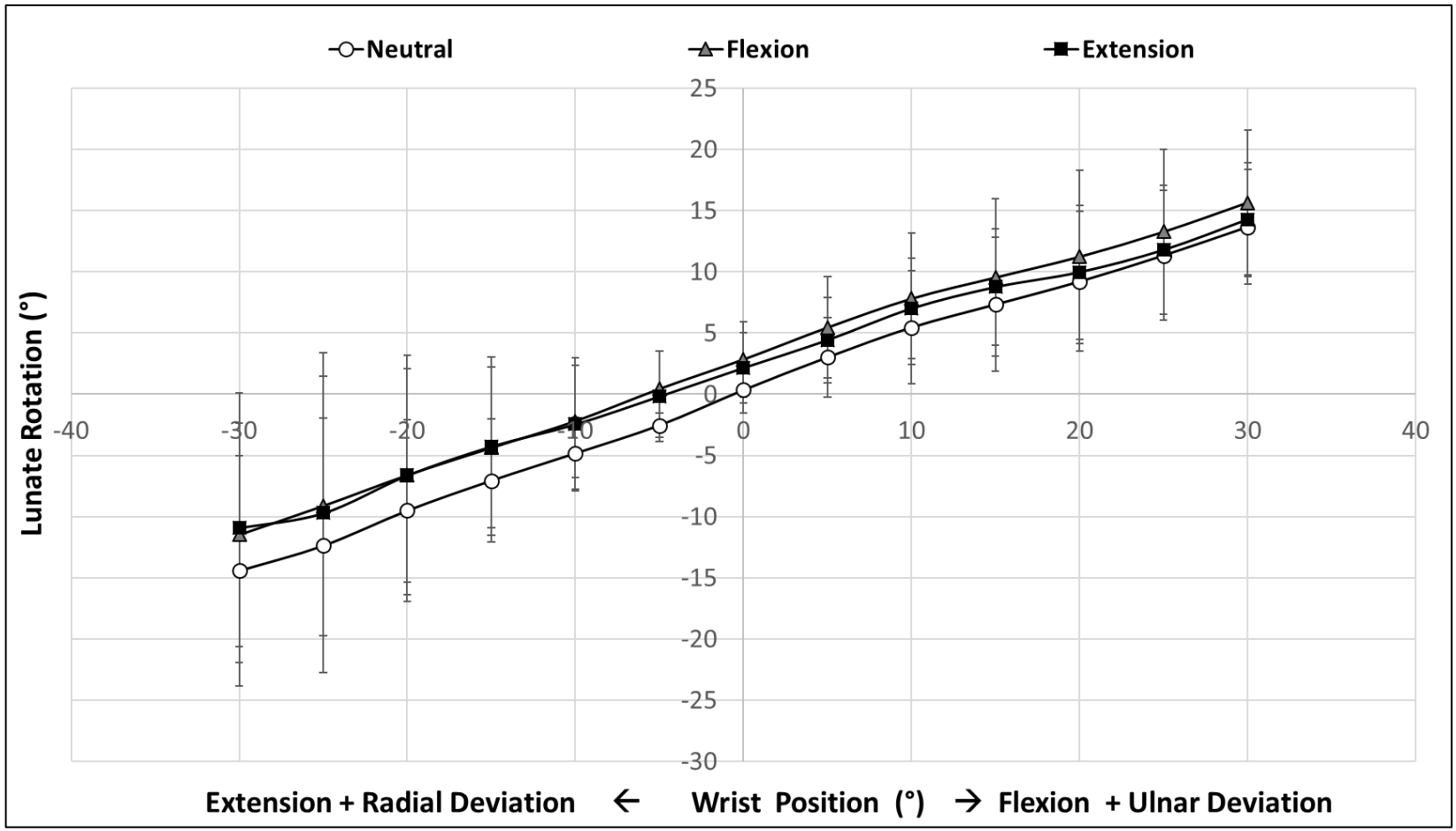

Figure 5-16: Angular Scaphoid Rotation in Three Forearm Orientations across DTM.

Mean angular rotation (mean ± 1 Standard Deviation) of the scaphoid in the neutral, gravity flexion and gravity extension forearm orientations during a flexion-extension wrist motion.

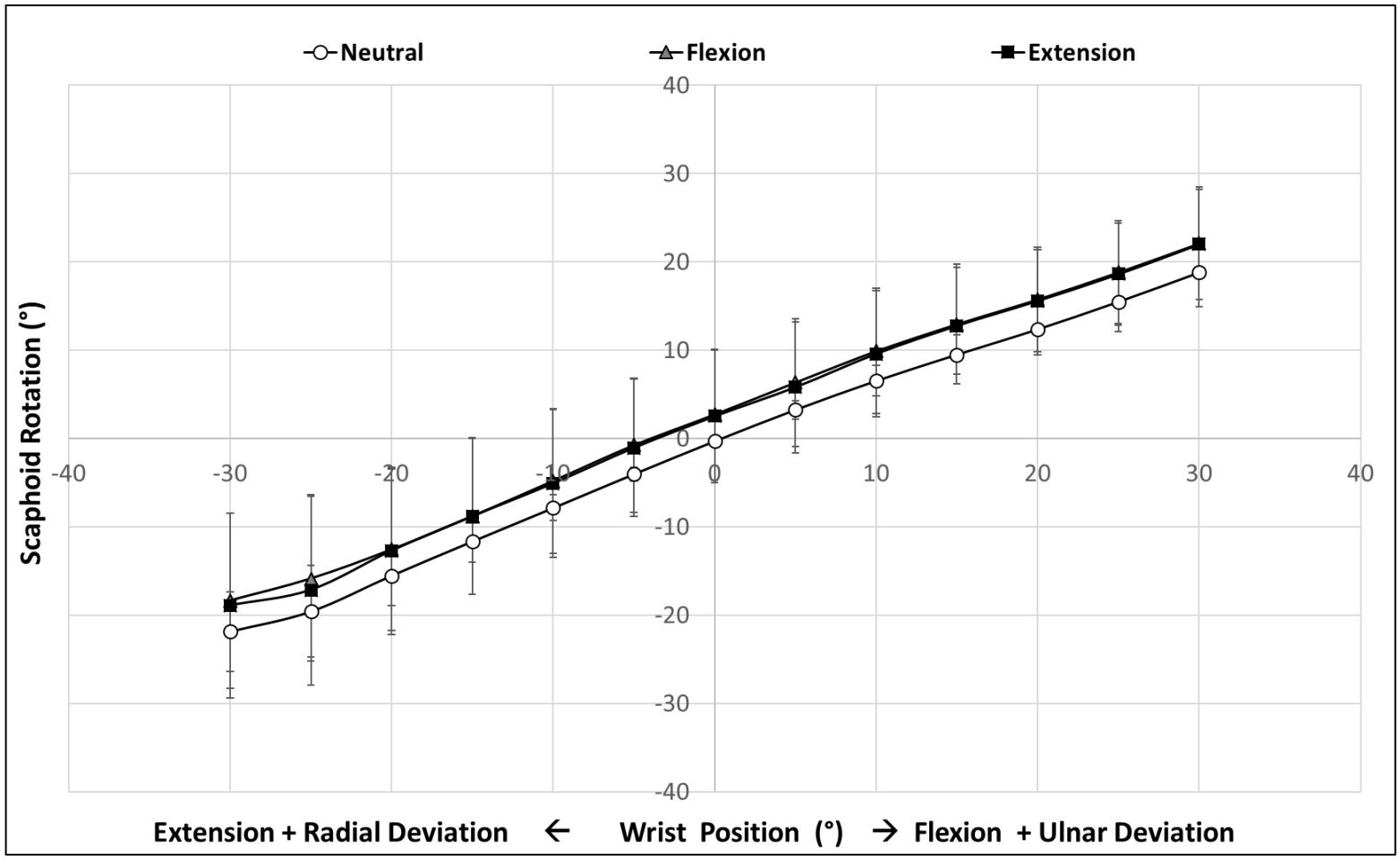

Figure 5-17: Angular Lunate Rotation in Three Forearm Orientations across DTM.

Mean angular rotation (mean ± 1 Standard Deviation) of the lunate in the neutral, gravity flexion and gravity extension forearm orientations during a flexion-extension wrist motion.

5.4 Discussion

This study demonstrated that radiocarpal contact is variable and dependent on forearm position (*i.e*. gravity flexion, gravity extension, and gravity natural) and wrist angle. Contact area at the radioscaphoid joint was maximal in the gravity extension orientation and radioscaphoid contact was greatest in wrist extension across all three forearm orientations during a flexion-extension wrist motion. These findings are consistent with literature, as reports indicate that radioscaphoid contact in highest in wrist extension.[9,10] Similarly, during DTM the gravity extension forearm orientation produced the greatest radioscpahoid joint contact area. Additionally, as the wrist moved toward the ulnar flexion component of DTM, there was trend towards decreasing radioscaphoid joint contact area. Radiolunate contact was similar between all three tested forearm orientations and wrist angles and was not found to be wrist angle dependent across a flexion-extension or dart thrower wrist motion. These finding again similar to previous literature that states that radiolunate contact is not wrist position dependent.[9] This study also reported higher average radioscaphoid and radiolunate contact areas across wrist motion than previously reported in literature.[9,11] Lastly, this study found that scaphoid rotation is affected by forearm rotation, but only at the extremes of wrist flexion-extension.

This study was the first to quantify radiocarpal contact and centroid position in three different forearm gravity orientations using ICD.[8] This previously validated non-inasive CT based method has been shown to be a sufficiently accurate measurement technique for predicting cartilage contact, as it accounts for regional variations in cartilage morphology at the distal radius. We showed that forearm orientation alters radiocarpal contact mechanics, illustrating that it is important to consider forearm orientation as a variable when interpreting and comparing results to previous studies.

Previous literature has assessed radioscaphoid and radiolunate contact area using a variety of different methodologies. Viegas et al. [12] was the first to document normal radiocarpal joint contact area using pressure sensitive film. Their study used a custom loading jig where each specimen was in a gravity neutral position and was loaded vertically by the jig. The study examined a truncated flexion-extension motion range (20° wrist flexion to 40° wrist extension), and the results showed that radioscaphoid joint contact area was 1.147 times that of radiolunate joint contact area, lunate contact area did not change relative to joint position, while scaphoid

contact area was greatest in wrist extension. Chen et al[9] examined normal radiocarpal contact mechanics using CT scans of 13 normal wrists in four static positions (20° of flexion, neutral, 20° of extension and 40° of extension). CT imagines were acquired in a gravity flexed position with the elbow flexed to 90°. The study reported a progressive increase in radioscaphoid contact area from 20° flexion, neutral, 20° wrist extension, to 40° wrist extension. In agreement with Chen et al. and Viegas et al, this study reported greater radioscaphoid contact area in simulated active wrist extension compared to wrist flexion in all three forearm orientations tested. Additionally, this study agrees with Viegas et al, who found that radiolunate joint contact area was not altered by wrist angle.

Unlike the flexion-extension wrist motion, DTM has been examined far less, and this is the first study to examine radiocarpal contact during active DTM. A similar trend was observed in radioscaphoid joint contact area, where the joint contact area was smaller in the ulnarly flexed position. Additionally, radioscaphoid contact was also found to be greatest in the gravity extension forearm orientation, which is in agreement with the flexion-extension results from this study. Also, in agreement with the flexion-extension results of this study, radiolunate joint contact area was similar across DTM, and was also not sensitive to forearm orientation.

Although, radiocarpal contact area has been previously documented for the flexion-extension wrist motion, the effect of forearm orientation has yet to be examined. Blevens et al [11] performed a study in the gravity neutral orientation and reported 52 mm^2 for radioscaphoid contact and 46 mm^2 for radiolunate contact in neutral wrist position [11]. While Tang et al performed study in the gravity flexion orientation and reported 76.6 mm^2 for radioscaphoid contact and 58.5 mm^2 for radiolunate contact in neutral wrist position [10]. Both Tang et al. and Blevens et al. applied similar loading conditions to the wrist and similar experimental set-ups with the exception of the forearm orientation (gravity flexion *versus* gravity neutral). The combined results from these two studies illustrate greater radiocarpal contact area in the gravity flexion orientation compared with the gravity neutral orientation. These results agree with this study and found that radioscaphoid joint contact area was greatest in the gravity flexion and gravity extension forearm orientations. The increased contact area observed in the gravity extension and gravity neutral forearm orientations in this study is an interesting finding. As the methodology used in this study did not consider the interaction of the contacting cartilage surfaces, it is difficult to draw conclusions regarding how contact area is correlated to contact

forces at the joint; however, the importance lies in the difference found between the tested forearm orientations.

Previous work by Shah et al, showed that that the horizontal forearm positions (palm facing down, with elbow at 90° elbow flexion) had the highest wrist extensor muscles forces in comparison to the other positions they evaluated.[1] Although this study did not report tendon loading, we do agree with Shah et al. that higher muscle forces tended to occur when working to overcome gravity. However, due to the complex shapes of the carpal bones, and their involved interactions with adjacent bones, higher loads may not always correlate to greater contact area or higher stresses.

The contact area centroid may be a more critical indicator of mechanism of degeneration. Although centroid location has been previously discussed by numerous investigators, a consensus has yet to be found regarding joint contact centroid translation during wrist motion. Tang et al. reported that radioscaphoid contact centroid moved dorsal and ulnar in flexion and volar and radial in extension. Conversely, Blevens et al. reported radioscaphoid and radiolunate centroids moving radial in flexion and ulnar in extension [11]. Viegas et al. reported a joint pressure centroid shift of the radioscpahoid and radiolunate joint in the volar direction when the wrist was extended to 20°; however, they reported seeing a dorsal shift of the centroid with further wrist extension. Rainbow et al [13] quantified joint space characteristics of the radioscaphoid and radiolunate joints and reported that in extreme wrist flexion, the radioscaphoid joint contact centroid translated towards the radial stylus and volar ridge of the radius, whereas in extreme extension, it shifted dorsally. The present study observed a radioscaphoid centroid translation in the radial and volar direction in flexion and only a marginal translation in the radial and dorsal directions in extension compared to neutral wrist position (Figure 5-12). Additionally, we noted that at extreme wrist flexion, the contact centroid on the radioscaphoid joint was radially translated in gravity neutral forearm orientation compared to the gravity flexion forearm orientation. The relative translations of the contact centroid for both radioscaphoid and radiolunate joints were small and potentially not clinically significant.

Joint contact centroid location was also quantified for DTM. To our knowledge this is the only study to examine radiocarpal joint contact during DTM and in three forearm orientations. Little

translation of the radiolunate joint contact centroid was noted between across the DTM. Furthermore, radiolunate joint contact centroid was not found to be sensitive to forearm orientation. The radioscaphoid joint contact centroid location was also found to stay relatively constant throughout DTM and was also not sensitive to forearm orientation. These findings support previously studies who have found that the lunate and scaphoid have minimal motion during DTM.

Carpal kinematics are a common outcome measure for biomechanical studies, while forearm orientation has yet to be investigated. The results of this study suggest that scaphoid rotation may differ in a flexion-extension motion pathway depending on the position of the forearm. While scaphoid rotation during flexion-extension motion was the only carpal rotation sensitive to forearm orientation, the contact mechanic outcomes from this study may better represent the influence of forearm orientation on the carpus. Additionally, the influence of forearm orientation may be more apparent in pathological wrist with ligamentous laxity or deficiency.

The strengths of this study included the use of a repeated measures study design, where each specimen served as its own paired control. Second, this study used a novel custom wrist simulator with the ability to position the forearm in three different position while allowing active simulation of wrist motion. Lastly, this study was able to investigate joint contact mechanics using a non-invasive method.

This study also had some limitations. The 3D models of each bone were based on CT imaging in air of the denuded specimens at the end of the experiment. Despite hydration with saline, desiccation may have occurred that may have shrunk the cartilage thickness of the model, thus decreasing contact area. However, the wrist capsule and skin were kept closed during the testing to avoid dessication and we observed larger contact areas than previously published. Additionally, the larger contact areas that we reported may be due to the cohort of specimens that were used were all males. Moreover, the ICD technique to quantify joint congruency is prone to model registration digitization error.

While statistical significance was found in this study, whether these differences are clinically significant is as yet unknown. Future work should aim to quantify the forces observed at the radiocarpal joint to gain a better understanding load transfer at the wrist. Lastly, this study only included an analysis of wrist flexion-extension in neutral forearm rotation, and in the future, it

would be pertinent to test other wrist motion pathways in addition to other forearm rotation (*i.e*. pronation, and supinations).

5.5 Conclusions

This study demonstrates that gravity affects wrist contact mechanics and kinematics. First, radiocarpal contact was found to be variable and dependent on forearm position and wrist angle. Contact area at the radioscaphoid joint was maximal in the gravity extension orientation and radioscaphoid contact was greatest in wrist extension across all three forearm orientations. Lastly, the results of this study demonstrated that scaphoid rotation is affected by forearm position but only at the extremes of wrist flexion-extension.

This study of importance to future biomechanical studies as the results elucidate the consequence of not considering forearm position when interpreting results. The results also show that certain forearm position may be more stable, and as future investigation evaluation novel surgical reconstitution techniques, they should subject their reconstructions to the worst-case-scenario forearm position to ensure the robustness of their repair. Furthermore, this study can aid in the development of rehabilitation protocols, by guiding therapist to use more stable forearm positions during rehabilitation. Lastly, this information can help guide the development of wrist arthroplasty by elucidating in which positions the wrist is most unstable.

5.6 References

1. Shah DS, Middleton C, Gurdezi S, Horwitz MD, Kedgley AE. The effects of wrist motion and hand orientation on muscle forces: A physiologic wrist simulator study. *J Biomech*. 2017;60:232-237. doi:10.1016/j.jbiomech.2017.06.017

2. Padmore CE, Stoesser H, Nishiwaki M, et al. The Effect of Dorsally Angulated Distal Radius Deformities on Carpal Kinematics: An In Vitro Biomechanical Study. *J Hand Surg Am*. 2018;43(11):1036.e1-1036.e8. doi:10.1016/j.jhsa.2018.02.017

3. Brown D, Mulligan MT, Uhl RL. Volar ligament repair for radiocarpal fracture-dislocation. *Orthopedics*. 2013;36(6):463-468. doi:10.3928/01477447-20130523-07

4. Padmore C, Stoesser H, Langohr GD, Johnson J, Suh N. Carpal Kinematics following Sequential Scapholunate Ligament Sectioning. *J Wrist Surg*. 2019;08(02):124-131. doi:10.1055/s-0038-1676865

5. Isa AD, Mcgregor ME, Padmore CE, et al. An In Vitro Study to Determine the Effect of Ulnar Shortening on Distal Forearm Loading During Wrist and Forearm Motion: Implications in the Treatment of Ulnocarpal Impaction. *J Hand Surg Am*. 2019;44(8):669-679. doi:10.1016/j.jhsa.2019.04.007

6. Rafehi S, Lalone E, Johnson M, King GJW, Athwal GS. An anatomic study of coronoid cartilage thickness with special reference to fractures. *J Shoulder Elb Surg*. 2012;21(7):961-968. doi:10.1016/j.jse.2011.05.015

7. Willing RT, Lalone EA, Shannon H, Johnson JA, King GJW. Validation of a finite element model of the human elbow for determining cartilage contact mechanics. *J Biomech*. 2013;46(10):1767-1771. doi:10.1016/j.jbiomech.2013.04.001

8. Lalone EA, McDonald CP, Ferreira LM, Peters TM, King GW, Johnson JA. Development of an image-based technique to examine joint congruency at the elbow. *Comput Methods Biomech Biomed Engin*. 2012;5842(January):37-41. doi:10.1080/10255842.2011.617006

9. Chen YR, Wu YF, Tang JB, Giddins G, Y. R. Chen1, Y. F. Wu1 JBT and GG.

Contact areas of the scaphoid and lunate with the distal radius in neutral and extension: correlation of falling strategies and distal radial anatomy. *J Hand Surg Am*. 2014;39E(4):379-383. doi:10.1016/j.jhsa.2006.05.002

10. Tang P, Gauvin J, Muriuki M, Pfaeffle JH, Imbriglia JE, Goitz RJ. Comparison of the "Contact Biomechanics" of the Intact and Proximal Row Carpectomy Wrist. *J Hand Surg Am*. 2009;34(4):660-670. doi:10.1016/j.jhsa.2008.12.004

11. Blevens AD, Light TR, Jablonsky WS, et al. Radiocarpal articular contact characteristics with scaphoid instability. *J Hand Surg Am*. 1989. doi:10.1016/S0363-5023(89)80076-0

12. Viegas SF, Tencer AF, Cantrell J, et al. Load transfer characteristics of the wrist. Part II. Perilunate instability. *J Hand Surg Am*. 1987;12(6):978-985. doi:10.1016/S0363-5023(87)80094-1

13. Rainbow MJ, Kamal RN, Leventhal E, et al. In vivo kinematics of the scaphoid, lunate, capitate, and third metacarpal in extreme wrist flexion and extension. *J Hand Surg Am*. 2013;38(2):278-288. doi:10.1016/j.jhsa.2012.10.035

Chapter 6

6 Effect of Gravity on Scapholunate Insufficiency: An in-vitro Biomechanical Study

OVERVIEW

Recent studies have focused less on investigations of flexion-extension (FEM) wrist motion and more on dart thrower's motion (DTM) in a rehabilitation setting. DTM is a movement pattern that may allow wrist mobility, while reducing SLIL strain. Previous cadaveric studies demonstrate minimal motion or dissociation of the scaphoid and lunate interval occurring with DTM. Forearm position is often not thought of during the creation of rehabilitation protocols, and yet differing forearm gravity positions may exacerbate certain injuries. This in-vitro biomechanical study aims to determine which gravity forearm position is optimal for scapholunate injury rehabilitation.

6.1 Introduction

As documented in Chapter 1 (Section 1.1.3.1), the scapholunate interosseous ligament (SLIL) is the most commonly injured wrist ligament. SLIL injuries frequently occur from a fall on an outstretched hand. SLIL tears are found to occur simultaneously with distal radius fracture in an estimated 54% of patient cases.[1] These injuries are often treated conservatively with rehabilitation, however they may also require surgical intervention. Following injury or repair, the wrist is often immobilized for 8 weeks or more to protect the SLIL in an effort to promote healing.[2] However, potential consequences of prolonged wrist immobilization include delayed return to work, permanent stiffness and reduced quality of life, which is why there is a need for SLIL rehabilitation protocol optimization in order to reduce permanent disability in patients with prolonged immobilization or those using conservative treatment methods.

The development of rehabilitation protocols is often an iterative process which incorporates both clinical and scientific knowledge. A fundamental understanding of carpal kinematics, specifically for the scaphoid and lunate is essential as their motion is complex. In the setting of SLIL injuries, studies have extensively looked at normal and pathological kinematics of the scapholunate (SL) joint and found that the kinematics of the SL joint are tightly governed by strength of the SLIL which connects the scaphoid to the lunate. As discussed in Chapter 1 (Section 1.2.2.2), the scaphoid and lunate rotate collectively in flexion or extension depending on the direction of motion.[3–5]

Recent studies have focused less on flexion-extension wrist motion (FEM) and more on dart thrower's motion (DTM) which is a common motion pattern in daily life. DTM is a movement pattern that may allow wrist mobility, while reducing SLIL strain. Defined as a coupled motion, DTM is oriented obliquely to orthogonal plane motion. Previous cadaveric studies have demonstrated minimal motion or dissociation of the SL interval occurring with DTM. Due to the minimal motion of the scaphoid and lunate, DTM is thought to be protective of the SLIL and therefore has provided the rational for including it in SL rehabilitation.

Following the discovery of the potential protective quality of the DTM, several studies investigated SL motion and dissociation following SLIL injury as a means to understand DTM's potential role in rehabilitation. These studies found that a truncated range of DTM should be used, as greater SLIL strain occurred at the maximum extension component of DTM,

while another study reported that the greatest SL interval gapping occurs that the maximum flexion component of DTM. Although these studies have begun to examine the utility of DTM in rehabilitation, other variables such at the influence of gravity should be investigated to further understand SLIL injuries to better rehabilitation protocols.

The effect of gravity on carpal biomechanics has only been briefly described. The study performed by Shah et al. in addition to the study from the previous chapter of this body of work (Chapter 5) are the first two to examine the effect of gravity on the biomechanics of the wrist. Shah et al. reported that the effect of gravity was most pronounced in the gravity flexion/horizontal orientation, resulting in higher extensor forces. Chapter 5 of this body of work, also found that forearm orientation influenced carpal biomechanics. Both studies also reported reduced muscle activity in the gravity neutral (upright forearm orientation), and therefore this forearm orientation may be optimal for SLIL rehabilitation, however further investigation is required to confirm this hypothesis.

The purpose of this cadaveric study was to analyze carpal kinematics and SL diastasis following complete SLIL sectioning in three different forearm orientations, simulating different gravity positions during active DTM.

6.2 Methods

6.2.1 Specimen Preparation

Eight fresh-frozen cadaveric upper limbs (mean age: 68 ± 10.1 years, 8R) were amputated mid-humerus. Prior to use, computed tomography (CT) scans of each limb were performed. Specimens with underlying static SL injury or arthritic changes of were excluded. The integrity of the SLIL, scaphotrapezial (ST) and radioscaphocapitate (RSC) ligaments were confirmed by stress testing under fluoroscopy and direct visualization during specimen preparation.

After thawing for 18 hours, specimen preparation was undertaken. A longitudinal dorsal wrist incision was performed, exposing the carpus. A second longitudinal central extended volar approach was then created. During the volar exposure, the volar SLL location was confirmed using fluoroscopy and marked with a simple suture for later easy identification. The capsule and extensor retinaculum were closed using interrupted 2-0 Vicryl sutures, and skin was closed to maintain hydration.

Following similar testing preparation as in Chapters 2, 4, and 5, optical tracking markers (Optotrak Certus; Northern Digital, Waterloo, Canada) were placed as previously described by Padmore et al [6] on the scaphoid, lunate, third metacarpal and radius to capture real time 3-dimensional motion. The scaphoid and lunate trackers were mounted using fluoroscopy, while the remaining trackers were inserted under direct visualization. The carpal trackers were secured using 2.7 diameter cortical bone screws, while the remaining trackers were secured with 3.5 diameter cortical bone screws. All trackers were oriented to maintain a perpendicular line of sight to the camera during testing, at a distance of approximately 2.5m. The tendons of the flexor carpi radialis (FCR), flexor carpi ulnaris (FCU), ECRL, extensor carpi radialis brevis (ECRB), pronator teres (PT), biceps brachii (BT) were isolated at the musculo-tendinous junction and a running locking stitch was placed using 100-pound fishing line (Shimano Canada Ltd. Reel Support Services, Peterborough, Canada). The specimens were mounted on a wrist active motion simulator as previously described in Chapter 5. After specimen mounting with the forearm held in neutral position, palpable anatomical landmarks on the radius and third metacarpal were digitized to create relevant coordinate systems such that the angles of the wrist, scaphoid, lunate could be calculated during DTM [6].

Loads were applied to each tendon through its respective servomotor and each specimen was taken through cyclic active motion trials of dart-thrower motion (DTM) (10° radial deviation, 30° flexion to 10° ulnar deviation, 30° extension). Five motion cycles were performed in the native state and 3 cycles for all subsequent stages. Preconditioning trials were also executed prior to the initial native testing.

6.2.2 Experimental Testing

A two-stage protocol was performed in which optical tracking DTM data was collected in the intact wrist and after complete SLIL sectioning. At each stage, data was collected in three gravity positions including gravity flexion, gravity neutral and gravity extension (as described in Chapter 5) (Figure 6-1). Data analysis involved the determination of: (1) scaphoid and lunate flexion and extension relative to the distal radius, (2) scapholunate angle, and (3) relative diastasis (translation) of the scaphoid articular surface with respect to the lunate's articular surface. These translations were calculated using a previously described inter-cartilage distance (ICD) technique (as described in Chapter 4). To obtain the mean diastasis of both the dorsal and volar regions of the SL articulation, the lunate's articular surface was bisected in the axial plane to create a dorsal half and a volar half. The relative diastasis at both the dorsal and volar regions was reported as a mean distance and compared to the native state.

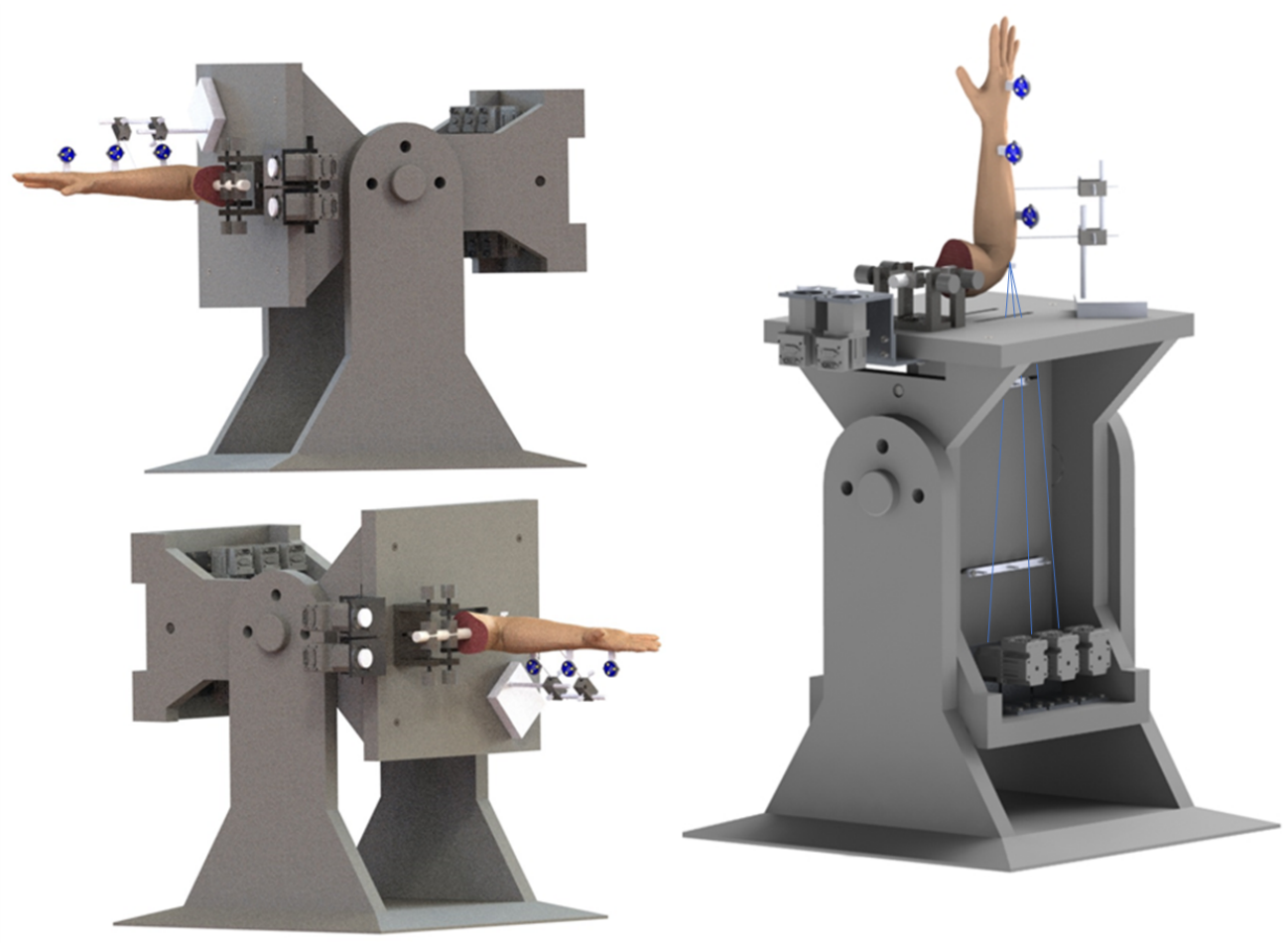

Figure 6-1: Active motion simulation platform.

Allows for three attainable positions: gravity flexion (left), gravity neutral (middle), and gravity extension (right). Optical tracking markers are shown on the radius, ulna and third metacarpal (Iglesias et al, 2015).

6.2.3 Statistical Methods

A three-way repeated-measures ANOVA analysis of variance (RM-ANOVA) with Greenhouse-Geisser correction was performed for analysis of scaphoid and lunate angulation (relative to the distal radius) and scapholunate angulation. The dependent outcome variables were carpal motion (scaphoid, lunate or scapholunate). The independent experimental variables were gravity position (gravity flexion, gravity neutral and gravity extension), sectioning states (native and complete SLIL sectioning), and wrist angle in 5° increments (10° radial deviation, 30° flexion to 10° ulnar deviation, 30° extension).

A three-way repeated-measures ANOVA analysis of variance (RM-ANOVA) with Greenhouse-Geisser correction was performed to evaluate dorsal and volar SL diastasis. The dependent outcome variable was mean diastasis (mm). The independent experimental variables were articular region (dorsal vs. volar aspect of SL articulation), sectioning states (native and complete SLL sectioning), and wrist angle in 5° increments (10° radial deviation, 30° flexion to 10° ulnar deviation, 30° extension). These tests allowed for the comparison of the intact SL diastasis to the diastasis of the subsequent stages of the protocol, in addition to the tested gravity positions for both the dorsal and volar aspects of the articulation. Additionally, we were able to determine whether the gapping of the dorsal and volar aspects of the articulation were symmetrical. Statistical significance was set at $p<0.05$.

6.3 Results

6.3.1 Kinematics

We compared the effect of complete SLIL sectioning in three gravity forearm positions (gravity neutral, gravity flexion, and gravity extension forearm positions). The data presented are the mean carpal rotations ± SD unless otherwise specified. No significant difference was detected between the forearm positions tested (gravity flexion, gravity extension and gravity neutral) when comparing scaphoid rotation following complete SLIL sectioning to the intact state (Figure 6-2, p =.22). The mean difference between the native state and complete SLIL sectioning in the three gravity forearm positions was, 8.8 ± 12.3° in the gravity neutral position, 9.6 ± 12.8° in the gravity flexion position, and 9.8 ± 13.0° in the gravity extension positions. Moreover, no significant difference was found between the three forearm positions (gravity flexion, gravity extension and gravity neutral), when comparing lunate rotation following complete SLIL sectioning to the intact state (Figure 6-3, p =.11). The mean difference between the native state and complete SLIL sectioning in the three gravity forearm positions was, 3.9 ± 6.4° in the gravity neutral position, 2.4 ± 6.7° in the gravity flexion position, and 1.4 ± 7.7° in the gravity extension positions. However, the differences in change in SL rotation were significant between the tested forearm orientations ($p < 0.001$). The greatest change in SL angle occurred in the gravity flexion orientation (palm facing down). On average SL angle following SLIL sectioning increased by 9.7 ± 8.6° more compared to the gravity neutral forearm orientation, and by 7.4 ± 5.4° more compared to the gravity extension orientation. Additionally, greater change in SL angle occurred near the end range of extension during DTM, while smaller changes occurred near the end range of flexion during DTM.

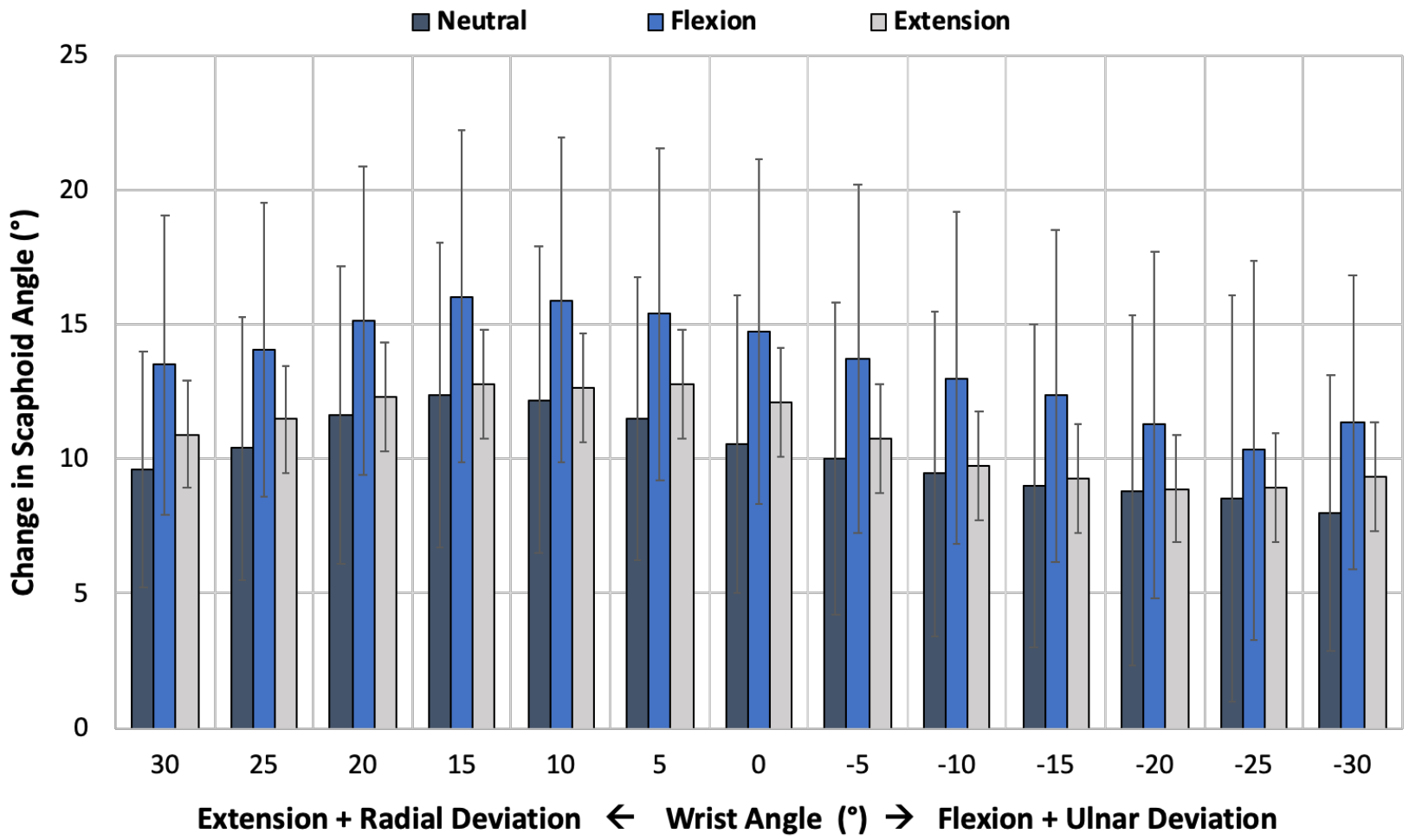

Figure 6-2: Scaphoid Rotation in Native State and Following Complete SLIL sectioning in Three Gravity Forearm Positions.

Mean change in angular rotation of the scaphoid in the native state and following complete SLIL sectioning in the neutral, gravity flexion and gravity extension forearm orientations during flexion-extension wrist motion.

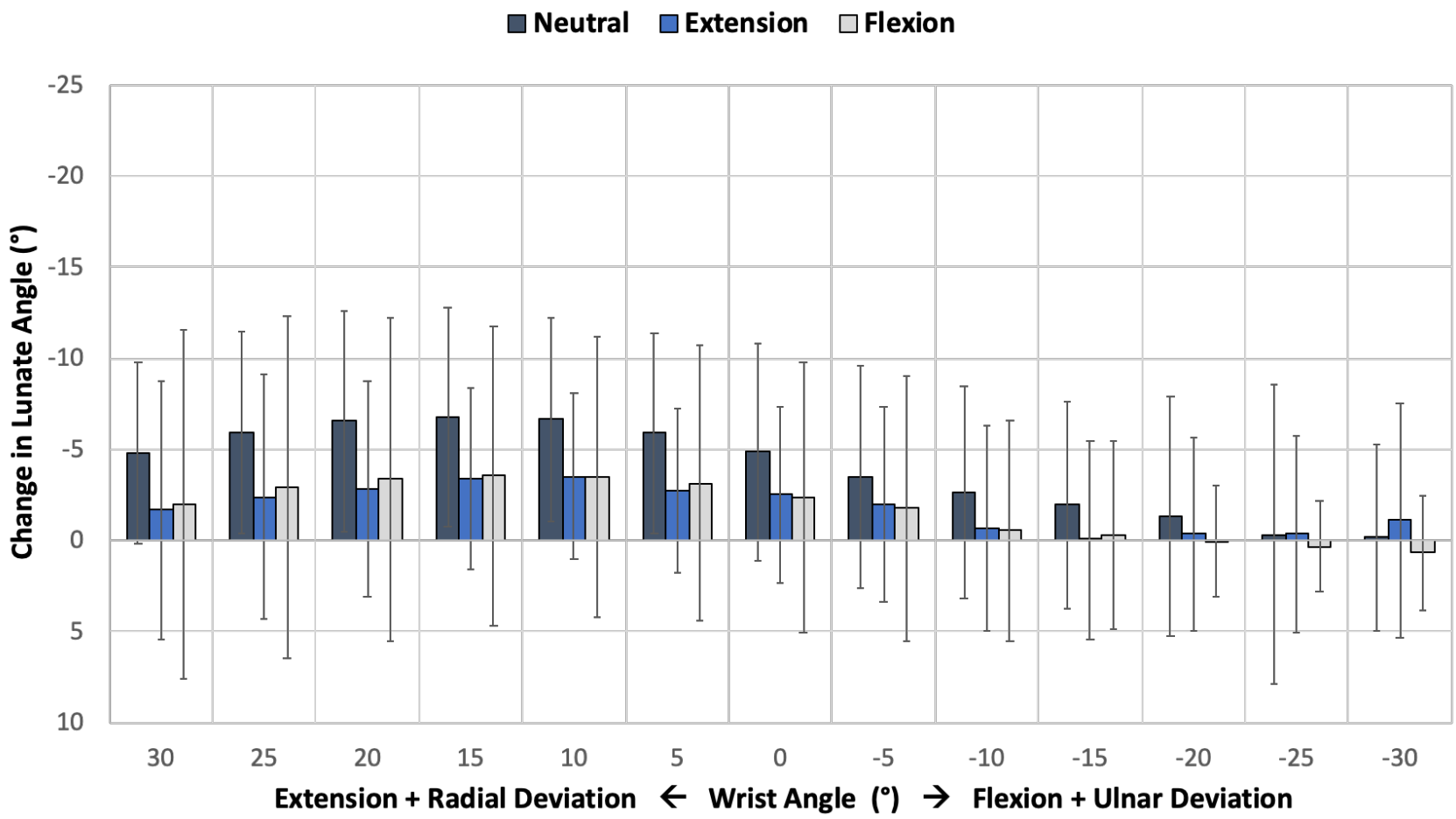

Figure 6-3: Lunate Rotation in Native State and Following Complete SLIL sectioning in Three Gravity Forearm Positions.

Mean angular rotation of the lunate in the native state and following complete SLIL sectioning in the neutral, gravity flexion and gravity extension forearm orientations during flexion-extension wrist motion.

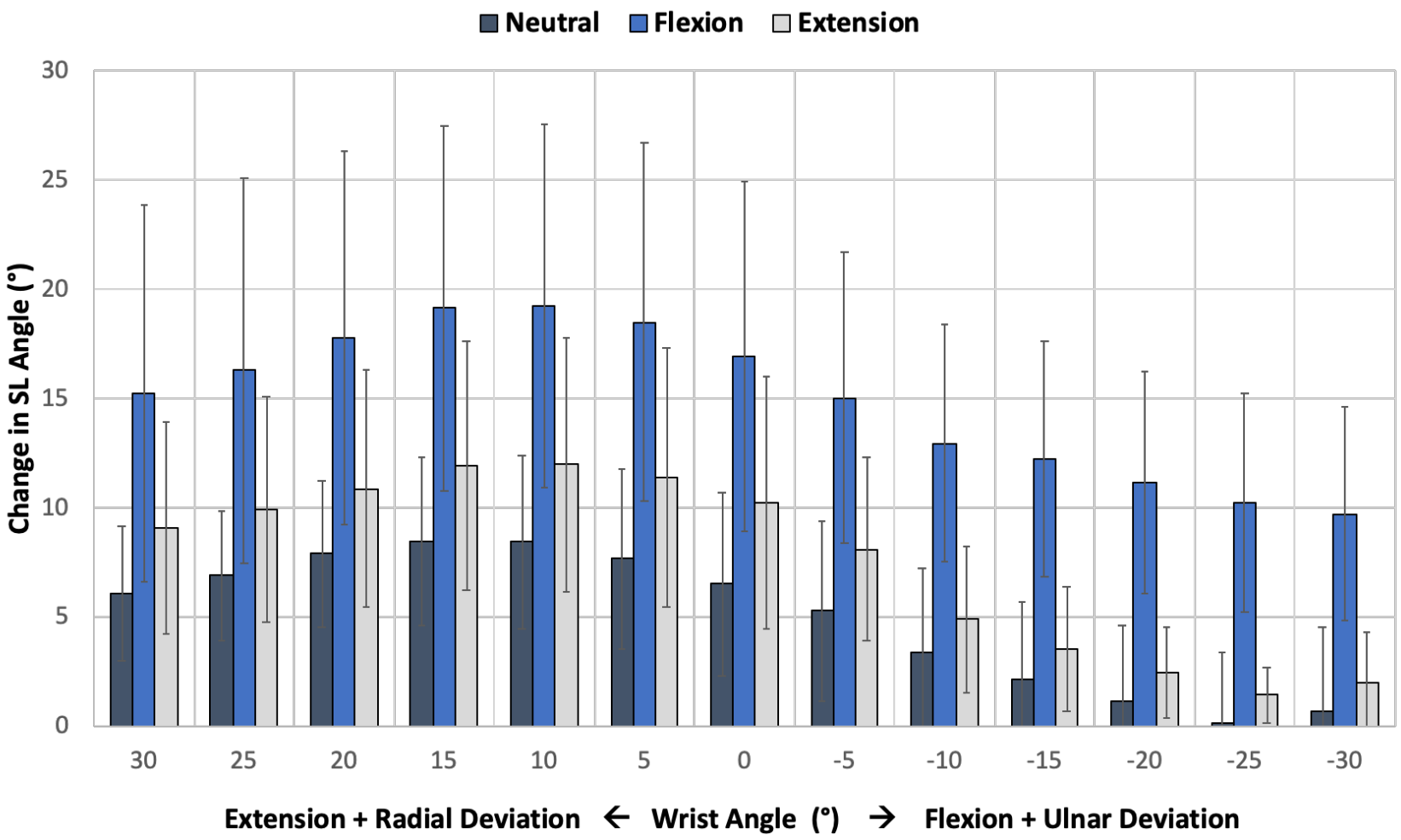

Figure 6-4: Scapholunate Rotation in Native State and Following Complete SLIL sectioning in Three Gravity Forearm Positions.

Mean angular scapholunate rotation in the native state and following complete SLIL sectioning in the neutral, gravity flexion and gravity extension forearm orientations during flexion-extension wrist motion.

6.3.2 SL Diastasis

The mean change in dorsal and volar SL diastasis between the intact state and complete SLIL sectioning was compared in the three gravity forearm positions (gravity neutral, gravity flexion, and gravity extension forearm positions) across the dart throwing motion arc. The data presented are the mean distance (mm) ± SD compared to the intact state unless otherwise specified. Significant increase in gapping of the dorsal SL interval occurred in all three forearm orientations ($p<.05$), but only during the flexion aspect of DTM (gravity neutral mean dif. = 1.0 ± 0.8 mm, gravity extension mean dif. = 1.1 ± 0.9 mm, gravity flexion mean dif. = 1.3 ± 1.1 mm) (Figure 6-5). Dorsal SL gapping during the extension aspect of DTM was not significantly different than the intact state in any of the forearm orientations tested. Volar SL gapping was also found to be similar in the SLIL injury state compared to the intact state in all three forearm orientations tested ($p=0.2$). There was a significant difference in dorsal and volar gapping in all three forearm orientations, but only during the flexion aspect of DTM ($p=0.4$).

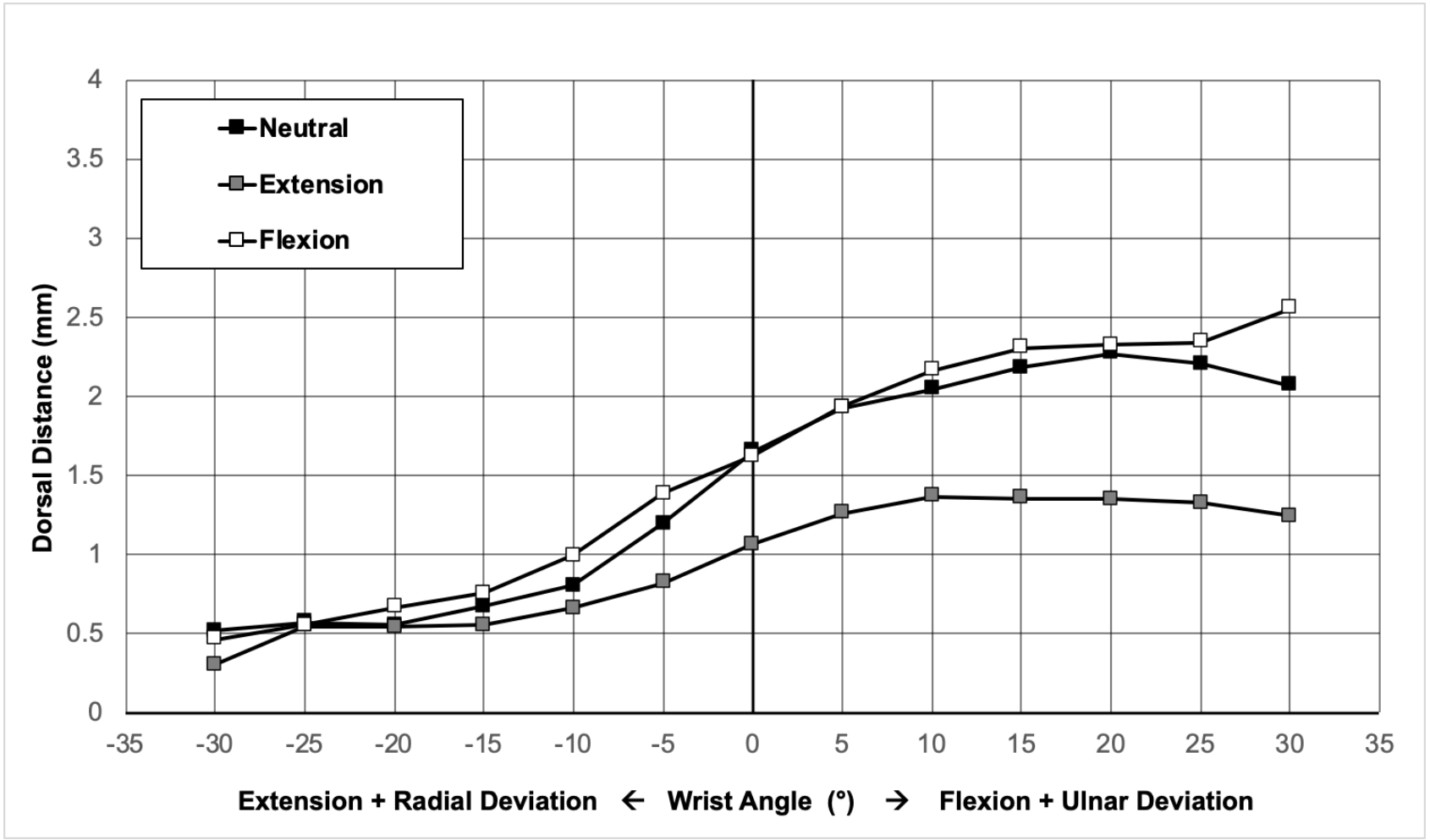

Figure 6-5: Change in Dorsal Scapholunate Diastasis Following Complete SLIL Sectioning in Three Gravity Forearm Positions.

Mean change in dorsal SL diastasis, normalized to the intact stage, following complete SLIL sectioning in the neutral, gravity flexion and gravity extension forearm orientations during flexion-extension wrist motion. Standard deviations were omitted for clarity but ranged from 0.7 to 1.6 for gravity neutral, 1.2 to 2.3for gravity flexion, and 0.8 to 1.2 for gravity extension.

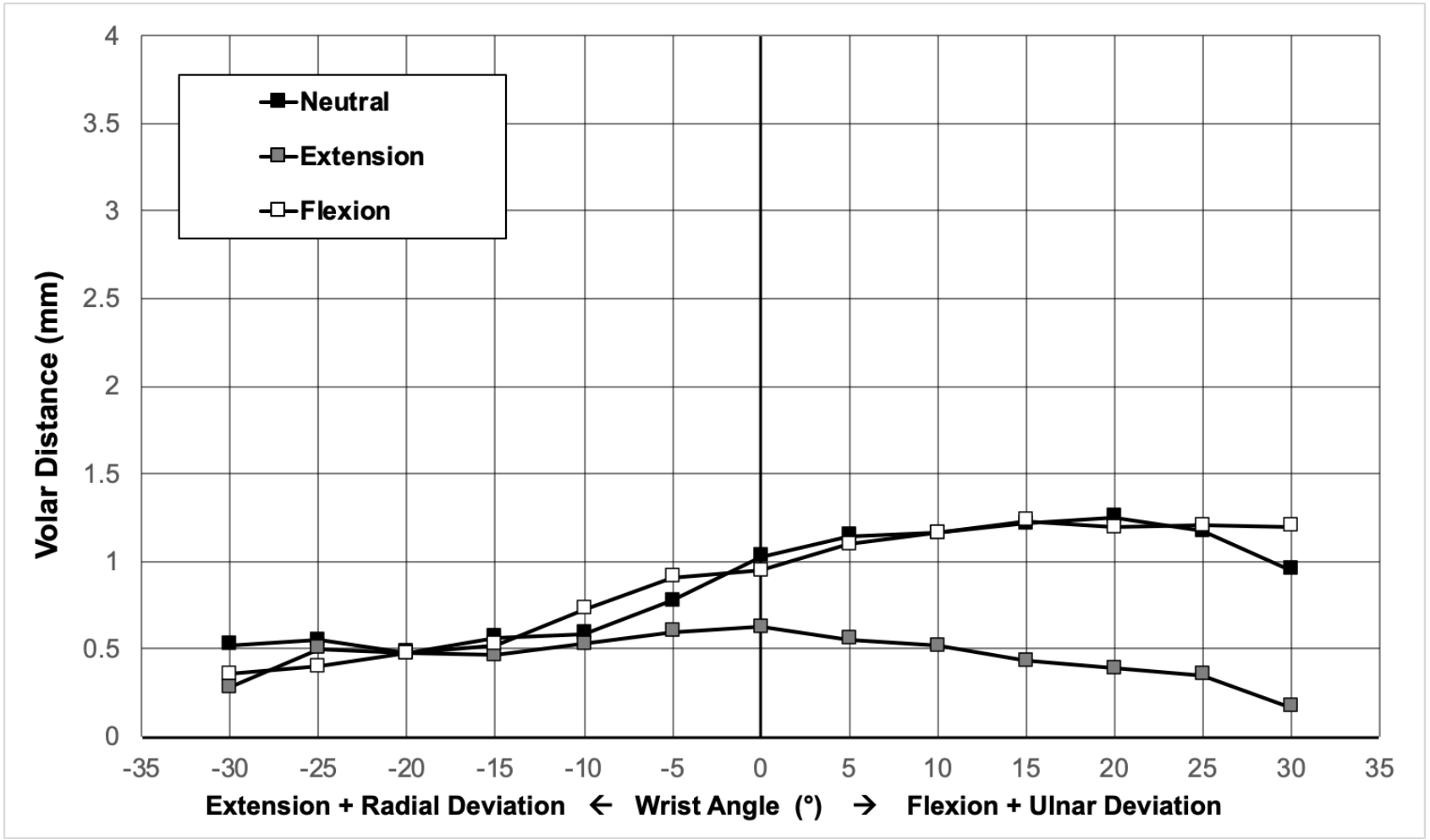

Figure 6-6: Change in Volar Scapholunate Diastasis Following Complete SLIL Sectioning in Three Gravity Forearm Positions.

Mean change in dorsal SL diastasis, normalized to the intact stage, following complete SLIL sectioning in the neutral, gravity flexion and gravity extension forearm orientations during flexion-extension wrist motion. Standard deviations were omitted for clarity but ranged from 0.6 to 1.0 for gravity neutral, 0.8 to 1.3 for gravity flexion, and 0.6 to 1.1 for gravity extension.

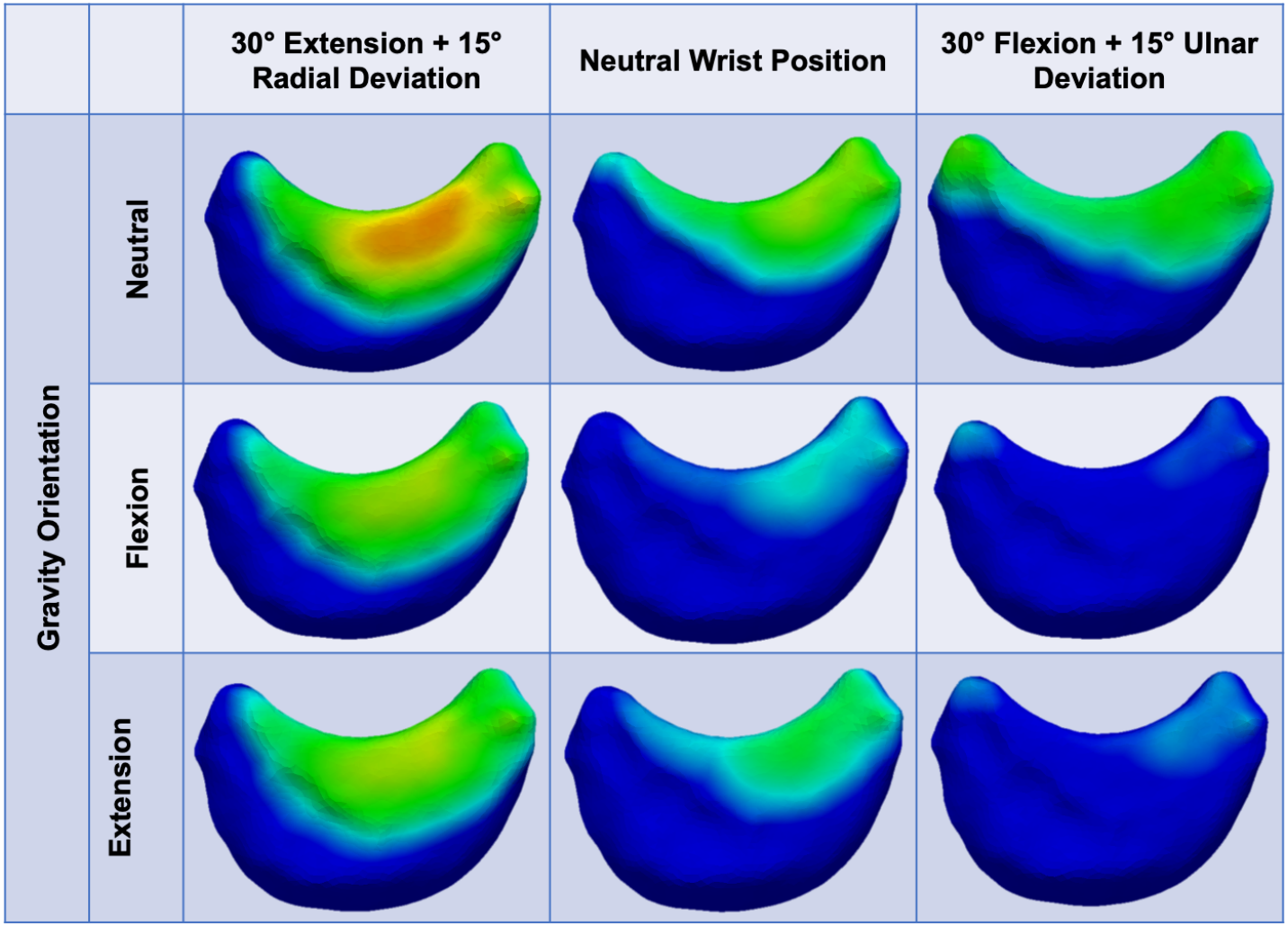

Figure 6-7: Scapholunate Diastasis in Three Gravity Positions.

Representative cross-sectional contact maps at the end points dart thrower motion and neutral wrist position following complete SLIL sectioning in three gravity forearm positions (gravity neutral, gravity flexion and gravity extension).

6.4 Discussion

SLIL injuries are treated conservatively with a period of immobilization or with surgical repair or reconstruction. Both non-operative and operative management require rehabilitation protocols which protect the SLIL yet allow motion to reduce stiffness. Recently, greater emphasis has been placed on the use of DTM in rehabilitation to restore wrist function while avoiding strain on the SLIL. The use of DTM in rehabilitation protocols has in part emerged from the knowledge produced by scientific and clinical evidence.[5,7–11] Previous work has found that scaphoid and lunate motion is minimized during DTM in the native wrist and is therefore thought of as protective of the SL interval.[8] Some works have cautioned incorporative the maximum extension component of DTM in rehabilitation protocols due to high SLIL strain[7], while others have suggested that the greatest gapping at the SL interval occurs at the maximum ulnar flexion component of DTM following SLIL injury.[12] Although recent studies have begun to elucidate the role of DTM in SLIL rehabilitation, this study provides greater insight into the effect of forearm orientation on SLIL injuries during DTM which will help to further evolve rehabilitation protocols.

In agreement with prior cadaveric studies, the results of this study show that sectioning of the SLIL causes changes in the relative angle between the scaphoid and lunate.[5,6,13–16] Waters et al. performed a cadaveric study using a large arc DTM and reported increased scaphoid flexion and lunate extension. Werner et al. executed a cadaveric study examining the *in-vitro* motion of the scaphoid and lunate during DTM. They also found SLIL sectioning caused increased scaphoid flexion and lunate extension. These aforementioned studies were performed on the same wrist joint motion simulator in the gravity neutral position (upright forearm orientation). The present study expands on the previous studies by investigating the role of gravity, and found that certain forearm orientations aggravate SLIL injuries. The gravity flexion forearm orientation caused significantly greater change in SL angle during DTM in comparison to the two other tested forearm orientations. On average the change in SL angle following SLIL sectioning was greater by $9.7 \pm 8.6°$ when compared to the gravity neutral forearm orientation, and by $7.4 \pm 5.4°$ when compared to the gravity extension orientation. Additionally, this study detected that the greatest change in SL angle occurred near the end range of extension during DTM, while smaller changes occurred near the end range of flexion during DTM.

Very few studies have examined SLIL gapping during DTM. In an *in-vivo* study, Garcia-Elias et al[17] compared subjects with SLIL insufficiency (n=6) to healthy patients (n=6). Dynamic 4-dimensional CT scans showed that when the SLIL was injured the scaphoid had significantly more radial translation in comparison to the lunate. Additionally, SL interval gapping was greatest at end-range ulnar flexion. Werner et al. investigated carpal translation and the minimum cortical distance between the scaphoid and lunate in a cadaveric study (n=37), that employed an active motion wrist joint simulator that uses the gravity neutral forearm orientation. The study reported dorsal translation of the scaphoid and radial translation of the lunate during DTM, however only reported the minimum cortical distance between the scaphoid and lunate for the flexion-extension and radial-ulnar deviation motion pathways. Although Dimitris et al[7] examined the forces across the SLIL during active motion of the wrist as opposed to SL interval gapping, they did find that SLIL force was greatest in the maximum extension component of DTM measured at 10° radial deviation, 30° extension which agree with the previous studies which suggest that end range DTM may not be suitable for rehabilitation. The results of the present study also agree with limiting end range DTM in rehabilitation as we found greater dorsal SL gapping at the end range of ulnar flexion during DTM. Similar to the kinematic changes that were noted, the greatest increase in dorsal gapping in the ulnar flexion aspect of DTM occurred in the gravity flexion orientation (1.3 ± 1.1 mm).

DTM is now commonly incorporated into SLIL injury rehabilitation protocols[9]. These protocols continue to evolve as cadaveric and clinical studies uncover new information. This study supports the use of DTM in rehabilitation protocols, however cautions the use of DTM in the gravity flexion or gravity extension forearm orientations as these positions caused greater angular changes between the scaphoid and lunate. Furthermore, similar to previous work, the authors suggest a truncated range of DTM, as maximum extension with radial deviation caused the greatest increase in relative SL motion.

There are limitations of this study. First, selective sectioning of cadaveric ligaments can serve to simulate wrist instability, the model may not be fully representative of the acute or chronic injury. Many previous studies that have examined SLIL insufficiency have also sectioned secondary stabilizers in addition to the SLIL[15,18]. Incorporating the sectioning of secondary stabilizers into future work would be beneficial to further the understanding the effect of forearm orientation on ligamentous injuries of the wrist. Second, the active motion simulator

used in this study simulated three gravity forearm positions, however, did not examine the effect of forearm rotation. Several previous studies have identified carpal posture differences as forearm rotation is varied, and this may be potentially of interest.

6.5 Conclusions

In conclusion, this cadaveric biomechanical study analyzes carpal kinematics and SL diastasis following complete SLIL sectioning using an active motion wrist joint simulator. From the results of this study, the authors recommend using a restricted range of DTM in acute SLIL injury and in post-reconstruction scenarios. Furthermore, the gravity flexion forearm position should be avoided as it appears to increase the gapping at the SL interval, potentially aggravating acute SLIL injuries or slowing healing following SLIL reconstruction.

6.6 References

1. Lindau T, Arner M, Hagberg L. Intraarticular lesions in distal fractures of the radius in young adults: A descriptive arthroscopic study in 50 patients. *J Hand Surg Eur Vol*. 1997;22(5):638-643. doi:10.1016/S0266-7681(97)80364-6

2. Skirven TM. Rehabilitation for Carpal Ligament Injury and Instability. In: *Rehabilitation of the Hand and Upper Extremity, 2-Volume Set*. ; 2011:1013-1023.e2. doi:10.1016/b978-0-323-05602-1.00075-1

3. Stoesser H, Padmore C, Nishiwaki M, Gammon B, Langohr G, Johnson J. Biomechanical Evaluation of Carpal Kinematics during Simulated Wrist Motion. *J Wrist Surg*. 2016;06(02):113-119. doi:10.1055/s-0036-1588025

4. Werner FW, Short WH, Fortino MD, Palmer AK. The relative contribution of selected carpal bones to global wrist motion during simulated planar and out-of-plane wrist motion. *J Hand Surg Am*. 1997;22(4):708-713. doi:10.1016/S0363-5023(97)80133-5

5. Waters MS, Werner FW, Haddad SF, McGrattan ML, Short WH. Biomechanical Evaluation of Scaphoid and Lunate Kinematics Following Selective Sectioning of Portions of the Scapholunate Interosseous Ligament. *J Hand Surg Am*. 2016;41(2):208-213. doi:10.1016/j.jhsa.2015.11.009

6. Padmore C, Stoesser H, Langohr GD, Johnson J, Suh N. Carpal Kinematics following Sequential Scapholunate Ligament Sectioning. *J Wrist Surg*. 2019;08(02):124-131. doi:10.1055/s-0038-1676865

7. Dimitris C, Werner FW, Joyce DA, Harley BJ. Force in the Scapholunate Interosseous Ligament During Active Wrist Motion. *J Hand Surg Am*. 2015;40(8):1525-1533. doi:10.1016/j.jhsa.2015.04.007

8. Bergner JL, Farrar JQ, Coronado RA. Dart thrower's motion and the injured scapholunate interosseous ligament: A scoping review of studies examining motion, orthoses, and rehabilitation. *J Hand Ther*. 2019. doi:10.1016/j.jht.2018.09.005

9. Wolff AL, Wolfe SW. Rehabilitation for scapholunate injury: Application of scientific and clinical evidence to practice. *J Hand Ther*. 2016;29(2):146-153. doi:10.1016/j.jht.2016.03.010

10. Crisco JJ, Heard WMR, Rich RR, Paller DJ, Wolfe SW. The mechanical axes of the wrist are oriented obliquely to the anatomical axes. *J Bone Jt Surg - Ser A*. 2011;93(2):169-177. doi:10.2106/JBJS.I.01222

11. Kakar S, Breighner R, Leng S, et al. The Role of Dynamic (4D) CT in the Detection of Scapholunate Ligament Injury. *J Wrist Surg*. 2016;05(04):306-310. doi:10.1055/s-0035-1570463

12. Garcia-Elias M, Alomar Serrallach X, Monill Serra J. Dart-throwing motion in patients with scapholunate instability: A dynamic four-dimensional computed tomography study. *J Hand Surg Eur Vol*. 2014;39(4):346-352. doi:10.1177/1753193413484630

13. Crisco JJ, Pike S, Hulsizer-Galvin DL, Akelman E, Weiss APC, Wolfe SW. Carpal Bone Postures and Motions Are Abnormal in Both Wrists of Patients with Unilateral Scapholunate Interosseous Ligament Tears. *J Hand Surg Am*. 2003;28(6):926-937. doi:10.1016/S0363-5023(03)00422-2

14. Werner FW, Short WH, Green JK. Changes in Patterns of Scaphoid and Lunate Motion During Functional Arcs of Wrist Motion Induced by Ligament Division. *J Hand Surg Am*. 2005;30(6):1156-1160. doi:10.1016/j.jhsa.2005.08.005

15. Short WH, Werner FW, Green JK, Masaoka S, Walter H. Short, MD, Frederick W. Werner, MME, Jason K. Green, BS, and Shunji Masaoka, MD P. Biomechanical Evaluation of Ligamentous Stabilizers of the Scaphoid and Lunate. *J hand surg am*. 2002;27(6):991-1002. doi:10.1053/jhsu.2002.35878.Biomechanical

16. Walter H. Short, MD, Frederick W. Werner, MME, Jason K. Green, BS, Levi G. Sutton, BS, and Jean Paul Brutus M, Schimmerl-Metz SM, Metz VM, et al. Biomechanical Evaluation of the Ligamentous Stabilizers of the Scaphoid and Lunate: Part III. *Hand*. 2018;32(3):297-309. doi:10.1016/j.neuron.2009.10.017.A

17. Garcia-Elias M, Alomar Serrallach X, Monill Serra J. Dart-throwing motion in patients with scapholunate instability: A dynamic four-dimensional computed tomography study. *J Hand Surg Eur Vol*. 2014;39(4):346-352. doi:10.1177/1753193413484630

18. Short WH, Werner FW, Green JK, Masaoka S. Biomechanical Evaluation of the Ligamentous Stabilizers of the Scaphoid and Lunate: Part II. *J Hand Surg Am*. 2005;30(1):24-34. doi:10.1016/j.jhsa.2004.09.015

Chapter 7

7 General Discussion and Conclusions

OVERVIEW

This chapter summarizes the objectives and hypotheses of this thesis, and discusses the studies performed to accomplish these objectives, as well as the findings of these investigations. The strengths and limitations of the current work are outlined as are the future directions of this wrist research.

7.1 Summary and Conclusions

To fully understand the biomechanics of the normal and pathological wrist, a more detailed understanding of the influence of experimental framework and how each decision made during development of experimental apparatus' or study protocol can affect study outcomes is essential. The present work describes several *in-vitro* wrist biomechanical cadaveric studies, the advancement and implementation of a non-invasive joint congruency technique, and application of this method to better understand a common clinical entity of scapholunate insufficiency. The specific objectives outlined in Chapter 1 have been accomplished with results supporting or rejecting our hypotheses.

The objectives of this thesis were:

1. To determine the radiocarpal and midcarpal joint contributions to global wrist motion
2. To assess current methodologies for generating wrist coordinate systems and compare how coordinate system selection effects the calculation of global wrist joint angle;
3. To develop and validate a CT-based joint congruency method to determine a reliable threshold value which accurately represents articular contact;
4. To assess the effect of forearm orientation on carpal kinematics and radiocarpal contact mechanics during simulated active wrist motion;
5. To evaluate the effect of forearm orientation on an injury model - particularly scapholunate insufficiency and determine which forearm orientation provides the greatest stability to the scapholunate joint.

7.1.1 Chapter 2: The Relative Contributions of the Radiocarpal and Midcarpal Joints to Wrist Motion: A Biomechanical Study

The first objective of this body of work was to investigate the relative contributions of the radiocarpal and midcarpal joints during wrist flexion and extension. This objective was achieved through the application of a passive wrist motion simulator. A constant load was applied to the wrist flexors and extensors throughout wrist motion to simulate the physiologic compressive force observed at the wrist. Planar wrist flexion-extension was simulated by passively guiding each specimen through the desired range of motion. Optical tracking was used to capture the 3D motion of the bones of interest, and custom data analysis software was

used to determine the relative contributions of the radiocarpal and midcarpal joints to motion through wrist flexion and extension.

The results of Chapter 2 suggest the radiocarpal joint contributes more to wrist extension than the midcarpal joint, while the midcarpal joint contributes more to global wrist motion in wrist flexion than the radiocarpal joint, while near neutral wrist position there is a relatively equal contribution from both joints to global wrist motion. The results of this study reject the hypothesis that the radiocarpal and midcarpal joint would contribute equally to global wrist joint motion as stated in Chapter 1.

In addition to examining the research question of joint contributions, this chapter served as the starting point for further investigation into wrist joint biomechanics. From this study we were able to identity opportunities for improvements in biomechanical testing techniques and analyses, in addition to spurring additional research questions including those related to joint contact mechanics in the native and pathological wrist.

7.1.2 Chapter 3: Investigation of the Effect of Coordinate System Selection on Wrist Kinematics

The second objective of this dissertation was to assess current methodologies for generating wrist coordinate systems and compare how joint coordinate system (JCS) selection affects the calculation of global wrist joint angle. This goal was accomplished using a wrist joint motion simulator. Planar wrist flexion-extension and radial-ulnar deviation was passively simulated by hand guiding the wrist through the motion pathways, while constant loads were applied to the wrist flexor and extensor muscle groups to simulate physiologic compressive forces at the wrist.

The results do not favor one JCS generation method over another, as all were found to be similar and the small differences observed were not thought to be clinically significant. These findings support the use of any of the currently employed JCS generation methods. A practical advantage of using the methods developed by Padmore et al, and Hillstrom et al. is that the required digitized points to form the JCSs are palpable. The results of this chapter reject the hypothesis stated in Chapter 1, which stated that a single coordinate system generation method will emerge as most consistent in describing wrist angle and will provide the smallest deviation from clinically measured wrist angle, as measured by a goniometer.

7.1.3 Chapter 4: Comparison of a CT-Based Joint Congruency Method for Assessing Joint Contact Mechanics of the Wrist

The third objective was to adapt and validate a CT-based joint congruency method for the wrist and to determine a reliable threshold value which accurately represents articular joint contact. The results from Chapter 4 described alterations to a previously validated non-invasive CT-based technique to predict joint contact at the wrist and then used Tekscan® to validate the technique. The threshold value which aligned with Tekscan® joint contact measurements, and reliably predicted joint contact area was markedly less than the value used in the elbow and at the distal radioulnar joint in other studies in our laboratory. This has important consequences to future studies using this technique to examine joint contact mechanics at the wrist. Investigators should use an appropriate threshold value depending on the joint of interest.

7.1.4 Chapter 5: Investigating the Effect of Forearm Orientation on Native Scapholunate Kinematics and Radiocarpal Contact Mechanics during Active Wrist Flexion-Extension

The fourth objective of this body of work was to assess the effect of forearm orientation on carpal kinematics and radiocarpal contact mechanics during physiologic active wrist motion. This goal was achieved by using a novel active motion wrist simulator, with the capacity to simulate wrist motion in different forearm gravity positions described in Chapter 5. The results of Chapter 5 demonstrated that the gravity loading affects wrist contact mechanics and wrist kinematics. First, radiocarpal contact was found to be variable and dependent on forearm position and wrist angle. Contact area at the radioscaphoid joint was maximal in the gravity extension orientation and wrist extension position. These findings were consistent with previous literature that reported increased radioscaphoid contact in wrist extension.[1,2] Second, this study found that radiolunate contact is not dependent on wrist angle or forearm position, which is not surprising as the joint is known to be very congruent with a very similar radii of curvature between the lunate fossa and the convex surface of the radius. Lastly, the results of this study demonstrated that scaphoid rotation is affected by forearm orientation but only at the extremes of wrist flexion-extension.

The novel information ascertained in this chapter will help guide future work and could also greatly impact rehabilitation protocols and post-operative care. In the case of wrist rehabilitation, one proposed standard protocol includes placing the forearm in the horizontal

orientation with neutral pronation, followed by the performance of exercises.[3] However, the results of Chapter 5 illustrate that there is increased joint contact in horizontal forearm orientations, and the gravity neutral forearm orientation may be more protective of the proximal carpal row and the radiocarpal joints.

7.1.5 Chapter 6: Examination of the Role of Forearm Orientation on Scapholunate Injuries with Applicability in Rehabilitation Protocols and Post-Operative Management

The fifth objective of this thesis was to evaluate the effect of forearm orientation on a clinically relevant injury model of scapholunate insufficiency and determine which forearm orientation provides the greatest stability to the scapholunate joint. Similar to Chapter 5, this goal was achieved by using a novel active motion wrist joint simulator, with the ability to simulate physiologic wrist motion in various forearm gravity positions, along with the joint congruency metod to assess contact. To adequately evaluate scapholunate joint stability, dart thrower motion was simulated as it has gained clinical acceptance as a protective motion pathway for scapholunate injury or rehabilitation. From the results of Chapter 5, the authors recommend using a restricted range of DTM in acute SLIL injury and in post-reconstruction scenarios due to greater SL gapping and intercarpal motion occurring at the end point of dart thrower motion. Furthermore, the results of Chapter 6 agree with Hypothesis 5, as the results showed that the gravity flexion and gravity extension forearm positions should be avoided as they appear to increase the gapping at the SL interval, causing unwanted stress of the SLIL. These results will aid clinicians and rehabilitation specialists in developing better management protocols for scapholunate injuries; as the gravity neutral position appears as the gravity neutral position. Additionally, although this study examined a single wrist pathology, the results illustrated that gravity does play a role in wrist injuries. As such the results of this body of work strongly recommend that gravity is considered when designing both experimental and clinical rehabilitation protocols.

7.2 Strengths and Limitations

Similar to all *in-vitro* biomechanical studies, the present work had various strengths and limitations.

A strength of this body of work was that despite smaller sample sizes all studies had adequate power, likely due to the highly repeatable experimental protocols of each study as well as the use of repeated measures data analysis which allowed for the evaluation of differences within each specimen. The studies discussed in Chapters 3-6 used a novel, but previously validated active motion joint simulator which accurately and repeatably simulated physiologic wrist motion. The active motion simulator used in body of work, in contrast to similar *in-vitro* biomechanics studies, maintained all soft tissue structures and specimen hydration was maintained through the closure of any incision. All studies employed a highly accurate motion capture system which likely reduced measurement error and increased the repeatability of results. Furthermore, the motion capture technique that was employed captured real time kinematic measurements through the entire tested range of motion; including complex wrist motions such as dart-thrower motion. Another strength of this study was the use of an advanced non-invasive CT-based technique to evaluate joint contact mechanics. This technique used accurate cartilage covered bone models to predict joint contact at the wrist.

This work also had limitations. Chapter 2 employed a passive motion joint simulator, and as such this could have affected the results, as varying physiological loads were not applied during flexion-extension motion. However, we attempted to mitigate the differences that may occur between active and passive motion by applying constant tone loads to the flexor and extensor muscles of the forearm. All studies included in this body of work analyzed a truncated range motion analysis, due to specimen variability, therefore the true extremes of motion were not analyzed. Furthermore, Chapter 2 neglected to investigate the effect of forearm orientation. Future work should examine how carpal contributions to motion are affected by forearm orientation, as this will further our understanding of normal wrist biomechanics. Chapters 2-5 analyzed planer wrist motions and did not account for complex multiplanar motion. However, Chapter 6 did build on previous work and included the analysis of dart thrower motions. Additionally, optical trackers were mounted in all studies, with the exception of Chapter 3, and tracker impingement within the carpal bones could have affected carpal bone rotation.

However, each tracker was checked fluoroscopically at the time of insertion and no impingement was evident within the arc of motion analyzed. We also acknowledge the inherent limitations of *in-vitro* cadaveric studies. Soft tissue adaptations and healing following injury could not of course be modeled *in-vitro*. Lastly, it is possible that while statistically significant differences were found in this body of work, these differences may not manifest in clinical significance.

7.3 Current and Future Directions

There exists an immense opportunity to further develop *in-vitro* wrist testing strategies to elucidate normal and pathological wrist biomechanics. First, the active motion joint simulator used in Chapters 4-6 of this thesis currently employs equal proportion of load to each flexor and extensor of the forearm, but further refinement using information from EMG studies could improve the performance of the active motion joint simulator, to allow for more accurate simulation of physiologic wrist motion. Additionally, these studies focused on planar wrist motion, and a single complex motion pathway called the dart thrower motion. *In-vitro* cadaveric testing would greatly benefit from focusing on more complex motion pathways, as they more realistically simulate physiologic motion. However, simulating more complex motion pathways comes with its own set of challenges.

Second, studies are already ongoing to incorporate surface registration into the current landmark registration protocol which was described in Chapter 4 of this thesis. A combination of surface registration in addition to landmark registration provide superior registration error and accuracy to the ICD technique. Further minimization of error when using the ICD technique in the wrist is imperative as the scale of the articulations of the wrist joint are small. Additionally, these ongoing studies strive to further automate the ICD procedure to decrease the data analysis time.

Finally, efforts should be made to develop finite element models of the wrist to examine joint contact forces. Although this body of work looked into changes in contact area, finite element modeling could impact our knowledge of disease progression and force transmission at the wrist. Through the use of the ICD technique to establish 3D bone and cartilage position in testing space, kinematic driven finite element models can be created to yield contact stress

information over a wrist motion arc, as opposed the traditional modeling of static positions. Furthermore, finite element modeling will extend our knowledge of contact mechanics by understanding the relationship between contact area and contact stress.

7.4 Conclusions

As the prevalence of wrist injuries is high, a greater understanding of native and pathological wrist biomechanics is paramount. The present work shows the importance of a rigorous experimental framework and developing an understanding of how each decision made during experimental apparatus or protocol development affects the study results. The potential consequences of not understanding base assumptions when designing testing apparatus or studies may lead to biased data reporting and thus misguided data interpretation. Furthermore, highly standardized experimental designs will lead to more accurate and repeatable results. Reliable results are paramount in knowledge translation as they affect an investigator's or clinician's ability to trust outcomes and advance research and clinical management of wrist pathologies. The results from this body of work will help investigators gain a greater understanding of how assessment techniques affect results and will help improve overall wrist biomechanics research.

7.5 References

1. Chen YR, Wu YF, Tang JB, Giddins G, Y. R. Chen1, Y. F. Wu1 JBT and GG. Contact areas of the scaphoid and lunate with the distal radius in neutral and extension: correlation of falling strategies and distal radial anatomy. *J Hand Surg Am*. 2014;39E(4):379-383. doi:10.1016/j.jhsa.2006.05.002

2. Tang P, Gauvin J, Muriuki M, Pfaeffle JH, Imbriglia JE, Goitz RJ. Comparison of the "Contact Biomechanics" of the Intact and Proximal Row Carpectomy Wrist. *J Hand Surg Am*. 2009;34(4):660-670. doi:10.1016/j.jhsa.2008.12.004

3. Hagert E. Proprioception of the Wrist Joint: A Review of Current Concepts and Possible Implications on the Rehabilitation of the Wrist. *J Hand Ther*. 2010. doi:10.1016/j.jht.2009.09.008

Appendix A - Glossary

This appendix contains a list of the terminology used through this thesis. Anatomical

ANOVA	Analysis of Variance, a statistical method for simultaneous comparisons between two or more means
Articular Cartilage	A specialized, fibrous connective tissue that covers the surface of synovial joints
Arthritis	Painful inflammation and stiffness of a joint Muscle
Cadaveric	Of, or pertaining to, a dead body preserved for anatomical study
Carpus	The bones of the wrist
Computed Tomography	Medical imaging method used to generate a three-dimensional image of the inside of an object using a series of two-dimensional images
Denude	To strip a bone of its soft tissue
Distal	Further from the beginning; opposite to proximal
Dorsal	Pertaining to the back, opposite to volar
Extension	The act of moving a part of the body, limb, from a bent to straight position; opposite to flexion
Extensor	Any muscle that extends a joint
Flexion	The action of bending or the condition of being bent; opposite to extension
Flexor	Any muscle that flexes a joint
Goniometer	An instrument for precise measurements of the joints of the body
In-Vitro	In an artificial environment
In-Vivo	Within the living body
Joint	The place of union or junction between two or more bones of the skeleton

Joint Congruency	The native osseous interaction and inherent stability of two bones
Kinematics	The study of motion of one body with respect to another
Kinetics	The study of forces acting on one body with respect to another
Ligament	A band of fibrous tissue connecting bones or cartilages serving to support and strengthen joints
Newton	The SI unit of force; it is equal to the force that would give a mass of one kilogram an acceleration of one metre per second per second
Pronation	Applied to the hand, the act of turning or placing the palm backward (posteriorly) or downward; opposite to supination
Proximal	Nearest to the point of reference; opposite to distal Pertaining
Radius	A long, slightly curved bone that lies to the lateral side of the forearm when in the anatomical position; it is the shorter and thicker of the two bones found in the forearm
Range of Motion	Amount of motion attained during an activity
Rotation Matrix	An algebraic description of rotation in three dimensions
Supination	Applied to the hand, the act of turning or placing the palm forward (anteriorly) or upward; opposite to supination
Tendon	A fibrous cord of connective tissue continuous with the fibers of a muscle and attaching the muscle to bone or cartilage
Transformation matrix	An algebraic description of rotation and translation in three dimensions
Ulna	The bone extending from the elbow to the wrist on the side opposite to the thumb; the inner and large bone of the forearm
Volar	Pertaining to the front or palm, opposite to dorsal

Appendix B – Carpal Tracker Mounts

Figure B-0-1 Scaphoid Tracker Mount.

Illustration of the scaphoid tracker mount inserted through a volar incision over the tuberosity. Secured with 2.7mm cortical bone screws.

Figure B-0-2 Lunate Tracker Mount.

Illustration of the lunate tracker mount inserted through a dorsal incision over the midpoint of the body. Secured with 2.7mm cortical bone screws

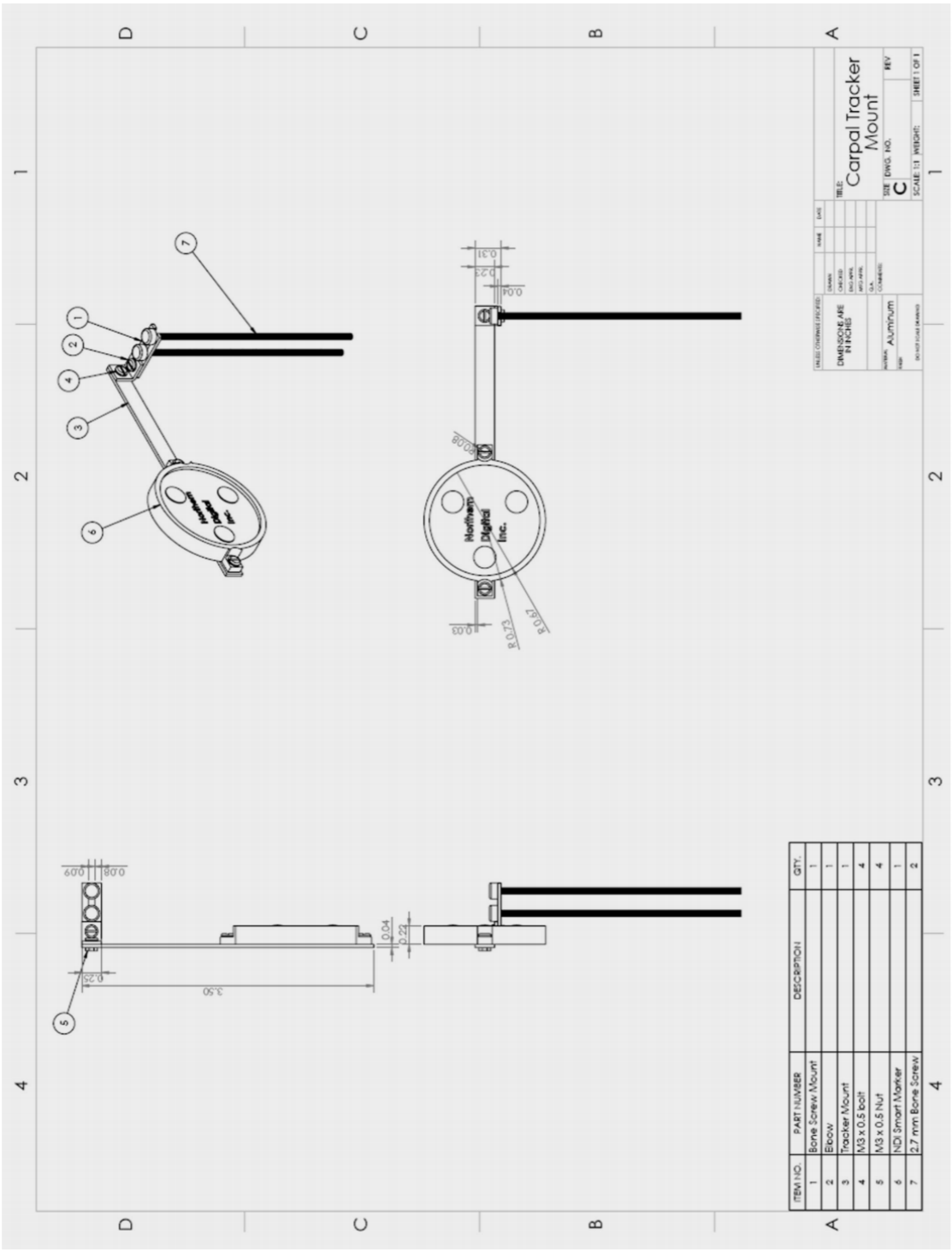

Figure B-0-3 Carpal Tracker Mount.

Drawing used to machine the carpal tracker mounts. The mounts were designed with three degrees of freedom allowing for variable set up. Accounts for inter-specimen variability and visibility issues.

Appendix C – Carpal Coordinate System Construction

Background

The International Society of Biomechanics (ISB) recommends carpal coordinate systems for each bone to be aligned with the radial coordinate system when the wrist is in the neutral anatomical position, when the long axis of the third metacarpal and radius are parallel. The volumetric centroid of the bone is defined as the origin of each carpal coordinate system. This method accounts for the variations between the different carpals and relates the coordinate systems to the relative geometry of the wrist.

Digitization and Registration

Following the completion of the investigation, the bones of interest were resected and isolated. The surface of the scaphoid, lunate, and capitate and third metacarpal were traced using an optical stylus (Certus Optotrack, Northern Digital Inc., Waterloo, Canada) and saved as a point cloud. A CT scan of each carpal bone was obtained and modified using 3-Matic (version 21.0, Materialise, Leuven, Belgium), to create an equally distributed surface mesh for each bone of interest. Using custom software, the mesh created from the CT scan and the digitization mesh were reoriented and registered into the same frame using a least-squares data fitting algorithm with visual confirmation. All digitization points were discarded, and the registered surface mesh was averaged to obtain the volumetric centroid and serve as the origin for each carpal coordinate system.

Coordinate Systems Construction

To report relative carpal kinematics during wrist motion, we determined the transformation required to bias the initial set of carpal data to the neutral reference frame. To construct this transformation, a regressive search algorithm was used to determine the instance of most neutral wrist position, obtained from the third metacarpal with respect to the radius, and a 4x4 transformation matrix was constructed using the origin of the carpal of interest and the 3x3 rotation matrix of the radius

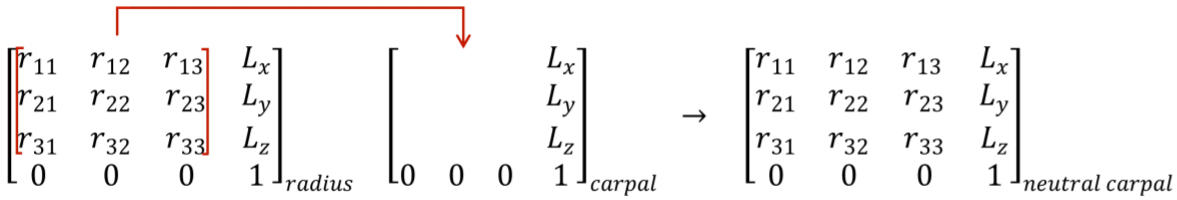

Figure C-1: Construction of the Neutral Carpal Frame

Following the construction of the neutral carpal frame, the transformation required to convert the original data from to the neutral frame can be calculated. Both frames share the same origin resulting in a rotation bias to convert one to the other. This transformation was collected for each carpal bone and applied to each frame within the data set.

$$[T_{NC}^{G}] = [T_{C}^{G}][T_{NC}^{C}]$$

Where:

$[T_{NC}^{G}]$ → Neutral carpal frame with respect to global

$[T_{C}^{G}]$ → Original carpal frame with respect to global

$[T_{NC}^{C}]$ → Original carpal frame with respect to neutral carpal frame

By rearranging the equation, we are able to isolate the necessary transformation, and apply it accordingly:

$$[T_{NC}^{C}] = [T_{C}^{G}]^{-1}[T_{NC}^{G}]$$

Curriculum Vitae

Clare Padmore MEng.

The Hand and Upper Limb Clinic
Lawson Health Research Institute, St. Joseph's Hospital

PhD Candidate
Biomedical Engineering Graduate Program
The University of Western Ontario

EDUCATION

Doctor of Philosophy Candidate - Biomedical Engineering, Biomechanics: Collaborative Training Program in Musculoskeletal Health Research — 2014 - Present
University of Western Ontario, London, Ontario

Master of Engineering – Mechanical and Materials Engineering (Medicine) — 2013-2014
University of Western Ontario, London, Ontario

Bachelor of Science - Civil Engineering (Psychology Minor) — 2009-2013
Rensselaer Polytechnic Institute, Troy, USA

HONOURS AND AWARDS

Joan Fich Padmore Memorial Scholarship: Award for Citizenship — 2018
Toronto Aeros Girls Hockey Association, Toronto, ON, Canada

CMHR Transdisciplinary Bone & Joint Training Award — 2017-2018
University of Western Ontario, London, Canada

Best Plastic Surgery Resident Project (co-author) — 2017
Schulich School of Medicine, University of Western Ontario, London, Canada

Top Guest Society Poster at American Society for Surgery of the Hand Annual Meeting — 2017
American Society for Surgery of the Hand San Francisco, CA, USA

Best Hand and Wrist Poster at Orthopedic Research Society Annual Meeting (co-author) — 2017
Orthopedic Research Society. San Diego, CA, USA

Best Orthopedic Trauma Podium Presentation at The Canadian Bone and Joint Conference — 2016
Canadian Bone and Joint Institute, London, ON, Canada

NCAA Division I Athletic Scholarship (Women's Ice Hockey) — 2009-2013
Rensselaer Polytechnic Institute, Troy, NY, USA

ECAC All – Academic Team (Women's D1 Ice Hockey) 2012-2013
Rensselaer Polytechnic Institute, Troy, NY, USA

Dean's Honour List 2012-2013
Faculty of Civil Engineering, Rensselaer Polytechnic Institute, Troy, NY, USA

RELATED WORK EXPERIENCE

Graduate Research Assistant
University of Western Ontario, London, ON
- Role: Senior graduate student, study design, data collection and analysis, manuscript preparation

Teaching Assistant
University of Western Ontario, London
- ESGSCI 9010 (3 semesters), MME 4469 (3 semesters), MME 2212 (2 semesters), MME 9601A (1 semester), MME 3381 (1 semester)

Western Summer Academy (Biomedical Engineering Camp) – Instructor
London, Canada
- Developed, implemented and lead high school student through an introduction to biomedical engineering

RCM Technologies – Project Management
Pickering, Ontario
- Updated and managed project databases, and drafted technical engineering documents (project reports, purchase orders, and building sketches).
- Assisted procurement engineering in the purchase of building materials and equipment, and reviewed documentation to ensure correctness.
- Provided overall technical support to the project management team.

Withrow Park Ball Hockey Association: Volunteer Coach
Toronto, Canada
- Head coach of the U16 Girls Provincial Ball Hockey Team
- Head coach of the U18 Girls House Ball Hockey Team (2 seasons)
- Co-Head coach of the Women's House League Ball Hockey Team (2 seasons)
- Assistant Coach of Women's Masters World Championship Team (Florida, USA)

Hart and Stride Hockey School - Coach
Toronto, Canada
- Development and executed practices and skills sessions to develop skating and hockey skills for a variety of skill levels and age groups (3-17 years)

Biomedical Engineering Graduate Department: Sports Rep
Western University, London
- Organized and lead Biomedical Engineering graduate sports teams and activities

PUBLICATIONS

PEER-REVIEWED RESEARCH PUBLICATIONS

1. Kadar, A., **Padmore, C.,** Fan, S., Langohr, GD., Grewal, R., Suh, N. "How Much Scaphoid Can be Safely Resected? A Biomechanical Analysis of the effects of Distal Scaphoid Resection". Hand (Submitted 2020)

2. Chambers, S. **Padmore, C.,** Fan, S., Grewal, R., Johnson, JA., Suh, N. "The Impact of Scaphoid Malunion on Carpal Motion: A Biomechanical Analysis". Journal of Wrist Surgery- American Ed. (Submitted)

3. **Padmore, C**. Chan, AHW., Langohr, GDG., Johnson, JA. Suh, N. "Wrist Joint Kinematics is Affected by Forearm Position during Active Flexion and Extension". Journal of Wrist Surgery (American Edition) (Submitted 2019)

4. Chan, AHW., **Padmore, C**., Langohr, GDG., Johnson, JA., Suh, N.A "Biomechanical Evaluation of the ECRL Tenodesis for Reconstruction of the Scapholunate Ligament". Journal of Hand Surgery (American Edition) (Submitted 2019)

5. **Padmore, C**. Chan, AHW., Langohr, GDG., Suh, N., Johnson, JA. "The Effect of Coordinate System Selection on Wrist Kinematics". Journal of Biomechanics (Submitted 2019)

6. Badre, A., Axford, D., **Padmore, C**., Faber, K., Johnson, JA., King, JW. "Effect of Ulnar Angulation and Soft Tissue Sectioning on Radial Head Stability in Anterior Monteggia Injuries: An In Vitro Biomechanical Study". *J Shoulder Elbow Surg*. 2020;29(6):1249-1258. doi:10.1016/j.jse.2019.10.025

7. Chambers, S., **Padmore, C**. Suh, N. "The Impact of Scaphoid Malunion on Radioscaphoid Joint Contact: A Computational Analysis". [published online ahead of print, 2020 Mar 24]. *J Hand Surg Am*. 2020;S0363-5023(20)30056-3. doi:10.1016/j.jhsa.2020.01.009

8. Isa, A., McGregor, M., **Padmore, C**., Langohr, GDG., Johnson JA., King, GW., Suh, N. "Effect of Radial Lengthening on Distal Forearm Loading Following Simulated in-vitro Radial Shortening." J Hand Surg Am. 2019 May 21. pii: S0363-5023(18)30457-X.

9. Isa, A., McGregor, M., **Padmore, C**., Langohr, GDG., Johnson JA., King, GW., Suh, N. "The effect of ulnar shortening on distal forearm loading during wrist and forearm motion: Implications in the treatment of ulnocarpal impaction". J Hand Surg Am. 2019 May 21. pii: S0363-5023(18)30457-X

10. **Padmore, C**., Stoesser, H., Langohr, G., Johnson, J., Suh, N. "Carpal Kinematics Following Sequential Scapholunate Ligament Sectioning". J Wrist Surg. 2019 Apr;8(2):124-131.

11. Wu, K., **Padmore, C**., Suh, N. "An Anthropometric Assessment of Proximal Hamate Autograft for Scaphoid Proximal Pole Reconstruction". J Hand Surg Am. 2019 Jan;44(1):60.e1-60.e8

12. **Padmore, C**., Stoesser, H., Nishiwaki, M., Gammon, B., Welsh, M., Langohr, G., Lalone, E., King, GJW., Johnson, JA. The Effect of Dorsally Angulated Distal Radius Deformities on Carpal Kinematics: An In-Vitro Biomechanical Study. J Hand Surg Am. 2018 Nov;43(11):1036.e1-1036.e8.

13. Stoesser, H., **Padmore, C**., Nishiwaki, M., Gammon, B., Langohr, GJW., Johnson, JA. Biomechanical Evaluation of Carpal Kinematics During Simulated Wrist Motion. J Wrist Surg. 2017 May;6(2):113-119.

SELECT PEER-REVIEWED ABSTRACTS AND CONFERENCE PRESENTATIONS

1. Badre A, **Padmore CE**, Axford DT, Faber KJ, King GJW, Johnson JA. (2019). The Role of Biceps Loading and Muscle Activation on Radial Head Stability in Anterior Monteggia Injuries. 74th Annual Meeting of the American Society for Surgery of the Hand, Las Vegas, NV, USA

2. Badre A, Axford DT, **Padmore CE**, Faber KJ, Johnson JA, King GJW. (2019). Effect of Ulnar Angulation and Soft Tissue Sectioning on Radial Head Stability in Anterior Monteggia Injuries. 74th Annual Meeting of the American Society for Surgery of the Hand, Las Vegas, NV, USA

3. Badre, A., Axford, A., **Padmore, C**., Berkmortel, C., Faber, KJ., Johnson, JA, King, GJW. "The Role of Biceps Loading and Muscle Activation on Radial Head Stability in Anterior Monteggia Injuries". International Combined Meeting Orthopedic Research Society (Jun 2019) Montreal, Canada

4. Badre, A., Axford, A., **Padmore, C**., Berkmortel, C., Faber, KJ., Johnson, JA, King, GJW. "Effect of Ulnar Angulation and Soft Tissue Sectioning on Radial Head Stability in Anterior Monteggia Injuries". International Combined Meeting Orthopedic Research Society (June 2019). Montreal, Canada
5. Chambers, S., **Padmore, C**., Suh, N. "The Association between Scaphoid Malunion and Radioscaphoid Joint Contact: A Computational Study". Association for Hand Surgery (Jan 2019). Palm Desert, California, USA.

6. Chan, A., **Padmore, C**., Suh, N. "Biomechanical Analysis of Extensor Carpi Radialis Longus Tenodesis for Scapholunate Ligament Reconstruction". American Association for Hand Surgery Annual Meeting (Jan 2019). Palm Desert, California, USA.

7. **Padmore, C**., Stoesser, H., Langohr, GDG., Johnson, JA., King, GJW., Suh, N. "Scapholunate Diastasis Following Sequential Sectioning of the Scapholunate Ligament and Secondary Stabilizers". World Congress of Biomechanics (July 2018). Dublin, Ireland.

8. Wu, K., **Padmore, C**., Suh, N. "Proximal Hamate Autograph for Scaphoid Proximal Pole Reconstruction: An Anthropometric Assessment". Canadian Orthopedic Association Annual Meeting (2018, June). Victoria, BC.

9. **Padmore, C**., Stoesser, H., Langohr, GDG., Johnson, JA., King, GJW., Suh, N. "Contact Mechanics of the Scapholunate Joint During Simulated Clench Fist Following Sequential Sectioning of the Scapholunate Ligament and Secondary Stabilizers." Canadian Research Society (2018, June). Victoria, BC, Canada

10. **Padmore, C.,** Chan, A., Suh, N. Biomechanical Evaluation of Extensor Carpi Radialis Longus Tenodesis for Scapholunate Ligament Reconstruction. Canadian Bone and Joint Conference (May 2018). London, ON.

11. **Padmore, C.,** Stoesser, H., Langohr, GDG., Johnson, Suh, N., JA., King, GJW., "Scapholunate Contact Mechanics Following Sequential Sectioning of the Scapholunate Ligament and Secondary Stabilizers". Orthopedic Research Society (2018, March). New Orleans, LA, USA

12. McGregor, ME., Isa, DA., **Padmore, C**., Welsh, MF., Langohr, GDG., King, GJW., Johnson, JA. "Loads in the Distal Radius and Ulna During Simulated Active Dart Throw Motion of the Wrist". Orthopedic Research Society (2018, March). New Orleans, LA.

13. Wu, K., **Padmore, C**., Lalone, E., Suh, N. "An Anthropometric Assessment of Proximal Hamate Autograft for Scaphoid Proximal Pole Reconstruction". American Society for Surgery of the Hand (Sept 2017). San Francisco, CA.Top Guest Society Poster Award

14. Stoesser, H., **Padmore, C**., Langohr, GDG., Suh, N., Johnson, JA., King, GJW. "Scaphoid and Lunate Kinematics Following Sequential Sectioning of the Scapholunate Ligament and Secondary Stabilizers". American Society for Surgery of the Hand (Sept2017). San Francisco, CA.

15. **Padmore, C**., Stoesser, H., Langohr, G., Lalone, E., Johnson, J A., King, G JW. "The Effect of Dorsal Angulation Deformities of the Distal Radius on Capitolunate Contact Mechanics".Canadian Orthopedic Research Society Conference (Jun 2017) Ottawa, ON.

16. Stoesser, H., **Padmore, C**., Langohr, G., Suh, N., Johnson, J A., King, GJW. "Scaphoid and Lunate Kinematics Following Sequential Sectioning of the Scapholunate Ligament and Secondary Stabilizers". Canadian Orthopedic Research Society Conference (Jun 2017). Ottawa, ON.

17. **Padmore, C**., Stoesser, H., Langohr, G., Lalone, E., Johnson, J A., King, GJW. "The Effect of Dorsal Angulation Deformities of the Distal Radius on Capitolunate Contact Mechanics". Orthopedic Research Society Annual Meeting (Mar 2017). San Diego, CA.

18. Stoesser, H., **Padmore, C**., Langohr, G., Suh, N., Johnson, J A., King, G JW. "Scaphoid and Lunate Kinematics Following Sequential Sectioning of the Scapholunate Ligament and Secondary Stabilizers". Orthopedic Research Society Annual Meeting. (Mar 2017) San Diego, CA. *Received the best hand and wrist poster/ poster teaser*

19. **Padmore, C.,** Stoesser, H., Nishiwaki, M., Gammon, B., Welsh, M., Langohr, G., Lalone, E., King, G JW., Johnson, J A. "The Effect of Distal Radius Deformities on Wrist Kinematics- An in-vitro Biomechanical Study".Canadian Orthopedic Research Society Conference (Jun 2016). Quebec City, QC

20. Stoesser, H., **Padmore, C.,** Nishiwaki, M., Gammon, B., Welsh, M., Langohr, G., Lalone, E., Johnson, J A., King, G JW. "Carpal Kinematics During Simulated Wrist Motion". Canadian Orthopedic Research Society Conference (June 2016). Quebec City, QC.

21. **Padmore, C**., Stoesser, H., Nishiwaki, M., Gammon, B., Welsh, M., Langohr, G., Lalone, E., King, G JW., Johnson, J A. “A Biomechanical Study of the Malunited Distal Radius and its Effect on Carpal Kinematics”. Canadian Bone and Joint Conference (Apr 2016). London, ON

22. Stoesser, H., **Padmore, C**., Nishiwaki, M., Gammon, B., Welsh, M., Langohr, G., Lalone, E., Johnson, J., King, G. “Carpal Kinematics During Simulated Wrist Motion”.Canadian Bone and Joint Conference (Apr 2016). London, ON

23. **Padmore, C**., Stoesser, H., Nishiwaki, M., Gammon, B., Welsh, M., Langohr, G., Lalone, E., King, G., Johnson, J. “The Effect of Distal Radius Deformities on Wrist Kinematics”. Orthopedic Research Society Annual Meeting (Mar 2016). Orlando, FL.

24. Stoesser, H., **Padmore, C**., Nishiwaki, M., Gammon, B., Welsh, M., Langohr, G., Lalone, E., Johnson, J., King, G. “Carpal Kinematics During Simulated Wrist Motion". Orthopedic Research Society Annual Meeting (Mar 2016). Orlando, FL

INVITED TALKS

Dr. Robert Zhong Department of Surgery Research Day “Scaphoid Malunion” – Co-author 2019
Western University, London, ON, Canada

Innovation in Motion Research Day. “Help! I’ve Fallen, and I Can’t Get Up…” 2019
London, ON

Biomechanics of the Musculoskeletal System, “Muscular Biomechanics” 2018
Western University, London, ON

Research Synopsis, “Current Hand and Wrist Research” 2017
Queens University, Kingston, ON

CIVE 460 Engineering Biomechanics, “Wrist Kinematics and Biomechanics” 2016
Waterloo University, Waterloo, ON